View metadata, citation and similar papers at core.ac.uk
brought to you by CORE
provided by ScholarBank@NUS

NONLINEAR DYNAMICS AND MODELING OF HEART AND BRAIN SIGNALS

KANNATHAL NATARAJAN

NATIONAL UNIVERSITY OF SINGAPORE
2008

NONLINEAR DYNAMICS AND MODELING OF HEART AND BRAIN SIGNALS

KANNATHAL NATARAJAN
(M.Sc., Nanyang Technological University)

A THESIS SUBMITTED

FOR THE DEGREE OF DOCTOR OF PHILOSOPHY

DEPARTMENT OF ELECTRICAL AND COMPUTER ENGINEERING

NATIONAL UNIVERSITY OF SINGAPORE
2008

Acknowledgements

It is a great pleasure to thank and convey my gratitude to the people who have helped me in this research work. First I would like to express my sincere thanks and gratitude to my supervisor **Dr. Sadasivan Puthusserypady** for his ever-present guidance and direction throughout this research work. He provided the counsel necessary for the completion of the thesis, and his advice and interest contributed immeasurable to this research work. Above all, he provided me constant encouragement and complete support in my research activities. I take this opportunity to thank **Dr. Vadakkepat Prahlad** for his timely help and support in completion and submission of the thesis.

I take this opportunity to thank Dr. Lim Choo Min, Dr. Rajendra Acharya and other staffs of Biomedical Engineering centre of NgeeAnn polytechnic for their help, support, interest and valuable suggestions for my research. I hereby express my sincere thanks to all the faculty and staff of National University of Singapore who has supported me to complete the research work. I also would like to thank all my family members and friends for their constant support and encouragement during all these years.

Special thanks to everyone who have, in one way or another, helped me to conduct this research.

Table of Contents

Summary

The theory of nonlinear dynamic systems provides new ways to handle complex dynamic systems. Chaos theory offers new concepts, algorithms and methods for processing, enhancing and analyzing the measured signals. In recent years, researchers have been applying the concepts of chaos theory to bio-signal analysis. In this work, the complex dynamics of the heart (Electrocardiogram (ECG)) and the brain (Electroencephalogram (EEG)) signals are analyzed in detail using the tools of chaos theory.

In the modern world, every year several thousands of people die of cardiac problems. This makes the automatic analysis and the assessment of risk for these problems a critical task. Analyses using the conventional linear methods are often found to produce inconclusive results. Therefore in this work we propose and apply unconventional methods of nonlinear dynamics to analyze ECG and EEG signals.

In the case of ECG, the heart rate variability (HRV) signal is analyzed using various complexity measures that are basing on symbolic dynamics. These complexity measures with the parameters in the frequency domain serve to be a promising way to get a more precise definition of individual risk. This is done in two stages: (i) feature extraction and (ii) classification. A feature library with more than ten features extracted from the HRV signal is developed for eight different cardiac health states. The measures

are then validated with neural network and fuzzy classifiers for their ability to do more precise classification. A classification accuracy of about 80-95% is achieved in our work.

In EEG analysis, the search for the hidden information for identification of seizures has a long history. In this work, an effort is made to analyze the normal and epileptic EEGs using the chaos theory. In this work, emphasis is made on the extraction and selection of key and relevant features that distinguish EEG (on the same subject) with and without the epileptic seizures. The features extracted include chaotic invariants and information theory features. Results obtained are promising and clear differences are seen in the extracted features between normal and epileptic EEGs.

At present, new biomedical signal processing algorithms are usually evaluated by applying them to signals acquired from real patients. Most cases, the signals are of short duration for the evaluator to decide on the accuracy and reliability of the given algorithm. To facilitate this evaluation, it is required to generate longer duration signals from these short duration signals while preserving the characteristics of the signal. In this work, we have proposed linear and nonlinear techniques to model the HRV and EEG signals from their respective short duration data. From the models, longer duration signals are synthesized for further analysis. Results of these generated signals show that the models can generate the HRV and EEG signals that approximate the real HRV and EEG signals. The HRV signal models are useful in the prediction of the heart rate signals and subsequently help in the analysis and diagnosis of cardiac abnormalities. The modeling of EEG signals can be a very useful tool in the prediction of seizures.

In this work, we have also proposed a new nonlinear model architecture using pipelined recurrent neural network (PRNN) to model the HRV and EEG signals. The new architecture performs better in terms of prediction error (measured as normalized root mean square error (NRMSE)) and signal to noise ratio (SNR). The signals modeled using the proposed architecture is able to successfully model the inherent nonlinear characteristics of the experimental signals. From the results it can be clearly seen that the proposed architecture clearly outperforms the linear models. This is due to the nonlinear model's inherent ability to model the underlying nonlinearity of the system under investigation.

List of Abbreviations

AF	Atrial Fibrillation
AIC	Akaike Information Criteria
AMI	Average Mutual Information
ANFIS	Adaptive Neuro Fuzzy Inference System
ANN	Artificial Neural Network
ANOVA	Analysis of Variance
APEN	Approximate Entropy
AR	Auto-Regressive
AV	Atrio-Ventricular
BBB	Bundle Branch Block
BPM	Beats Per Minute
BPTT	Back Propagation Through Time
CA	Cardiac Arrest
CAD	Coronary Artery Disease
CHB	Complete Heart Block
CJD	Creutzfeldt–Jakob Disease
CTM	Central Tendency measure

CTSA	Chaotic Time-Series Analysis
DFA	Detrended Fluctuation Analysis
ECG	Electrocardiogram
EEG	Electroencephalogram
FD	Fractal Dimension
FNN	False Nearest Neighbor
FPE	Final Prediction Error
FT	Fourier Transformation
FFT	Fast Fourier Transform
HF	High Frequency
HRV	Heart Rate Variability
ISCH	Ischemic/Dilated Cardiomyopathy
IVCD	Intraventricular Conduction Defects
KSEN	Kolmogorov-Sinai Entropy
LBBB	Left Bundle Branch Block
LF	Low Frequency
MA	Moving Average
NN	Neural network
NRMSE	Normalized Root Mean Square Error
NSR	Normal Sinus Rhythm
NTSA	Nonlinear Time-Series Analysis
PRNN	Pipelined Recurrent Neural Network

Pdf	Probability density function
PSD	Power Spectral Density
PVC	Pre-Ventricular Contraction
RBF	Radial Basis Functions
REN	Renyi's Entropy
RNN	Recurrent Neural Networks
RSA	Respiratory Sinus Arrhythmia
RTRL	Recurrent Time Recurrent Learning
SA	Sino-Atrial
SD	Standard Deviation
SNR	Signal to Noise Ratio
SEN	Spectral Entropy
SSS	Sick Sinus Syndrome
VF	Ventricular Fibrillation
VLF	Very Low Frequency
VT	Ventricular Tachycardia
WT	Wavelet Transform

List of Tables

List of Figures

Chapter 1 Introduction

1.1 Introduction

Computer technology has an important role in structuring biological systems. The explosive growth of high performance computing techniques in recent years with regard to the development of good and accurate models of biological systems has contributed significantly to new approaches to fundamental problems of modeling transient behavior of biological systems.

The importance of biological time series analysis, which exhibits typically complex dynamics, has long been recognized in the area of non-linear analysis. Several approaches have been proposed to detect the (hidden) important dynamical properties of the physiological phenomenon. The nonlinear dynamical techniques are based on the theory of chaos and have been applied to many areas including the areas of medicine and biology [1].

A great deal of attention has been focused on the extraction of dynamical information from chaotic time series [1-3]. Chaos is the state in which a nonlinear dynamical system exhibits bounded motion, with exponential sensitivity to initial conditions. The initially neighboring state of a chaotic system diverges exponentially as

the system evolves forward in time [4]. Chaotic time series analysis has greatly enhanced the understanding of chaos in experimental systems by allowing multidimensional dynamical information to be recovered from a time series of measurements of a single variable [1-3]. This is achieved using the method of time delay embedding, which allows the recovery of information from all degrees of freedom which are coupled to the observable [1]. This allows the strange attractor[1] of a chaotic dynamical system to be extracted from a time series of measurements of a single variable. The simplicity of the technique and the accessibility of experimental time series have encouraged the rapid exploration of numerous fields as varied as plasma fluctuations [2], climatic variations [5], non-equilibrium chemical systems [6], etc.

In this work, methods of chaotic time series analysis are applied to bio-signals such as the heart rate variability (HRV) signal and the electroencephalogram (EEG) signal. The HRV is extracted from the electrocardiogram (ECG) signal. The ECG is the electrical signal generated by the heart's muscles measured on the skin surface of the body. On the other hand, the EEG represents the time series that maps the voltage corresponding to neurological activity of the brain as a function of time. These two signals are essentially non-stationary in nature; they display a fractal[2] like structure. They may contain indicators of current disease, or even warnings about impending diseases. The indicators may be present at all times or may occur at random in the time scale.

---

[1] An aattractor is a set of states to which a dynamical system evolves after long enough time. An attractor is described as strange attractor if it has non-integer dimension and dynamics on it are chaotic.
[2] Fractal is a fragmented geometric shape that exhibits self similarity by having same type of structures on all scales.

However, to (study and) pinpoint anomalies in voluminous data collected over several hours is strenuous and time consuming. Therefore, computer based analytical tools for in-depth study and classification of data over day long intervals can be very useful in diagnostics.

1.2 Motivation

ECG has a basic role in cardiology since it consists of effective simple noninvasive low cost procedures for the diagnosis of cardiac disorders that have high epidemiological incidence and are very relevant for their impact on patient life and social costs. Pathological alterations observable by ECG are cardiac rhythm disturbances (or arrhythmia), dysfunction of myocardial blood perfusion (or cardiac ischemia), chronic alteration of the mechanical structure of the heart. Arrhythmias are considered to lead to life threatening conditions and the patients with arrhythmias are subjected to continuous monitoring in the intensive care units. Thus the automated and reliable detection of abnormalities in intensive care patients is very essential and critical. Recently lot of research is being carried out for automating the detection of abnormalities by applying various engineering methods and unconventional techniques to help the doctor to diagnose and act faster in case of emergency conditions. And also designing low cost high performance simple to use and portable equipment for ECG offering a combination of diagnostic features seem to be globally worthwhile. Such equipment should embed and integrate several techniques of data analysis such as signal processing, pattern

detection and recognition, decision support and human computer interaction. Thus computerized methods are to be applied for detection and classification of abnormalities.

Epilepsy is a pathological condition characterized by spiky patterns in continuous EEG and seizure at times [7]. Approximately one percent of the world's population has epilepsy, one third of whom have seizures not controlled by medications [7, 8]. Individuals with epilepsy suffer considerable disability from seizures and resulting injuries, the stigma and social isolation attached to having seizures, and from side effects of medical and other therapies. In some patients, whose seizures reliably begin in one discrete region, usually in the mesial (middle) temporal lobe, may be cured by surgery. This requires removing large volumes of brain tissues, due to the lack of a reliable method for accurately locating the region of seizure onset and the pathways through which seizures spread. Successful surgical treatment of focal epilepsies requires exact localization of the epileptic focus and its delineation from functionally relevant areas. For this purpose, different pre-surgical evaluation methodologies are currently in use [9]. Neurological and neuropsychological examinations are complemented by neuro-imaging techniques that try to identify potential morphological correlates. Currently, for localization of the epileptic focus, the patient's spontaneous habitual seizure is recorded using electroencephalography. Depending on the individual occurrence of seizures this task requires long lasting and continuous recordings of EEG. In case of ambiguous scalp EEG findings, invasive recordings of electrocorticogram and stereo-EEG via implanted depth electrodes are used. This procedure is time consuming and offers greater risk to the

patient. Thus reliable EEG analysis techniques are required to localize and to demarcate the epileptic focus.

1.3 Objectives

The present work is to perform nonlinear time series analysis on ECG and EEG signals and use neural network techniques to classify and model these signals. Various milestones in this work are:

- To identify appropriate and relevant set of features to detect various cardiac abnormalities from the HRV signals.
- To analyze EEG signals and to identify set of features that distinguishes different types of EEG, specifically the epileptic EEG.
- To identify suitable network architecture to classify the signals for the abnormalities based on the chosen feature set.
- To identify and implement a suitable algorithms for dynamic reconstruction model of the signals.

1.4 Contributions

The contributions derived from this research are summarized below:

- The implementation of an automatic approach to achieve highly reliable detection of cardiac abnormalities, which entails feature extraction, feature selection, feature fusion, event classification and assessment.

- Evaluation of large set of features extracted using nonlinear time series analysis techniques for detection of cardiac abnormalities.

- Identification of suitable classifier architecture and classifier inputs to reliably detect various cardiac abnormalities.

- Characterization of normal and epileptic EEG signals using chaotic invariants and information theory.

- Identification of the classifier architecture and classifier inputs to classify EEG signals from the extracted features.

- Implementation of linear and nonlinear models for the reconstruction of HRV and EEG signals.

- Developed a new model architecture based on pipelined recurrent neural network (PRNN) for the reconstruction of HRV and EEG signals.

- Comparison and validation of the performance of the proposed architecture with existing linear and nonlinear architectures.

1.5 Organization of the Thesis

The thesis is organized in a systematic manner starting from introduction to literature review, nonlinear analysis of signals, modeling of signals and finally the conclusion.

- Chapter 1 - Introduction

The introduction to the current work in terms of motivation, objectives and the contributions is discussed in this chapter.

- Chapter 2 – Literature Review

Review of the previous research work done by others in the area of cardiac health diagnosis, chaotic signal processing, EEG signal analysis and linear and nonlinear modeling of signals.

- Chapter 3 – Chaotic analysis of heart signals

In this chapter, the chaotic invariants (fractal dimensions, correlation dimension, Lyapunov exponent, Hurst exponent) and information theory features of HRV signals are extracted and analyzed in detail.

- Chapter 4 – Nonlinear dynamics of EEG signals

In this chapter, a comprehensive chaotic analysis of the normal, background and epileptic EEG signals is carried out. The chaotic measures distinguish the different types of EEG signals and offer insight into the dynamical nature and variability of these signals.

- Chapter 5 – Classifier architectures for cardiac health state diagnosis and mental health diagnosis

The neural network classifier, fuzzy classifier and adaptive neuro fuzzy inference system (ANFIS) classifier are presented as diagnostic tools to aid the physician in the analysis of heart diseases. The characteristic features of the HRV signals from the feature library are evaluated for the suitability to do classification. A comparative analysis of the results of the classifiers is presented and the performances of the classifiers are evaluated in terms of classification accuracy.

Similarly, the ability and effectiveness of the nonlinear measures of EEG in diagnosing various mental states are evaluated using neural network classifier, fuzzy classifier and ANFIS classifier.

- Chapter 6 – Linear modeling of heart and brain signals

The HRV and EEG signals are modeled using linear modeling methods such as the Welch method and Burg's method. The performances of the two methods in modeling

these signals are analyzed. The dynamic characteristics of the modeled signals are compared with the original signals.

- Chapter 7 – Nonlinear modeling of heart and brain signals

The nonlinear model using Elman neural network is developed to model the HRV and EEG signals individually. A novel nonlinear modeling architecture is proposed using pipelined recurrent neural network (PRNN). The results of the proposed architecture and the Elman model are compared and evaluated using the dynamic characteristics of the reconstructed signals.

- Chapter 8 – Conclusion

The conclusion and comments of the work done in this project are discussed. Various suggestions for future work are also given.

Chapter 2 Literature Review

Physiological time series such as ECG and EEG typically are short, nonlinear and noisy. Such time series usually cannot be studied satisfactorily by linear time series analysis. Although linear techniques such as Fourier analysis are useful to study characteristic oscillations in detail, these methods fail to detect any non-linear correlations present and cannot provide a complete characterization of the underlying dynamics.

Over the last two decades many non-linear time series methods have been developed in the theory of non-linear dynamics, commonly known as chaos theory. These methods are suited to characterize the dynamics in noise free, low-dimensional deterministic systems and have proven highly successful in characterizing irregular (chaotic) time series from mathematical models and well controlled physical experiments. Biological systems are subjected to changes in their environment triggered both by stochastic sources and feedback control mechanisms. Thus the time series recorded from the natural world consist of a mixture of random and deterministic features. Hence, in early 90's investigators explored the way to apply the nonlinear time series analysis techniques [10-13] to analyze and characterize apparently irregular behavior – a distinct feature of physiological signals. Later researchers tuned the focus of attention in applying chaos theory to bio-signal analysis in two directions. They are the

detection and characterization of nonlinear dynamics of the underlying physiological system and to develop new and robust nonlinear measures that are more suited to all types of data. Various techniques discussed in the literature of chaos theory to characterize the nonlinear behavior include the estimates of an effective correlation dimension, entropy related measures, Lyapunov exponents, measures for determinism, self-similarity, interdependencies, recurrence quantification and tests for nonlinearity.

In 1991, Kaplan *et. al*. applied the theory of chaos to detect the cardiac arrhythmia such as ventricular fibrillation (VF) [14]. They tried to identify whether the fibrillation originates from a chaotic system by constructing a dynamical system representation of the signal and testing directly for signs of chaos by calculating Lyapunov exponents. However they were unsuccessful in constructing a phase-space representation of ventricular fibrillation that distinguishes between ventricular fibrillation and a similar, but random, signal. Researchers have applied the concepts of chaos in cardiology and tried to address the different heart diseases including whether chaos represents the healthy or diseased state. As most of these approaches to chaotic modelling rely on discrete models of continuous problems, in 1995, Cohen *et. al.* developed a continuous nodal based on a conjectured solution to the logistic equation [15]. As a result of this approach, two practical methods for quantifying variability in data sets have been derived. The first method is a graphical representation obtained by using second-order difference plots of time series data [15]. The second is a central tendency measure (CTM) that quantifies this degree of variability [15]. The CTM is then used as a feature for a neural network to differentiate congestive heart failure patients as compared to normal controls.

Efforts have been made in estimating nonlinear characterizing parameters like correlation dimension for pathological signals and it has been shown that they are useful indicators of pathologies. Further progress made in the field using measures of chaos has attracted scientific community applying these tools in studying physiological systems. Several methods for estimating invariants from nonlinear dynamical systems is reported in the literature[16-23]. Crucial for the application of nonlinear methods is the reconstruction (embedding) of the time series in a phase space with appropriate dimension. In 1999, Fell *et. al.*[16], in their work have demonstrated the importance of embedding the time series in a state-space with appropriate dimension in nonlinear analysis. In their study, only healthy subjects were considered and the necessity to choose the proper embedding dimension is explained. In their work, proper embedding dimension was determined by application of two techniques, the false nearest neighbours method and the saturation of the correlation dimension. Results are then compared with findings for simulated data (quasiperiodic dynamics, Lorenz data, and white noise) and for phase randomized surrogates. This result paved the foundation to find the proper embedding dimension and used by most of the current research in the nonlinear analysis of bio signals to appropriate embedding dimension for the topologically proper reconstruction of the bio signals considered.

Khadra *et. al.*[17] have proposed classification of life-threatening cardiac arrhythmias using Wavelet transform. In this work, three types of arrhythmia such as ventricular fibrillation, atrial fibrillation and ventricular tachycardia were identified using the energy parameter from the wavelet transform. Later, Al-Fahoum *et. al.*[18], extended

the study by using six different energy descriptors from the wavelet transformations. They tried with nine different wavelets and generated a feature vector using these wavelet energy descriptors and used as an input to radial basis function (RBF) neural networks for classifying the above mentioned three arrhythmias and the normal class. Further, the studies using wavelet transform was extended to identify the underlying phenomenon of the physiological process. Paul *et. al,* [19] showed that the coordinated mechanical activity in the heart during ventricular fibrillation may be made visible in the surface ECG using wavelet transform (WT). The results have been demonstrated using an animal model for cardiac arrest that the WTs allow this underlying the coordinated atrial activity to be detected using the non-invasive ECG recording. These results paved a way for many other researchers to look into different nonlinear parameters that differentiate the diseased states in physiological signals and also to apply these features as inputs to the different classifiers architectures and study the performance.

Sun *et. al.*[20] included few other additional types of arrhythmia such as pre-ventricular contraction in their analysis for detection of arrhythmia using nonlinear techniques. Then, Owis *et. al.*[21] applied the features extracted based on nonlinear dynamical modeling in ECG signals for arrhythmia detection and classification. In their work, they have used correlation dimension and Lyapunov exponents for classification using three different classifiers such as the minimum distance, Bayesian and the k-nearest neighbors. Six signal classes have been shown to be statistically different but poor classification results were observed, indicating that their distributions have significant overlap. This suggests that the proposed features were able to detect the presence of

abnormality rather than to specify the type of abnormality. Dingfei *et. al.*[22] evaluated different types of classifier architectures to classify cardiac arrhythmia into six classes using autoregressive (AR) modeling parameters. All these work shows the horizon of research on application of nonlinear techniques for ECG analysis even tough consistent and clinical application results are yet to be reached.

During the past decades, a great deal of work has been devoted in understanding the physiological information behind the variability of the cardiac cycle. Task force (1996) gave guidelines for Heart rate variability (HRV) - standards of measurement, physiological interpretation for clinical use [23]. Since then many researchers started to try to apply the nonlinear techniques to these HRV signals and look into feasibility of using the HRV signal as a reliable diagnostic tool.

Methods based on chaos theory have been applied in tracking the HRV signals. Researchers have used phase-space technique to distinguish normal and abnormal cardiovascular signals [24]. In this effort, it has been shown that phase space representation differentiated the HRV signals and the arterial pressure signals into two classes such as the normal and abnormal class. Further research in literature, indicates the importance and evolution of application of nonlinear techniques to study HRV in both healthy and many diseased subjects [16-25].

It has been shown that the variability in heart rate reflects the vagal and sympathetic function of the autonomic nervous system, and can be used as a monitoring tool in clinical conditions characterized by altered autonomic nervous system function.

Spectral analysis of beat-to-beat variability is applied as a non-invasive technique to evaluate autonomic dysfunction. Radhakrishna *et. al.* [25] have tried the nonlinear analysis of HRV signals to investigate the autonomic changes associated with panic disorder. Even though well established analysis tools from linear system theory can provide valuable information for physiological and clinical interpretation of the HRV, it has been speculated that methods from nonlinear dynamics may provide a powerful tool to deduce more information for better understanding the mechanisms of cardiovascular control [23].

From the literature studies, it can be seen that there has been extensive research done on applying nonlinear techniques to ECG signals as compared to HRV signals for identification of cardiac abnormalities. There is still the problem in the automatic identification of cardiac abnormalities as there is no specific methods or features has been identified to classify the many different types of cardiac abnormalities. Accordingly in this work, we address the problem of characterizing the nonlinear dynamics of the HRV signals of different cardiac abnormalities and access their suitability for classifying many cardiac abnormities rather than just a few. This is required as healthcare industry is getting more and more sophisticated and looking for ways for more automated diagnosis and indices for rapid diagnosis.

Many investigators, for example, Duke *et. al.* [12] has proved that complex dynamical evolutions lead to chaotic regimes. In the last thirty years, experimental observations have pointed out that, in fact, chaotic systems are common in nature [26]. In

theoretical modeling of neural systems, emphasis has been put mainly on either stable or cyclic behaviors. In the past, a wide range of work has been done in understanding the complexities associated with the brain through multiple windows of mathematics, physics, engineering and chemistry, physiology etc [27]. Until about 1970, EEG interpretation was mainly heuristic and of a descriptive nature. Although several papers have discussed quantitative techniques to assist in EEG interpretation [28], in clinical terms the situation remained unchanged. Nonlinear dynamics theory opened new and powerful window for understanding behavior of the EEG. In 1985, first Babloyantz *et. al.*, used nonlinear techniques to study the slow wave sleep signal [29]. According to their research, the analysis of electroencephalogram data from the human brain during the sleep cycle reveals the existence of chaotic attractors for sleep stages two and four. The onset of sleep is followed by increasing "coherence" towards deterministic dynamics involving a limited set of variables. They have applied techniques such as Phase space representations and Lyapunov exponents and provided the possibility for these techniques to be further explored in the analysis of EEG signals.

Subsequently there has been a sustained interest in describing neural processes and brain signals, especially the EEG, within the context of nonlinear dynamics and theory of deterministic chaos [30]. Rapp *et. al.* indicated that the correlation dimension estimate of the EEG signal can distinguish between a subject at rest and a cognitively active subject (doing mental subtraction or addition). These results also suggested that nonlinear analysis techniques can provide a characterization of changes in cerebral electrical activity associated with changes in cognitive behaviour. Since that time,

applications of EEG to several research areas have significantly increased and researchers further tired to apply the nonlinear techniques on brain signals for understanding the chaotic behavior and the dynamic process at neural level for various brain disturbances such as the schizophrenia, insomnia, epilepsy and other disorders [31-33].

In 1997, Stam *et. al*. [34] studied the abnormal dynamics of cortical neural networks in Creutzfeldt–Jakob disease (CJD) by applying nonlinear techniques to the EEG signals. They showed that in the EEG the CJD episodes coincide with the occurrence of periodic slow waves and can be predicted much better than the irregular background activity. The results suggested the usefulness of non-linear models to gain a better understanding of brain dynamics. Later, Rezek *et. al*. [35] applied four stochastic-complexity features on EEG signals recorded during periods of Cheyne–Stokes respiration, anaesthesia, sleep, and motor-cortex investigation. They successfully demonstrated the use of entropy measures for characterising the various phenomenons from the EEG signals even though these techniques were not applied for identification of any brain disorders. Jaeseung *et. al.* [32] further investigated the use of nonlinear parameters for identification of brain disorders such as Alzheimer's disease and vascular dementia. In this work, to assess nonlinear EEG activity in patients with Alzheimer's disease (AD) and vascular dementia (VaD), the authors estimated the correlation dimension (D2) and the first positive Lyapunov exponent (L1) of the EEGs in both patients and age-matched healthy control subjects. The AD patients had significantly lower D2 and L1 values than the normal control subjects whereas the VaD patients had relatively increased values of D2 and L1 compared with the AD patients. In addition, the

authors detected that the VaD patients had an uneven distribution of D2 values over the regions than the AD patients and the normal control subjects whereas AD patients had uniformly lower D2 values in most regions, indicating that AD patients have less complex temporal characteristics of the EEG in entire regions. These nonlinear analyses of the EEG signals paved a way to provide insight in understanding the nonlinear dynamics of the observed EEG activity in different brain disorders. Further studies has been done in understanding the EEG dynamics for prediction of epileptic seizures [36,37], characterization of sleep phenomena [38], encephalopathy's [39] or Creutzfeldt–Jakob disease [34] and monitoring of depth of anesthesia [35,40]. Eventually, researchers started exploring the application of these techniques in a clinical scenario.

In the analysis of EEG data for clinical applications, different chaotic measures such as the correlation dimension, Lyapunov exponent and entropy are used in the literature [41 - 46]. Jing and Takigawa [41] applied the correlation dimension techniques to analyze EEG at different neurological states. These estimates of correlation dimensions were calculated for control EEG, ictal and inter-ictal EEG signals. The estimates were calculated for different regions of the brain and also with respect to the different frequency ranges. This study provided an in-depth analysis of application of correlation dimension to EEG signals and their conclusions on the variation of the dimension estimates proved as an evidence to apply correlation dimension estimate for future analysis of brain states from EEG signals. Lehnertz and Elger [42] used the correlation dimension to test whether a relationship exists between spatio-temporal alterations of neuronal complexity and spatial extent and temporal dynamics of the epileptogenic area.

Casdagli *et. al.*[43] showed that the techniques developed to study of nonlinear systems can be used to characterize the epileptogenic regions of the brain during the inter-ictal period. The correlation integral, a measure sensitive to a wide variety of nonlinearities, was used for detection. And statistical significance was determined by comparison of the original signal to surrogate datasets. The results showed that statistically significant non-linearities were present in signals generated by the epileptogenic hippocampus and inter-ictal spike foci in the temporal neocortex. These results indicated that techniques developed for the study of non-linear systems can be used to characterize the epileptogenic regions of the brain during the inter-ictal period and can elucidate the dynamical mechanisms of the epileptic transition. Further adding to the research, investigators explored the ways to apply the nonlinear analysis for prediction of seizures and measure the level of synchronization in the brain during different mental states. [44-46]. Arnhold *et. al.* [46] have used measures such as correlation dimension and mean phase coherence to characterize the inter-ictal EEG for prediction of seizures. The effective correlation dimension revealed that values calculated from inter-ictal recordings were significantly lower for the epileptic focus as compared to remote areas of the brain. Also the epileptogenic process during the inter-ictal state is characterized by a pathologically increased level of synchronization as measured by the mean phase coherence. All the above mentioned research proved that nonlinear analysis techniques can be used for analysis of EEG signals but they are all specific for the scenario or the problem that is considered. Lot more research is required to identify the specific techniques for diagnosis of different and more specific brain disorders or states.

Despite the many applications of EEG in clinical neurophysiology [47-52], its visual interpretation is very subjective and does not lend itself to statistical analysis. As a result, a number of research groups have proposed methods to quantify the information content of the EEG. Among these are the Fourier transform (FT), WT, chaos, entropy, and sub-band wavelet entropy [53-56]. The importance and necessity for EEG signal modeling to achieve a better understanding of the physical mechanisms generating these signals and to identify the causes of EEG signals changes was emphasized by Bai *et. al.*[57]. The results lead to the application of estimated model parameters for identification and classification of EEG abnormalities in future research. Modeling can also be used for predicting the future neurological outcome and for data compression. Simulation based on EEG signal model can be used to better demonstrate the effectiveness of a certain quantitative analysis method or EEG feature extraction system.

There are many publications relating to the prediction of seizures by analyzing the EEG with characterizing measures [58]. However in these studies, the authors have envisioned the feasibility of predicting the seizures. There are work done [59] to statistically validate these measures that are used to predict seizures. One such method is application of surrogates to evaluate the performance of seizure prediction algorithms and has concluded that the approach of surrogates is a promising work in this field. The analysis and prediction of epileptic seizures is still strong area to research and conclusive results are yet to be obtained.

With this scenario, in this work, the control, background and epileptic EEGs are characterized using various nonlinear measures and their suitability for diagnosis are assessed. The possibilities of predicting the seizure horizon is also explored and attempted in this work by dynamically reconstructing the EEG signals and evaluate using a set of chosen nonlinear features. Furthermore, in this work, attempt is made to analyze both heart and brain signals using nonlinear techniques and evaluate the cardiac and mental health states. This attempt is essential as the future in healthcare is to provide more and more sophisticated and automated monitoring and diagnosing using multimodal physiological signals.

Considering a scenario of Cardiac arrest (CA), which is one of the most commonly occurring critical coronary unit disorders, due to the technological developments of implantable and portable defibrillators, most of the patients of CA have successful resuscitation in or outside the hospital. However, a large majority of resuscitated patients are left with significant neurological impairment. Neuronal damage from CA occurs within minutes and rapidly devastates brain function with permanent consequences shortly after its onset. These patients usually have undetected seizures and are mostly known after the brain is damaged. This lead to situation of patients with the heart functioning but the brain damaged. Furthermore, the lack of sensitive detection and monitoring methods has impeded clinical investigations into improving diagnosis and recovery of brain function. Still, the overall compelling goal is to bring to the bedside state-of-the art equipment for rapid and accurate detection and monitoring of both heart and brain functions [60].

Here in this work, a different approach of application of non-linear time series analysis techniques is adopted to demonstrate that concepts originating from the theory of non-linear dynamics can be used to characterize the underlying dynamics of EEG and HRV signals. In particular, recently developed statistical and non-linear time series methods are applied to evaluate the feasibility of diagnosing the cardiac and mental health states from the predicted EEG and HRV signals.

Chapter 3 Chaotic Analysis of HRV Signals

The process of analyzing time series using mathematical and numerical data transformations or even appropriate graphical displays constitutes a field of science known as time-series analysis. Conventional signal processing techniques include FT, autocorrelation functions and AR data modeling. These methods generally are and have often been found insensitive for describing the nonlinear structure of chaotic time series. Chaotic time-series analysis (CTSA), or nonlinear time-series analysis (NTSA), refers to a class of data-analysis techniques employed to provide a richer description of time series generated for chaotic systems. In this chapter, various techniques of nonlinear time series analysis which are based on the paradigm of deterministic chaos are discussed.

The HRV signal, extracted from the ECG signal can be used as a reliable indicator of heart diseases. Using the HRV signal as the base signal, a feature library with more than ten features is developed for diagnosis of eight different cardiac health states. In this work, parameters such as correlation dimension (D_2), largest Lyapunov exponent (λ_1), Kolmogorov-Sinai entropy (*KSEN*), spectral entropy (*SEN*), approximate entropy (*APEN*) and Renyi's entropy (*REN*) are used to quantitatively describe the attractor in multidimensional space. The extracted chaotic features are accurate only if the signals are

reconstructed in a multi-dimensional state-space with optimal embedding dimension (m) and embedding time delay (τ). The optimal τ and m are determined before proceeding with the chaotic features extraction. The signals are tested for nonlinearity and stationarity as well, as the measurements of these parameters are valid only if the data under consideration are nonlinear and stationary.

3.1 Description of the Data

ECG data for the analysis was obtained from PhysioBank Biomedical Signals Archive[3][61]. The ECG signals available in the database were pre-processed to remove noise due to power line interference, respiration, muscle tremors, spikes etc. The sampling frequency of the data is 360 Hz. The number of dataset chosen for each of the eight classes of cardiac health states is given in Table 3.1. Each dataset consists of around 10,000 samples. The heart rate is calculated by identifying the R peaks of ECG signals using Tompkins's algorithm [62]. The interval between two successive QRS complexes is defined as the RR interval (t_{R-R}) and the heart rate (HR) in beats per minute (BPM) is given by,

$$HR = \frac{60}{t_{R-R}} \tag{3.1}$$

[3] http://www.physionet.org/physiobank/database/

In this work, an effort is made to characterize and classify eight different classes with one normal class and seven different cardiac abnormalities. The HRV signal is extracted from the ECG signal for each class.

Type	NSR	PVC	CHB	SSS	LBBB	ISCH	AF	VF
No. of datasets	100	75	53	52	46	52	55	53

Table 3.1 ECG Data for eight cardiac health states

The eight cardiac states are:

Normal Sinus Rhythm (NSR): All P-waves upright, rounded and similar in size and shape. A P-wave exists for every QRS complex. Each P-wave is the same distance from the QRS complex – less than 0.20 seconds. All QRS complexes are the same size and shape and point in the same direction. Each QRS is the same distance from the T-waves and the QRS the duration is 0.10 seconds or less. The heart rate in this case varies between 60-100 BPM and is rhythmic.

Preventricular Contraction (PVC): In this case, extra beats occur in the normal sinus rhythm causing irregularity in the usual rhythm of the heart. These extra beats occur when there is an ectopic focus in the ventricle, causing it to send premature electrical impulse that spreads to the sino-atrial (SA) node. The QRS complex is widened and not associated with the preceding P-wave. The T-wave is inverted after PVC. It is often followed by a compensatory pause. In couplets, there are two consecutive PVCs exist. In Bigeminy, there is PVC after every other NSR. In this case, heart rate increases from normal rhythm and varies between 100- 160BPM.

Complete Heart Block (CHB): In this case, the heart rate will be usually between 30-35BPM. P-waves are not conducted to the ventricles because of the block at the atrio-ventricular (AV) node. In this case, the P-waves show no relation to the QRS complexes. They 'probe' every part of the ventricular cycle but are never conducted. All the impulses generated from the sinus node are not conducted to the ventricle. No impulses are conducted and the ventricular rate becomes dependent on spontaneous ventricular depolarizations. In this case, the ECG exhibits bradycardia with HR = 20-40 BPM. The ventricles are depolarized by a ventricular escape rhythm.

Sick Sinus Syndrome (SSS): It is a disturbance of the normal rhythm of the heart. The electrical impulse that drives the heart beat starts in the SA node of the heart, and then spreads through specialized conduction pathways, causing orderly depolarization and contraction of the heart muscle. This can be traced on an ECG. There is rhythmic variation in the heart rate swinging between higher and lower heart rates.

Atrial Fibrillation (AF): In AF, sinus rhythm does not occur. Instead, multiple "patterns" of electrical impulses travel randomly through the atria, leading to random activation of different parts of the atria at different times. Because the tissues of the right and left atria are not stimulated to contract in an organized manner, the walls of the atria quiver resulting in an irregular ventricular rhythm. Sometimes on a first look the rhythm may appear regular but on closer inspection it is clearly irregular.

Ischemic/Dilated Cardiomyopathy (ISCH): Ischemic cardiomyopathy is the ventricular systolic dysfunction caused by the atherosclerotic coronary artery disease (CAD). As a

result of smoking, hypertension, diabetes mellitus, lipid disorders, chronic inflammation, and genetic susceptibility, atherosclerotic plaque accumulates in the walls of coronary arteries resulting in reduced flow of blood and oxygen to the heart. Irregular heartbeats can be observed under this condition.

Left Bundle Branch Block (LBBB): This belongs to a group of heart problems called intraventricular conduction defects (IVCD). Patients with LBBB may have left ventricular disease or cardiomyopathy. The pattern seen in the ECG indicates pulses in a heart beat and their duration. QRS duration of greater than 110 milliseconds is a diagnostic indication of LBBB.

Ventricular fibrillation (VF): Ventricular fibrillation causes rapid, ineffective and uncoordinated contractions of the heart. It is caused by abnormal heart beats which are initiated by electrical activity in the lower heart chambers or ventricles. This condition is a common complication of heart attacks and can also be caused by electrocution or drowning. The ECG is bizarre, irregular and random.

Using the HRV signal as the base signal, the eight cardiac states are characterized using the nonlinear, chaotic and information theory features. These signals are analyzed using fractal dimensions, correlation dimension, Lyapunov exponent, entropies and detrended fluctuation analysis.

3.2 Fractal Dimension Analysis

The term "fractal" was first introduced by Mandelbrot in 1983 [63]. A fractal is a set of points that when looked at smaller scales, resembles the whole set. The concept of fractal dimension (FD) refers to a non-integer or fractional dimension and originates from fractal geometry. In traditional geometry, the topological or Euclidean dimension of an object is the number of independent directions that the object occupies in space. This definition of dimension works well for geometrical objects whose level of detail, complexity or "space-filling" is the same. However, when considering two fractals of the same topological dimension, their level of "space-filling" is different, and that information is not given by the topological dimension. The FD emerges to provide a measure of how much space an object occupies between Euclidean dimensions. The FD of a waveform represents a powerful tool for transient detection. This feature has been used in the analysis of ECG and EEG to identify and distinguish specific states of physiologic function. Many algorithms are available to determine the FD of the waveform. In this work, algorithms proposed by Higuchi and Katz [64, 65] are implemented for analysis of ECG and EEG signals.

3.2.1 Higuchi's Algorithm

Consider $\{x(i); i = 1,2,\ldots,N\}$, the time sequence to be analyzed. Here N is the total number of samples in the dataset. Construct k new time series $x_m^k \ as: \ x_m^k = \{x(m), x(m+k), x(m+2k), ..., x(m+\lfloor \frac{N-m}{k} \rfloor k), \}$ for m=1, 2, …, k, where m indicates

the initial time value, and *k* indicates the discrete time interval between points, and $\lfloor a \rfloor$ means the integer part of *a* or *a* rounded down to the nearest integer. For each of the *k* time series or curves x_m^k, the length $L_m(k)$ is computed by,

$$L_m(k) = \frac{\sum_{i=1}^{\lfloor a \rfloor} \left| x(m+ik) - x(m+(i-1)k) \right| (N-1)}{\lfloor a \rfloor k}, \tag{3.2}$$

where $(N-1)/\lfloor a \rfloor k$ is a normalization factor and $a = \frac{N-m}{k}$. An average length is computed as the mean of the *k* lengths $L_m(k)$ for $m = 1, 2, ..., k$. This procedure is repeated for each *k* ranging from 1 to $k_{\max}$, obtaining an average length for each *k*. In the curve of ln($L_m(k)$) versus ln(1/*k*), the slope of the least-squares linear best fit is the estimate of the FD ($D^{Higuchi}$) [64].

3.2.2 Katz Algorithm

Using Katz's method [65], the FD of a curve can be defined as,

$$D^{Katz} = \frac{\log_{10}(L)}{\log_{10}(d_x)}, \tag{3.3}$$

where *L* is the total length of the curve or sum of distances between successive points, and d_x is the diameter estimated as the distance between the first point of the sequence and the point of the sequence that provides the farthest distance. Mathematically, d_x can

be expressed as $d_x = \max\left(\|x(1), x(i)\|\right)$ for $i = 2, 3..., N$. Here $\|x(i), x(j)\|$ represents the Euclidean norm of the distance between the points $x(i)$ and $x(j)$.

Considering the distance between each point of the sequence and the first, point *i* is the one that maximizes the distance with respect to the first point. The FD compares the actual number of units that compose a curve with the minimum number of units required to reproduce a pattern of the same spatial extent. FDs computed in this fashion depend upon the measurement units used. If the units are different, then so are the FDs. Katz's approach solves this problem by creating a general unit or yardstick: the average step or average distance between successive points, d_{av}. Normalizing the distances, D^{Katz} is then given by,

$$D^{Katz} = \frac{\log_{10}(L/d_{av})}{\log_{10}(d_x/d_{av})}. \tag{3.4}$$

3.2.3 Validation of the FD Algorithms

The FD algorithms discussed above are validated using synthetic data generated using the Weiestrass cosine function [66] given by,

$$W_Y(t) = \sum_i \gamma^{-iY} \cos(2\pi\gamma^i t), \quad 0 < Y < 1, \tag{3.5}$$

where $\gamma > 1$. The FD (theoretical) of this signal is given by $D = 2 - Y$. FD's of this synthetic signal range from 1.001 to 1.991. Figure 3.1 shows the FD values obtained by

each of the analysis methods plotted against the theoretical FDs of the synthetic data. The perfect reproduction of the theoretical FDs should yield a straight line of slope equal to one. From this study, it is seen that the Higuchi's algorithm provides the most accurate estimate of FD.

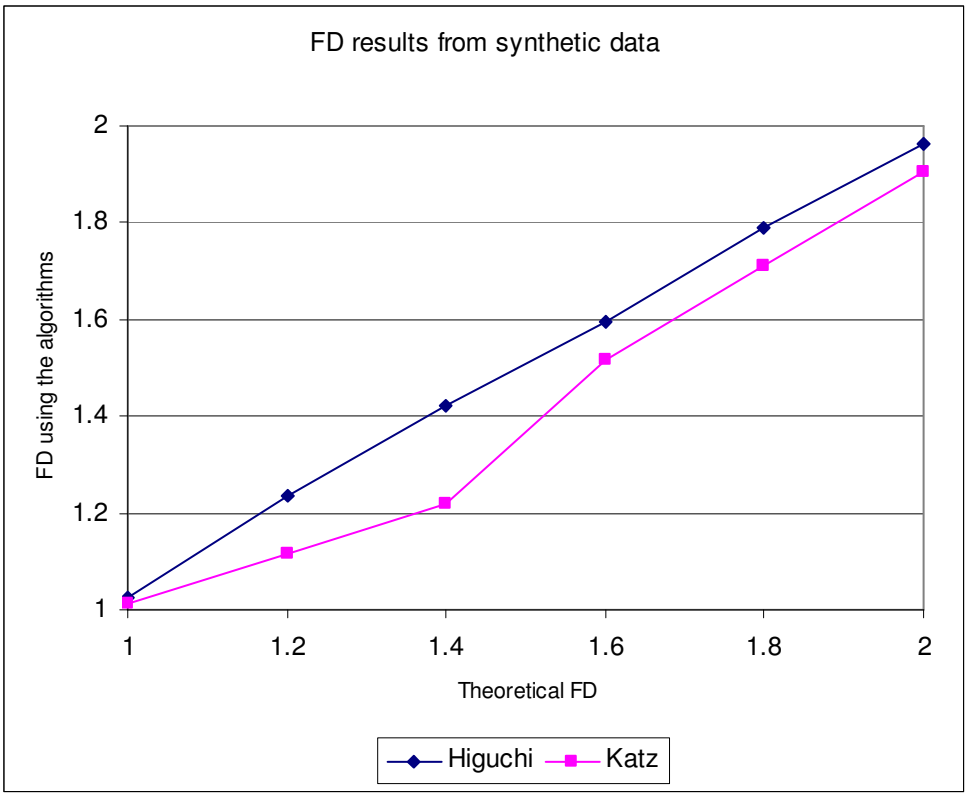

Figure 3.1 FD computed using Higuchi and Katz method versus theoretical FD

3.3 State-space Reconstruction

All further analysis of the time series depends on the precondition of a successful reconstruction of the state-space of the underlying process. There exist a number of

rigorous theorems about the possibility to reconstruct a state-space from a scalar time series. The reconstructed attractor from the observed scalar data must preserve the invariant characteristics of the original unknown attractor. This is done by using an appropriate embedding dimension, *m,* and embedding delay time, τ (delay coordinate method). Taken's embedding theorem [67] allows for the reconstruction of the attractor in the time delayed embedded space, preserving its topological characteristics. The reconstruction of the attractor is done from a finite time series of the observation of a single variable. Takens embedding theorem asserts that if a time series ($x(1), x(2),..., x(N)$) is one component of an attractor that can be represented by a smooth *d*-dimensional manifold (where *d* is an integer), then the topological properties of the attractor such as dimensions and Lyapunov exponents are equivalent to the topological properties of the embedding formed by the *m*-dimensional state-space vectors,

$$\mathbf{x}_i = [x(i),\, x(i+\tau),\, x(i+2\tau),\, \ldots\ldots,\, x(i+(m-1)\tau)]\,, \qquad (3.6)$$

for $m \geq 2d+1$. In equation (3.6), τ is the embedding delay time and m is the embedding dimension. Different choices of m and τ yield different reconstructed trajectories. There exist several methods for estimating the optimum values τ and m, which are summarized as follows [68]:

Analytical methods for estimating τ :

- Autocorrelation and power spectrum functions
- Average mutual information (AMI) function

- Degree of separation function
- Lyapunov exponents

Analytical methods for estimating m:

- False nearest neighbor method (FNN)
- Bad prediction method
- Fractal and correlation dimensions

Empirical methods (for estimating both τ and m):

- Neural networks (NN)
- Derivative-free global optimization methods, like genetic algorithms

3.3.1 Estimation of Embedding Dimension

The dimension m is the minimum number of time-delay coordinates needed so that the trajectories $\mathbf{x}_i$ do not intersect in m dimensions. In dimensions $< m$, trajectories can intersect because they are projected down into too few dimensions. Subsequent calculations, such as predictions, may then be corrupted. If it is too large, noise and other contamination may corrupt other calculations because noise fills any dimension.

Sauer et al. [69] has generalized the Taken's theorem to find an optimal embedding dimension. If the attractor has a box counting dimension D_0, then an embedding dimension of $m \geq 2D_0 + 1$ is sufficient to ensure that the reconstruction is a

one to one embedding. If the attractor has a correlation dimension D_2, then an embedding dimension of $m \geq D_2$ is sufficient to measure the D_2 from the embedding. In practical applications, the Grassberger-Procaccia algorithm [70] is used to measure the D_2 of reconstructions for different embedding dimensions. The minimum embedding dimension of the attractor is $m+1$, where m is the embedding dimension above which the measured value of the D_2 saturates.

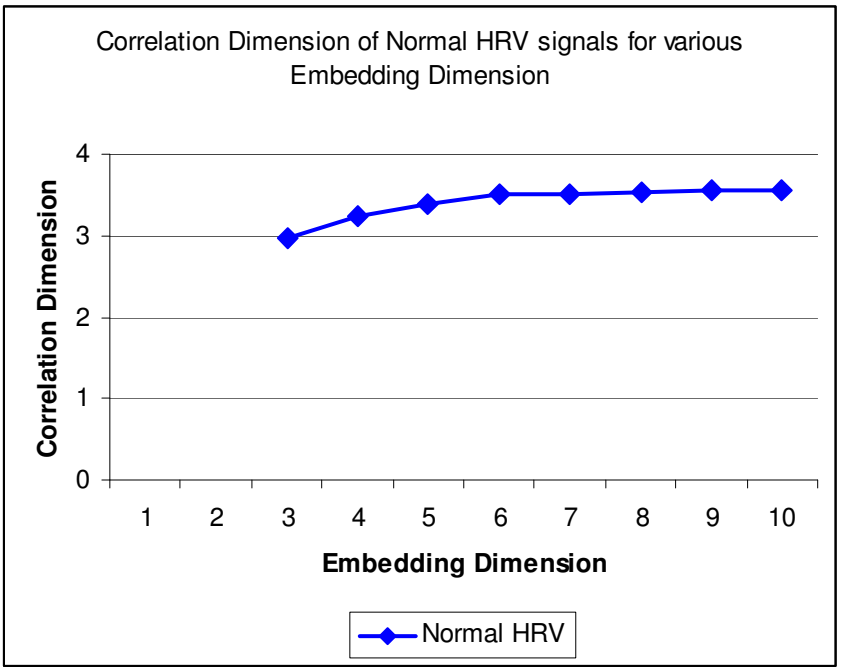

Figure 3.2 Variation of correlation dimension for different embedding dimension

Using the Grassberger-Procaccia algorithm (discussed in Section 3.6.1), D_2 of the HRV signals are estimated for different embedding dimensions. The optimum embedding dimension of the attractor is $m = m_{sat} + 1$, where m_{sat} is the embedding

dimension above which the measured value of D_2 saturates. The graph of D_2 vs. m for normal HRV signal is shown in Figure 3.2. It is observed that the D_2 saturates at $m_{sat} = 6$ and the optimum embedding dimension is chosen as $m = 7$ for the analysis of HRV signals.

3.3.2 Estimation of Embedding Delay Time

A one-to-one embedding can be obtained for any value of $\tau > 0$. However, both too small and too large values for τ will cause failures of the reconstruction.

- *Small time delay*: If τ is small, the values of $x(i)$ and $x(i+\tau)$ will be almost equal, since the system did not have time to change its state significantly. So there is little gain of information between them. Then each reconstructed vector consists of almost equal components *i.e* redundant information. Therefore the reconstructed attractor will be concentrated around the main diagonal of the reconstruction space forming a long and thin object in the state-space.

- *Large time delay*: If τ is large and the dynamical system is chaotic, the effect of sensitive dependence on the initial conditions will make the information about the state of the system at instant i almost irrelevant for the state at instant $i+\tau$. During the time interval $(i, i+\tau)$ the system has almost forgotten the state $x(i)$ and the deterministic correlation between

the states at both times could be detected by resolving very small scales in the reconstruction space for which high precision measurements are required.

The optimal time delay is determined by using the AMI function. The delay at which first minimum of the AMI function occurs is identified to be the optimum τ. Mutual information function for normal HRV signal is given Figure 3.3. It can be clearly seen that the mutual information reaches its first minimum at $\tau = 4$. Hence the optimal embedding delay τ is chosen as 4 for our analysis of HRV signals.

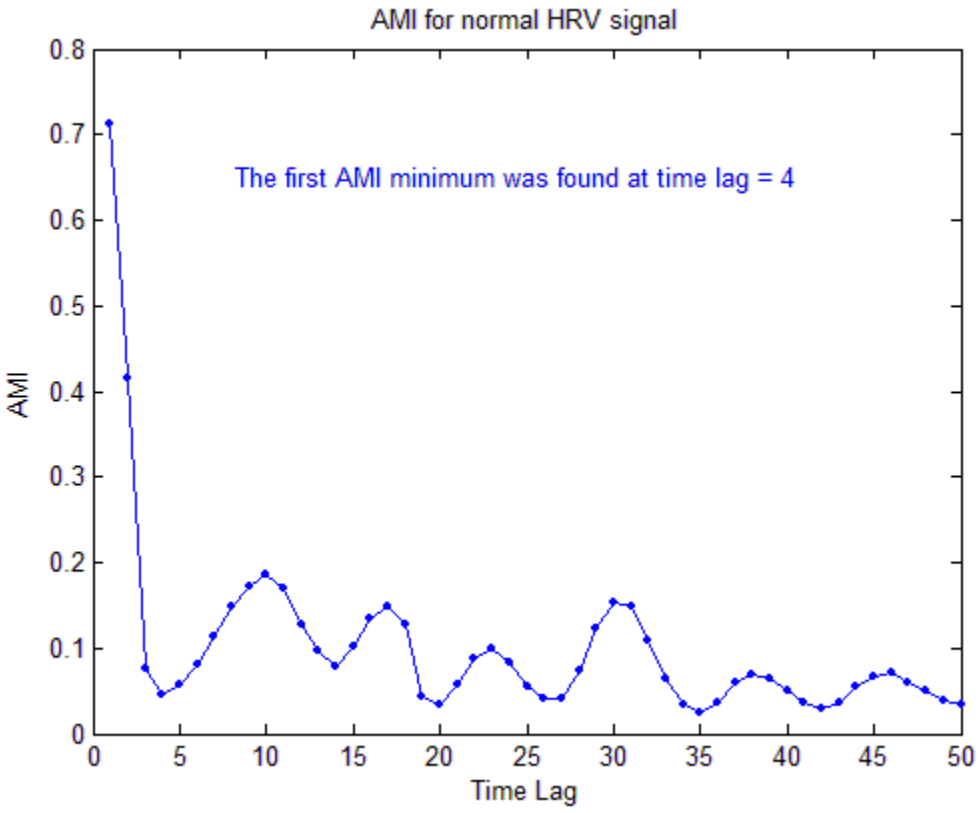

Figure 3.3 AMI of normal HRV signal

Figure 3.4 shows the 3-D plot of the reconstructed attractor of the HRV signals with a time delay of $\tau = 4$. As dimensions greater than three cannot be shown graphically, unfolding of the attractor in three dimensions is given. It can be seen from this Figure 3.4 that even in three dimensions, the attractor show clear differences in their structure between the eight classes of cardiac abnormalities. The plot of the attractors serve as a descriptive representation of the signal and still parametric representations of the reconstructed attractor are needed to quantify the signals. $x(n)$

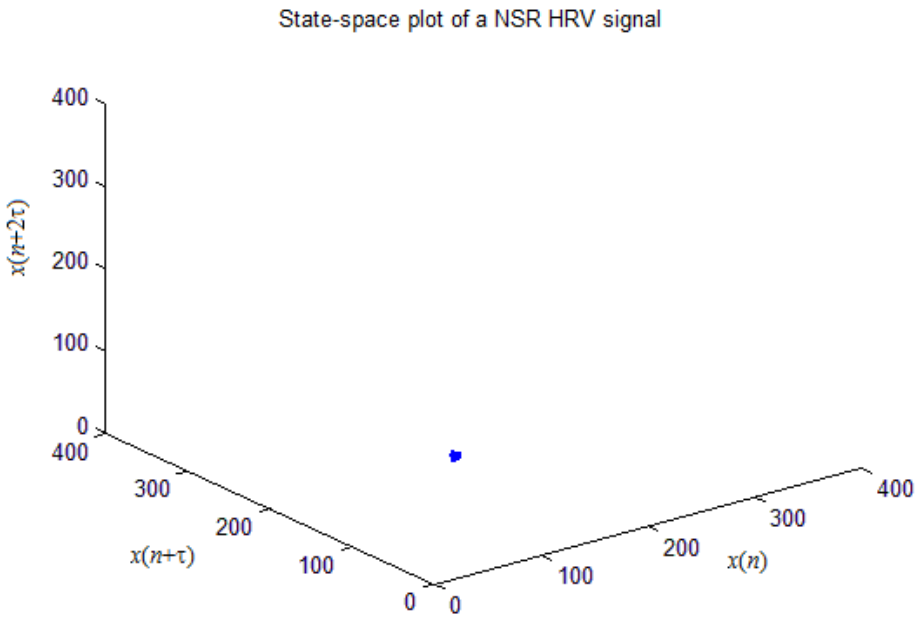

(a)

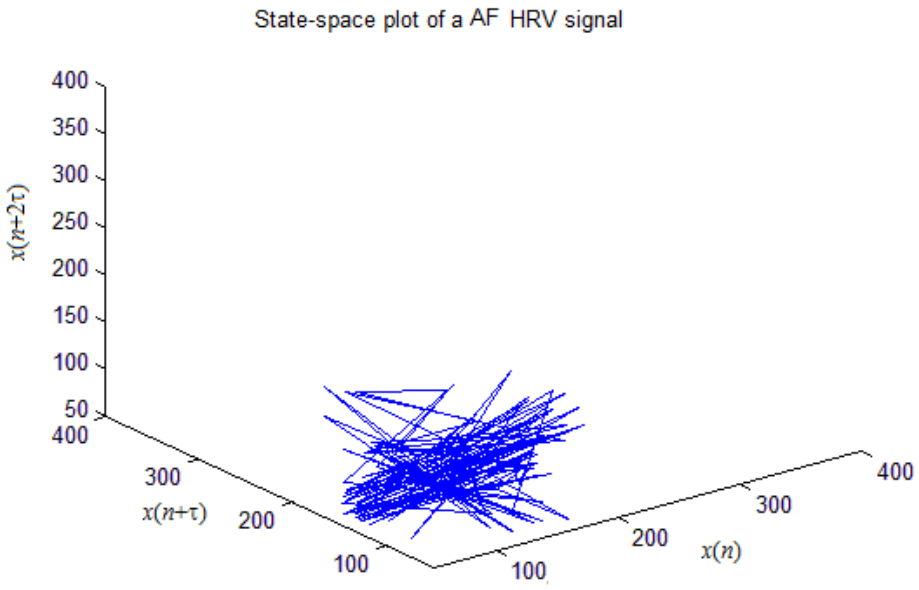
State-space plot of a AF HRV signal
400
350
300
250
200
150
100
50
x(n+2τ)
400
300
x(n+τ)
200
100
100
200
300
400
x(n)

(b)

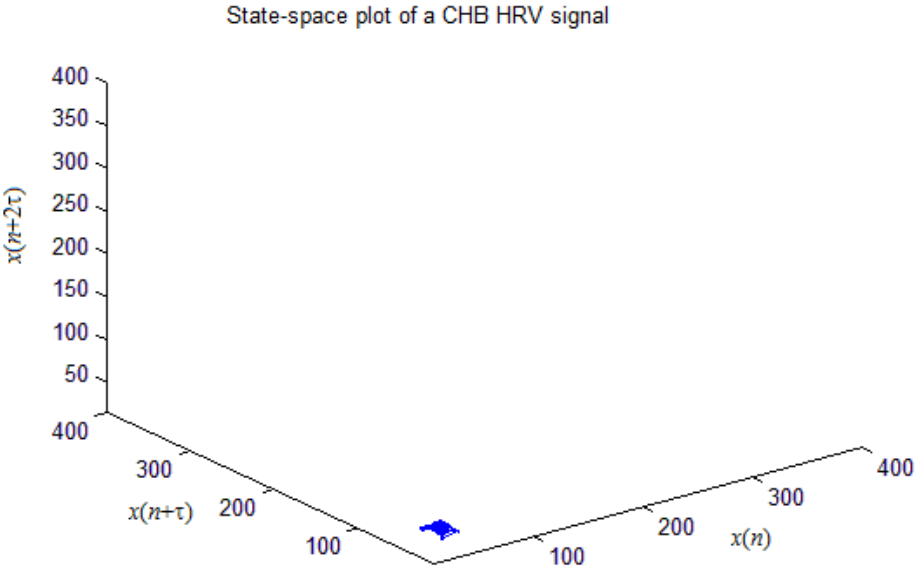
State-space plot of a CHB HRV signal
400
350
300
250
200
150
100
50
x(n+2τ)
400
300
x(n+τ)
200
100
100
200
300
400
x(n)

(c)

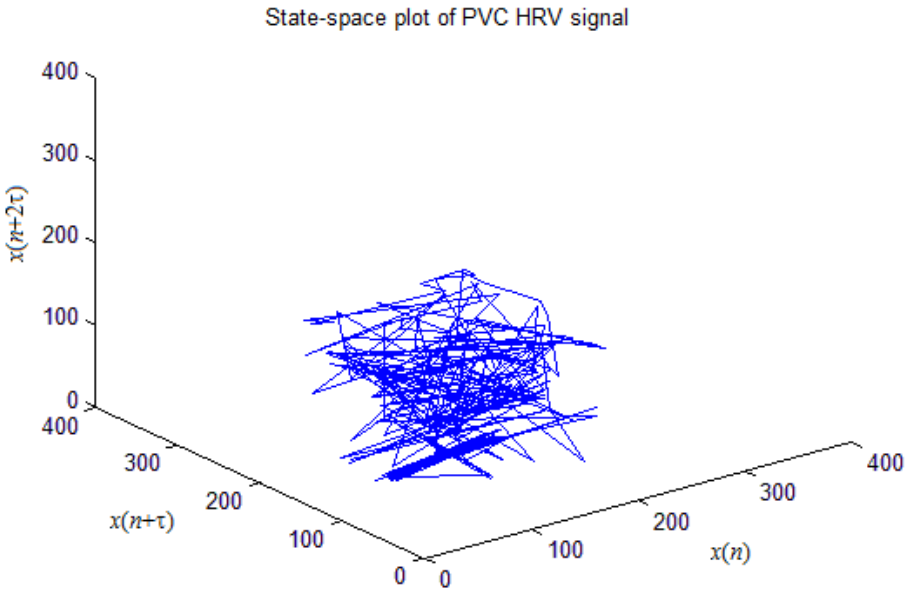
State-space plot of PVC HRV signal
400
300
200
100
0
x(n+2τ)
400
300
200
100
0
x(n+τ)
0
100
200
300
400
x(n)

(d)

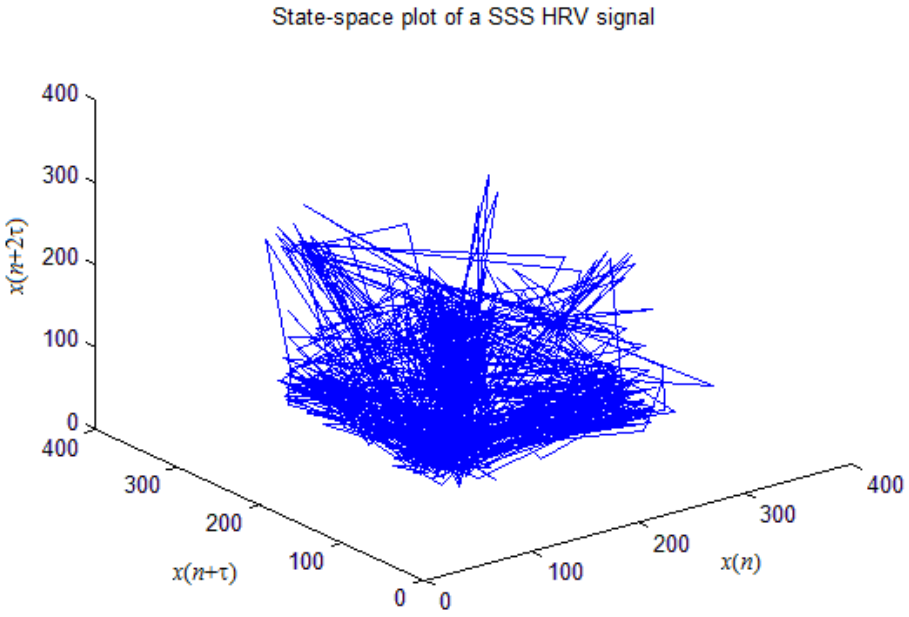
State-space plot of a SSS HRV signal
400
300
200
100
0
x(n+2τ)
400
300
200
100
0
x(n+τ)
0
100
200
300
400
x(n)

(e)

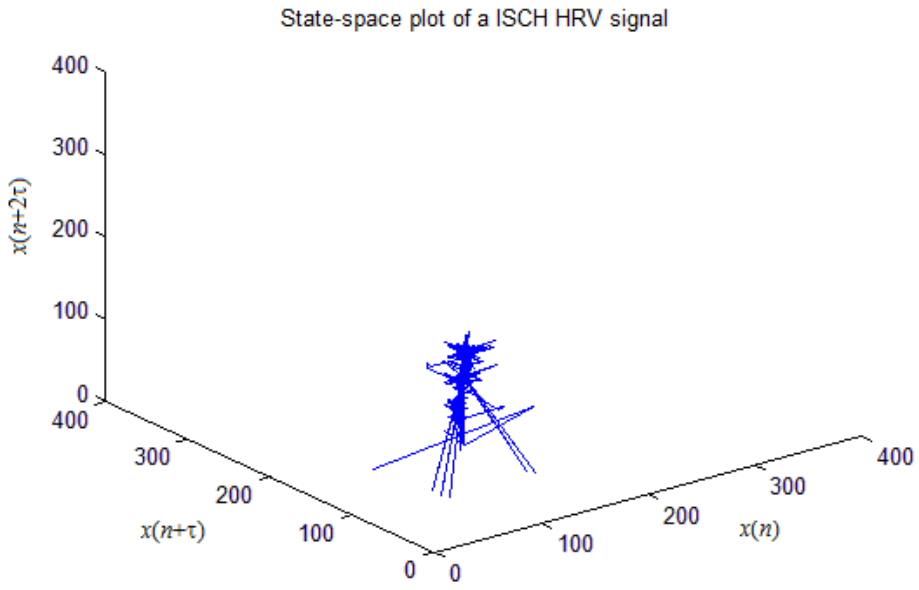
State-space plot of a ISCH HRV signal
400
300
200
100
0
x(n+2τ)
400
300
200
100
0
x(n+τ)
0
100
200
300
400
x(n)

(f)

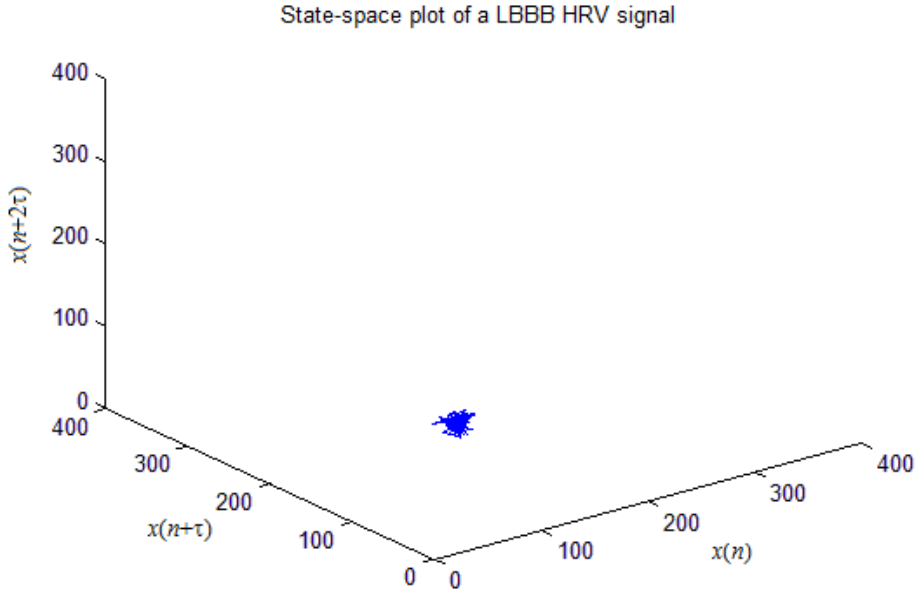
State-space plot of a LBBB HRV signal
400
300
200
100
0
x(n+2τ)
400
300
200
100
0
x(n+τ)
0
100
200
300
400
x(n)

(g)

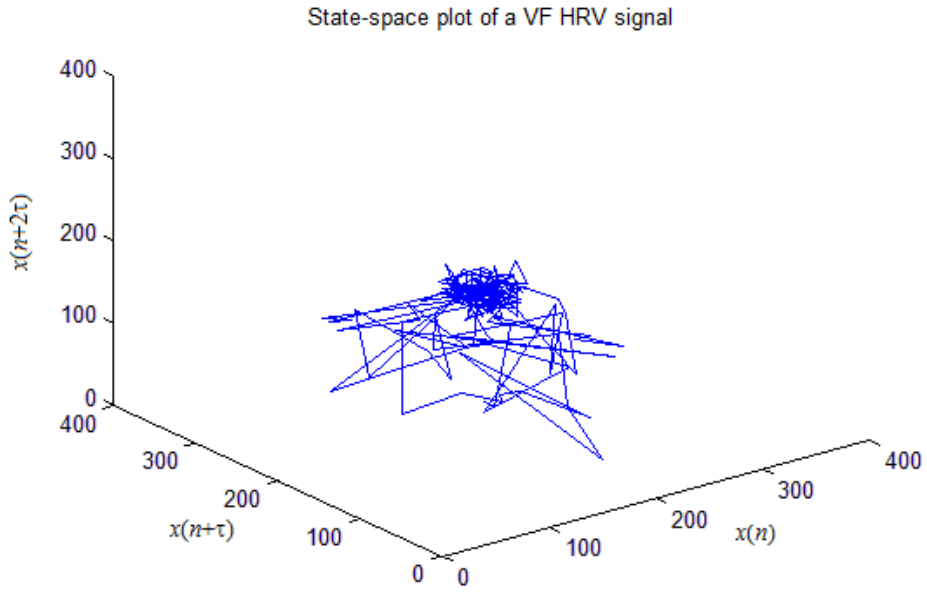

(h)

Figure 3.4 Phase-space plot of eight classes of HRV signals

3.4 Nonlinearity

One of the objectives of this work is to determine the nonlinear dynamics of the HRV and EEG signals. Before applying any nonlinear time series analysis algorithms on the data, it is necessary to test the presence of nonlinearity in the data under consideration. One of the efficient methods to test for nonlinearity in the data is the surrogate data test proposed by Theiler *et. al.* [71] in 1992.

3.4.1 Test for Nonlinearity

Surrogate signal is produced by phase randomizing the original data. It has similar spectral properties as of the given data. The surrogate data sequence has the same mean, the same variance, the same autocorrelation function and therefore the same power spectrum as the original sequence, but phase relations are destroyed. In the case of data shuffling, the histograms of the surrogate sequence and the reference sequence are identical. The random phase spectrum is generated by using any of the three methods described below.

1. *Random phase*: here the complex phase values of the Fourier transformed input signal are chosen randomly.

2. *Phase shuffle*: here the phase values of the original spectrum are used in random order.

3. *Data shuffle*: here the phase values of the original spectrum are used in random order and the sorted values of the surrogate sequence are substituted by the corresponding sorted values of the reference sequence additionally.

The measured topological properties of the experimental time series are then compared with that of the measured topological properties of the surrogate data sets. If both the experimental data and the surrogate data yield the same results then by the null hypothesis, the experimental data is set of random noise and the underlying process is linear.

Type	**NSR**	**PVC**	**LBBB**	**AF**	**VF**	**CHB**	**SSS**	**ISCH**
$APEN(Original)$	1.75	1.51	1.47	1.57	1.09	0.97	1.57	0.76
$APEN(Surrogate)$	0.78	0.67	0.61	0.73	0.45	0.43	0.73	0.26
% Difference	55.43%	55.63%	58.50%	53.50%	58.72%	55.67%	53.50%	65.79%
$D_2(Original)$	3.58	2.29	3.2	2.58	2.9	2.72	2.35	3.3
$D_2(Surrogate)$	1.34	1.11	1.28	1.08	1.12	1.12	1.06	1.11
% Difference	62.57%	51.53%	60.00%	58.14%	61.38%	58.82%	54.89%	66.36%

Table 3.2 Surrogate Data analysis for eight cardiac health states

In this work, the surrogates for the HRV signals are generated by the Fourier decomposition with the same amplitudes as the empirical data decomposition but with random phase components. 20 sets of surrogate data are generated for each of the eight classes. Approximate entropy (*APEN*) and D_2 are obtained for both the original and surrogate data sets and given in Table 3.2. It has been found that, the surrogate data *APEN* and original data *APEN*, are different from each other by more than 50%. Similar procedure is repeated for D_2 as well. The surrogate data D_2 and the original data D_2 are different from each other by more than of 50%. This rejects the null hypothesis and confirms that the original data is nonlinear.

3.5 Stationarity

A scientific measurement of any kind is only useful if it is reproducible. In the case of time series measurements, the dynamic properties of the data under consideration are relevant and valid only if the data is stationary. Stationarity requires that all parameters of the studied system relevant for its dynamics have to be fixed and constant during the measurement period. Recurrence plots (RPs) are used to reveal non-

stationarity of a series. It was first proposed by Eckmann *et. al.*[72] in order to study state-space orbits. RP is a graphical to represent the hidden drift and periodicities in the signal. It is an array of dots in an $N \times N$ square where a dot is placed at (i, j) whenever $\mathbf{x}_j$ is closer to $\mathbf{x}_i$ within a small radius r_i around $\mathbf{x}_i$. To obtain the recurrence plot from time series $\{x(n); n = 1,2,\ldots,N\}$, *m*-dimensional orbit of $\mathbf{x}_i$ is constructed by method of delays. Then r_i is chosen such that reasonable of $\mathbf{x}_j$ points are around $\mathbf{x}_i$ within the radius r_i. Finally, the recurrence plot is obtained by plotting a dot at each point (i, j) when $\mathbf{x}_j$ is within the ball of radius r_i centered at $\mathbf{x}_i$.

The RP is illustrated for periodic, stationary and non-stationary process [Figure 3.5]. The RPs are constructed with $m = 2, \tau = 5$ and $r = 0.15 \times$*standard deviation of the signal*. The 10Hz sinusoidal signal and its recurrence plot is given in Figure 3.5a and Figure 3.5b, respectively. The diagonal lines segments parallel to $i = j$ indicate the periodic nature of the signal. The exponentially damped sinusoidal signal and its RP is given in Figure 3.5c and Figure 3.5d, respectively. The fading pattern in the RP is due to the non-stationarity in the signal. The white Gaussian noise and its RP is given in Figure 3.5e and Figure 3.5f. The plot is uniform indicating stationary process without any periodicity.

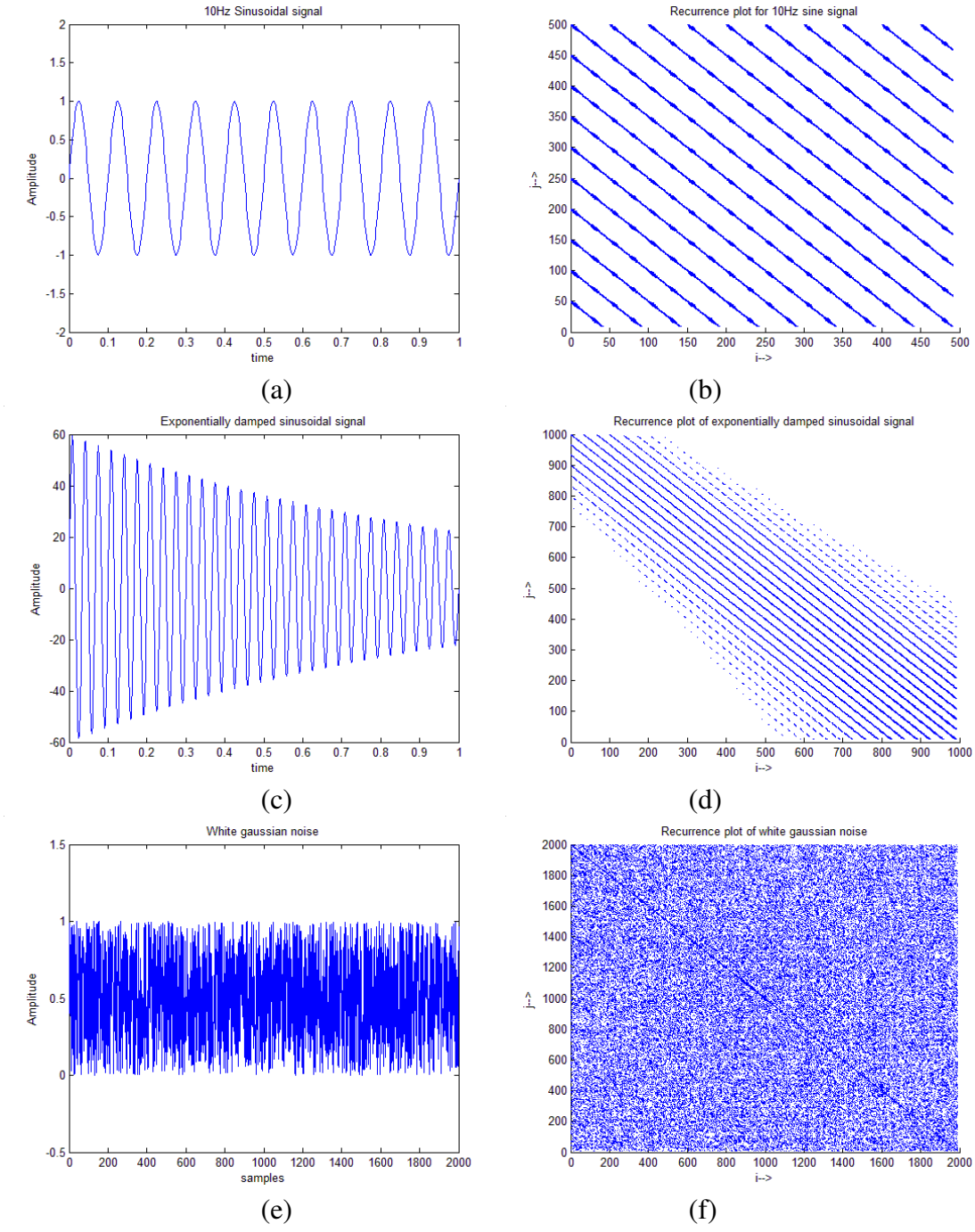

Figure 3.5 Illustration of Recurrence plots

For a stationary system, the RP is homogeneous along the diagonal. The RP of HRV signals of eight cardiac states are shown in Figure 3.6. The RP is constructed with $m = 2, \tau = 5$ and $r = 0.15 \times$ *standard deviation of the signal.* It can be seen that the plot is symmetric along the diagonal and the overall pattern is fairly uniform. The uniform distribution of the pattern indicates that the underlying process for the HRV signal is a stationary process.

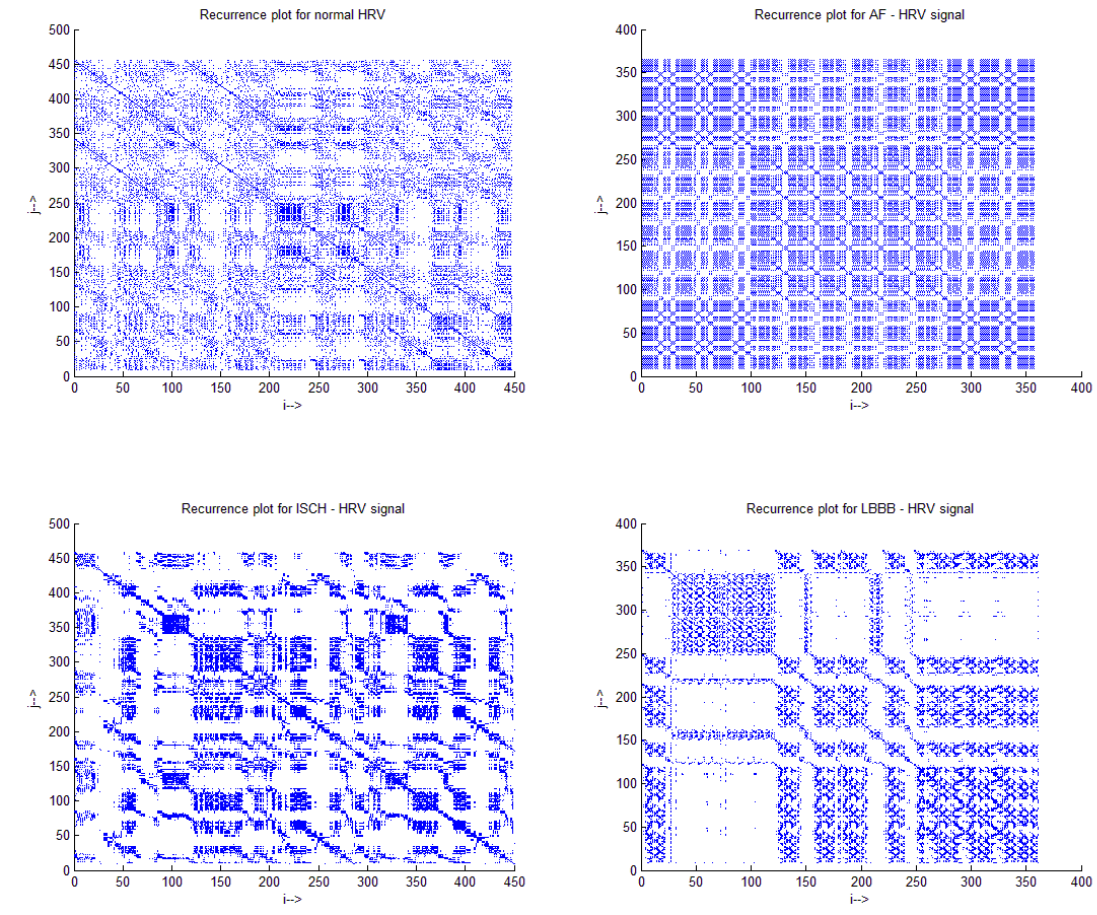

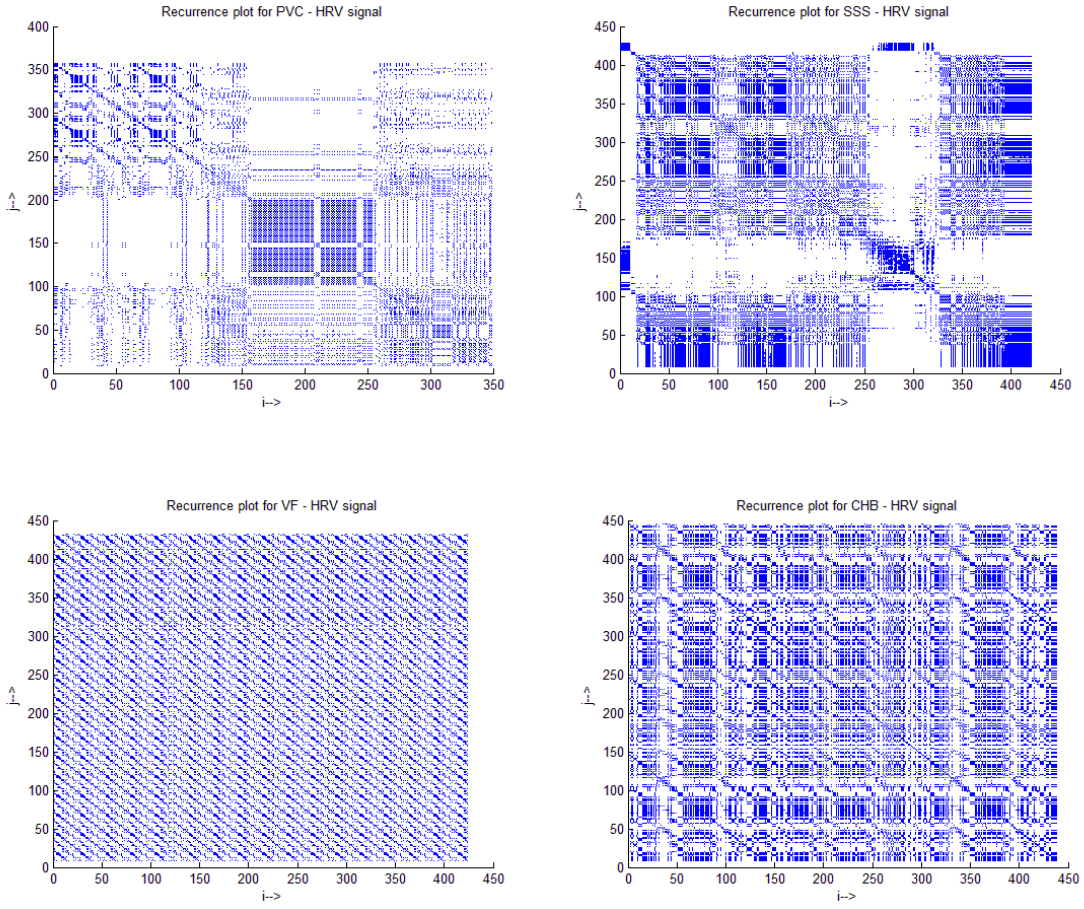

Figure 3.6 Recurrence plot of the HRV signals of eight cardiac states.

3.6 Chaotic Invariants Analysis

The dimension of a system can give much information about the nature of the system. The estimation of the dimension from the experimental data (time series) is therefore very useful to the understanding of the system, particularly if the system is periodic, chaotic, or noisy. There is a broad spectrum of dimensions used to characterize nonlinear systems. In particular, D_2 is discussed here in detail. Besides the spectrum of

generalized dimensions, there are other geometric quantities like the spectrum of Lyapunov exponents and entropies that are invariant under embedding. Lyapunov exponent and entropies characterize the dynamics of the deterministic systems.

3.6.1 Correlation Dimension

D_2 is one of the most widely used measures of FD. Here we adapt the algorithm proposed by Grassberger and Procaccia [70] to estimate D_2 values of the experimental time series. The idea is to construct a correlation function $C(r)$ that is the probability that two arbitrary points on the orbit are closer together than *r* in the state-space. Here *r* is the radial distance around each reference point $\mathbf{x}_i$ in the state-space. This is done by calculating the separation between every pair of *N* data points and sorting them into bins of width *dr* proportionate to *r*. The D_2 can be calculated using the distances between each pair of points $\mathbf{x}_i$ and $\mathbf{x}_j$ in the state-space ($s(i, j) = \left\| \mathbf{x}_i - \mathbf{x}_j \right\|, i, j = 1,2, \cdots, N$), in the set of *N* number of points.

A correlation function, *C(r)*, is then calculated using,

$$C(r) = \frac{2}{N(N-1)} \sum_{i=1}^{N} \sum_{\substack{j=1 \\ j \neq i}}^{N} \Theta\left(r - \left\| \mathbf{x}_i - \mathbf{x}_j \right\|\right), \tag{3.7}$$

where, Θ is the Heaviside function.

D_2 is calculated using the fundamental definition

$$D_2 = \lim_{r \to 0} \frac{\log C(r)}{\log(r)}. \tag{3.8}$$

The data points used in calculating the *C(r)* comes from a time series, which has too small or too large time resolution may introduce spurious effects. If the time resolution is too small, the data may contain multiple copies of essentially the same measurements, which leads to multiple-counting. The D_2 is then artificially low because all the points are temporally close to each other. This effect occurs when the time resolution of the analyzed data is much smaller than the τ (or any characteristic time scale).

The correction proposed by Theiler [73] is, for each reference point $\mathbf{x}_i$ to include measurements $\mathbf{x}_j$ which are at least τ steps away from $\mathbf{x}_i$

$$C'(r) = \frac{2}{N(N-1)} \sum_{i=1}^{N} \sum_{j=i+\tau}^{N} \Theta\left(r - \left\| \mathbf{x}_i - \mathbf{x}_j \right\|\right). \tag{3.9}$$

This correlation integral $C'(r)$ is used in equation (3.8) to calculate D_2.

3.6.2 Lyapunov Exponents

Lyapunov exponents (λ) is a quantitative measure of the sensitive dependence on the initial conditions. It defines the average rate of divergence or convergence of two neighboring trajectories in the state-space. An exponential divergence of initially nearby trajectories in state-space coupled with folding of trajectories, to ensure that the solutions

will remain finite, is the general mechanism for generating deterministic randomness and unpredictability. Therefore, the existence of a positive λ for almost all initial conditions in a bounded dynamical system is the widely used definition of deterministic chaos. To discriminate between chaotic dynamics and periodic signals, λs are often used. The trajectories of chaotic signals in state-space follow typical patterns. Closely spaced trajectories converge and diverge exponentially, relative to each other. A negative exponent implies that the orbits approach a common fixed point. A zero exponent means the orbits maintain their relative positions; they are on a stable attractor. Finally, a positive exponent implies the orbits are on a chaotic attractor.

The algorithm proposed by Wolf *et. al.* [74] is used to determine the largest Lyapunov exponent (λ_1) in this study. For two nearby points in a state-space $\mathbf{x}_i$ and $\mathbf{x}_i + \Delta\mathbf{x}$, that are function of time and each of which will generate an orbit of its own in the state, the separation between the two orbits $\Delta\mathbf{x}$ will also be a function of time. This separation is also a function of the location of the initial value and has the form $\Delta\mathbf{x}(\mathbf{x}_i, K)$, where K is the value of time steps forward in the trajectory. For chaotic data set, the mean exponential rate of divergence of two initially close orbits is characterized by,

$$\lambda = \lim_{K \to \infty} \frac{1}{K} \ln \frac{\left|\Delta\mathbf{x}(\mathbf{x}_i, K)\right|}{\left|\Delta\mathbf{x}\right|}. \tag{3.10}$$

The maximum positive λ is chosen to be λ_1.

3.6.3 Hurst Exponent

The Hurst exponent (*H*) is a measure that has been widely used to evaluate the self-similarity and correlation properties of fractional Brownian noise, the time series produced by a fractional (fractal) Gaussian process. *H* is used to evaluate the presence or absence of long-range dependence and its degree in a time series. However, local trends (nonstationarities) are often present in physiological data and may compromise the ability of some methods to measure self-similarity. *H* is the measure of the smoothness of a fractal time series based on the asymptotic behavior of the rescaled range of the process. The *H* is defined as [75],

$$H = \frac{\log\left(\frac{R}{S}\right)}{\log(N)}, \tag{3.11}$$

where *N* is the duration of the sample of data and *R/S* the corresponding value of rescaled range. The rescaled range *R/S* is the ratio of the range of values in the time series to the standard deviation of the values of the considered time series. The above expression is obtained from the Hurst's generalized equation of time series that is also valid for Brownian motion. If H=0.5, the behavior of the time-series is similar to a random walk. If H<0.5, the time-series cover less "distance" than a random walk. But if H>0.5, the time-series covers more "distance" than a random walk. *H* is related to the dimension D_2 by,

$$H = d + 1 - D_2 . \tag{3.12}$$

Here, *d* is the Euclidean dimension.

3.6.4 Poincare Geometry

HRV analysis provides a noninvasive measure to asses the autonomic status of the heart. Under abnormal heart conditions, there will be perturbations to this autonomic activity, which is reflected as fluctuations in the heart rate. These fluctuations can be characterized using Poincare plots.

The Poincare plot, a technique taken from nonlinear dynamics, portrays the nature of R-R interval fluctuations. It is a graph in which each R-R interval is plotted as a function of the previous R-R interval. Poincare plot analysis is an emerging quantitative-visual technique whereby the shape of the plot is categorized into functional classes that indicate the degree of the heart failure in a subject [76]. The plot provides summary information as well as detailed beat-to-beat information on the behavior of the heart [77].

The geometry of the Poincare plot provides information on the beat-to-beat variation of the HRV signal. A common way to describe the geometry is to fit an ellipse to the graph. The ellipse is fitted onto the so called line-of-identity at 45^0 to the normal axis. The standard deviation of the points perpendicular to the line-of-identity denoted by SD1 describes short-term variability which is mainly caused by respiratory sinus arrhythmia (RSA). The standard deviation along the line-of-identity denoted by SD2 describes long-term variability.

Statistically, the plot displays the correlation between consecutive intervals in a graphical manner. Nonlinear dynamics considers the Poincare plot as the two dimensional (2-D) reconstructed R-R interval state-space, which is a projection of the reconstructed attractor describing the dynamics of the cardiac system. The R-R interval Poincare plot typically appears as an elongated cloud of points oriented along the line-of-identity. The dispersion of points perpendicular to the line-of-identity reflects the level of short term variability. The dispersion of points along the line-of-identity is thought to indicate the level of long-term variability.

The Poincare plot may be analyzed quantitatively by calculating the standard deviations of the distances of the points *x(i)* in the time series to the lines $y = x$ and $y = x + 2\bar{x}$, where $\bar{x}$ is the mean of all *x(i)* [77]. The standard deviations are referred to as *SD1* and *SD2*, respectively. *SD1* related to the fast beat-to-beat variability in the data, while *SD2* describes the longer-term variability of *x(i)*. The ratio *SD1*/*SD2* may also be computed to describe the relation between these components. The Poincare plots of the eight classes of HRV signals are given in Figure 3.7. From the results it can be seen that the pattern of the Poincare plots, the position of the ellipse and the ranges of *SD1* and *SD2* values are distinct for each type of cardiac abnormality. For NSR HRV signal, the R-R interval dispersion is more as the rhythm is more periodic. More ball shaped plot is seen for PVC and CHB characterizing the symmetrical R-R interval clusters around the centre of the plot. The narrow plot for ISCH indicates very low dispersion of R-R

intervals. These plots are quantatively described using the ratio *SD1/SD2* and the results are given in Table 3.3.

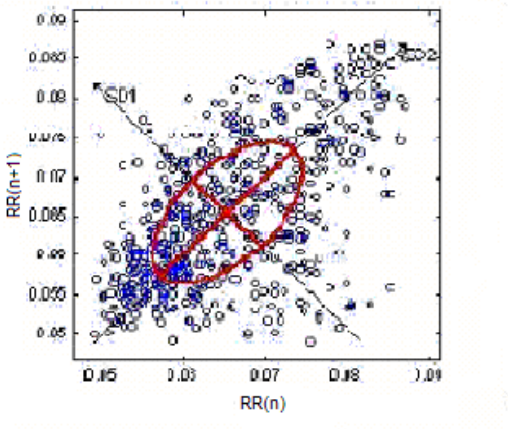

(a) Poincare plot for Normal

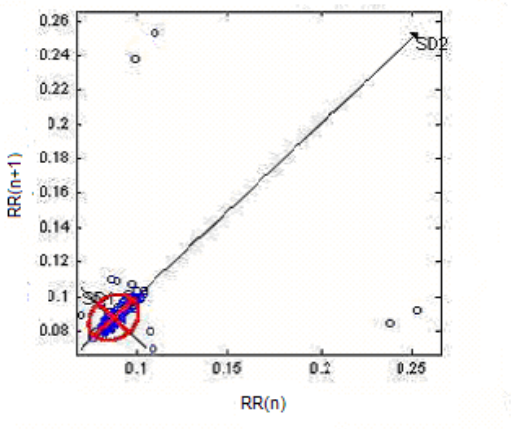

(b) Poincare plot for PVC

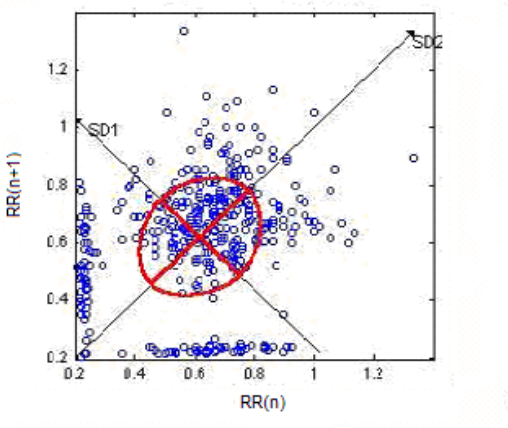

(c) Poincare plot for AF

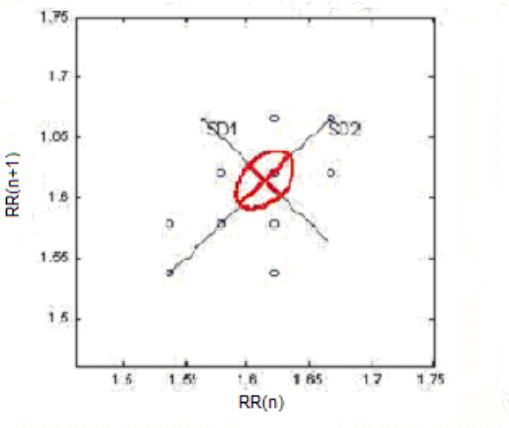

(d) Poincare plot for CHB

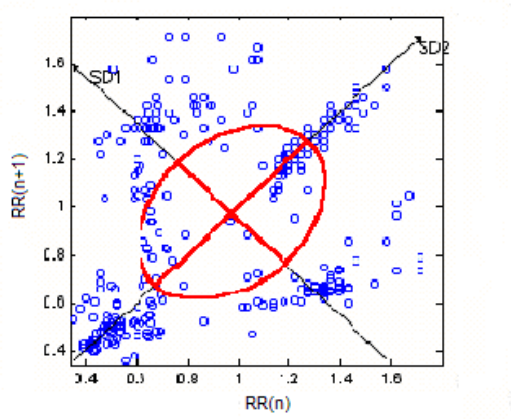

(e) Poincare plot for SSS

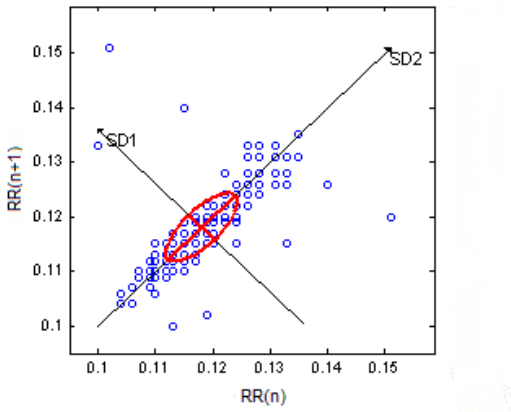

(f) Poincare plot for ISCH

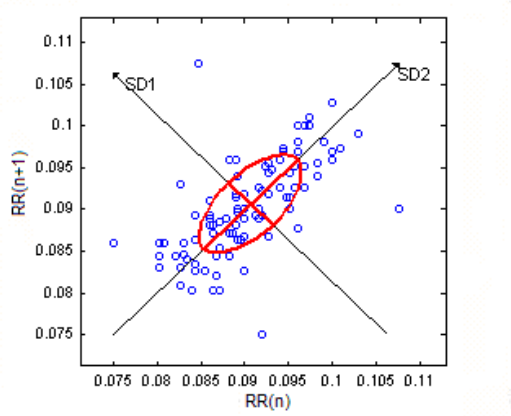

(g) Poincare plot for LBBB

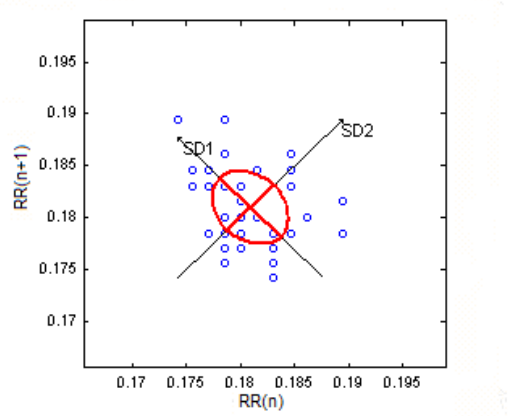

(h) Poincare plot for VF

Figure 3.7 Poincare plot for the 8 classes of HRV signals

3.6.5 Detrended Fluctuation Analysis

The concept of a fractal is most associated with geometrical objects satisfying two criteria: self-similarity and fractal dimensionality. Self-similarity means that an object is composed of sub-units and sub-sub-units on multiple levels that statistically resemble the structure of the whole object. The second criteria for fractal object is that it has a FD, also

called fractal, that can be defined to be any curve or surface that is independent of scale. This concept of fractal structure can be extended to the analysis of heart rate signals.

The detrended fluctuation analysis (DFA) is used to quantify the fractal scaling properties of short interval R-R signals. This technique is a modification of root-mean-square analysis of random walks applied to non-stationary signals [78]. The root-mean-square fluctuation of an integrated and detrended time series is measured at different observation windows and plotted against the size of the observation window on a log-log scale.

First, the R-R time series (of total length *N*) is integrated using the equation,

$$y_k = \sum_{i=1}^{N} [RR_k(i) - RRav_k], \quad k = 1,2,\cdots,L] \tag{3.13}$$

where y_k is the k^{th} value of the integrated series, L is the number of the datasets, $RR_k(i)$ is the i^{th} inter beat interval, and the $RRav_k$ is the average inter beat interval over the entire series.

Then, the integrated time series is divided into windows of equal length, *n*. In each window of length *n*, a least-squares line is fitted to the R-R interval data (representing the trend in that window). The *y* coordinate of the straight line segments are denoted by $y_k(n)$. Next, we detrend the integrated time series, $y_k(n)$, in each window. The root-mean-square fluctuation of this integrated and detrended series is calculated using the equation:

$$F(n) = \sqrt{\frac{1}{N}\sum_{k=1}^{N}[y_k - y_k(n)]^2} \ . \qquad (3.14)$$

This computation is repeated over all time scales (window sizes) to obtain the relationship between *F(n)* and the window size *n* (i.e., the number of beats in a window that is the size of the window of observation). Typically, *F(n)* will increase with window size. The fluctuation in small windows are characterized by a scaling exponent (self-similarity factor), α, representing the slope of the line relating *log F(n)* to *log n*. In this method, a fractal like signal results in a scaling exponent value of 1 (α=1). White Gaussian noise (totally random signal) results in a value of 0.5, and a Brownian noise signal with spectrum rapidly decreasing in power in the higher frequencies results in an exponent value of 1.5 [78].

The value of α can be viewed as an indicator of the "roughness" of the original time series: the larger the value of the α, the smoother the time series is. A good linear fit of the $log_{10}F(n)$ to $log_{10}n$ plot indicates *F(n)* is proportional to n^{α} where α is the single exponent describing the correlation properties of the entire range of heart rate signal. In most cases, the linear fit for the entire range data is not feasible. So it was suggested to use two different slopes to fit the data – with one above the breakpoint and one below the breakpoint. This results in one short range scaling exponent α_s and a long range exponent α_l as shown in Figure 3.8 for a normal heart rate signal.

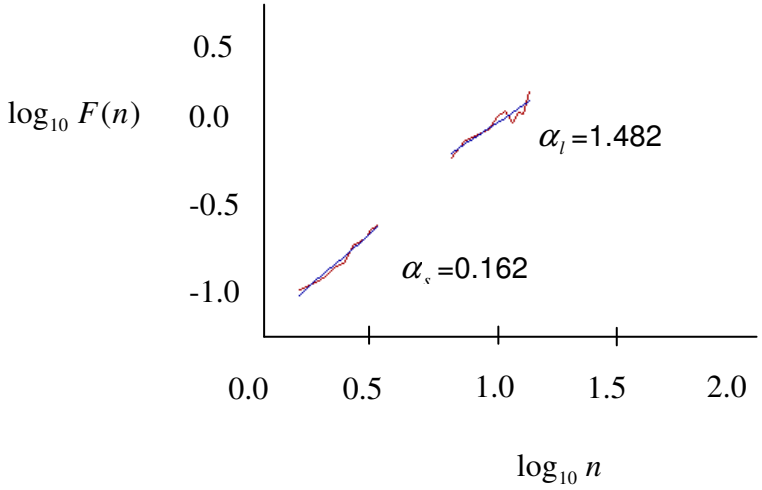

Figure 3.8 $F(n)$ plotted against several box sizes, n, on a log-log scale

3.7 Entropy Analysis

Entropy is a thermodynamic quantity describing the amount of disorder in the system. From an information theoretic perspective, the above concept of entropy is generalized as the amount of information stored in a more general probability distribution. First, Shannon applied the concept of information or logical entropy to the science of information theory and data communications. Recently a number of different entropy estimators [79] have been applied to quantify the complexity of the signal. Entropy estimators are broadly classified into two categories: (i) spectral entropies and (ii) embedding entropies. The spectral entropies use the amplitude components of the power spectrum of the signal as the probabilities in entropy calculations. In this topic the spectral entropies – Shannon entropy and Renyi's entropy are discussed. The embedding

entropies use the time series directly to estimate the entropy. Kolmogorov-Sinai entropy and the approximate entropy are the embedding entropies discussed here.

3.7.1 Spectral Entropy

Spectral entropy (*SEN*) [80] is the normalized form of Shannon's entropy. It quantifies the spectral complexity of the time series. A variety of spectral transformations exist. Of these the FT is most probably the well-known transformation method from which the power spectral density (PSD) can be obtained. Thus normalization of PSD with respect to the total spectral power will yield a probability density function (pdf). Application of Shannon's channel entropy gives an estimate of the spectral entropy of the process where entropy is given by

$$SEN = \sum_{f} p_f \log\left(\frac{1}{p_f}\right), \tag{3.15}$$

where p_f is the pdf value at frequency *f*. Heuristically, the entropy has been interpreted as a measure of uncertainty about the event at *f*. Thus, entropy *SEN* may be used as a measure of system complexity. It measures the spread of data. Data with broad, flat probability distribution have high entropy where as data with narrow, peaked distribution will have low entropy. *SEN* is also a special case of a series of entropies termed Renyi entropies.

3.7.2 Renyi's Entropy

Renyi's entropy [81] is generalization of Shannon spectral entropy to quantify the diversity, uncertainity and randomness of the system. The Renyi's entropy of order β is defined as,

$$REN = -\frac{\beta}{1-\beta}\sum \log p_f^{\beta} \qquad (\beta \neq 1). \tag{3.16}$$

where p_f is the pdf value at frequency *f*. In this work, we have used the value of $\beta = 2$ and determined the *REN* for biosignals. *REN* differs from *SEN* in that the sum is weighted towards frequencies in the lower frequency band (1-20 Hz). In the higher frequency band (20-45 Hz), the *SEN* and *REN* are similar. This is particularly helpful in the analysis of EEG.

3.7.3 Kalmogorov Sinai Entropy

Entropy is determined from the embedded time series data by finding points on the trajectory that are close together in state-space but which occurred at different times (i.e., are not time correlated). These two points are then followed into the future to observe how rapidly they move apart from one another. The time it takes for point pairs to move apart is related to the so-called Kolmogorov entropy [10], *KSEN*, by $\langle t_{div} \rangle = 2^{-(KSEN)t}$ where $\langle t_{div} \rangle$ is the average time for the pair to diverge apart and *KSEN* is expressed in bits per second. Entropy reflects how well one can predict the behavior of

each respective part of the trajectory from the other. Higher entropy indicates less predictability and a closer approach to stochastic nature.

3.7.4 Approximate Entropy

KSEN entropy measure diverges to a value of infinity when the signal is contaminated by the slightest noise. Pincus [82] proposed Approximate Entropy (*APEN*) as a solution to these problems and successfully applied it to relatively short and noisy data. The *APEN* was used by Bruhn [83] to analyze EEG signals in patients under general anesthesia. In the calculation of *APEN* , two parameters *m* and *r* must be chosen prior to the computation of *APEN* . The *APEN* measure is obtained by

$$APEN(m, r, N) = \frac{1}{N-m}\sum_{i=1}^{N-m}\log C_i^{m+1}(r) - \frac{1}{N-m+1}\sum_{i=1}^{N-m+1}\log C_i^{m}(r), \tag{3.17}$$

where $C_i^m(r)$ is the correlation integral with embedding dimension *m* and time lag of 1.

For this study, *m* is set to 2 and *r* is set to 15% of the standard deviation of each time series. These values are selected on the basis of previous studies indicating good statistical validity for *APEN* within these variable ranges [84].

3.8 Feature Extraction Results and Discussion

Methods derived from the field of nonlinear dynamics and chaos has resulted in the investigation of cardiovascular systems and has been utilized with the main purposes of classifying and detecting different signals. A complex system such as a cardiovascular system cannot be linear by nature, and by considering it as a nonlinear system, better understanding of the system dynamics can be achieved. Since a linear method fails to extract the nonlinear properties of heart dynamics [28, 29, 36], we prefer to use nonlinear methods rather than linear methods. For example, if the time series is stationary, we can apply standard spectral analysis techniques and calculate the power spectrum. But heart rate time series are not really stationary, because the signal generated by a fractal process is nonstationary. Heart rate dynamics even under normal conditions displays nonequilibrium fluctuations that cannot be detected or analyzed with traditional methods.

In this study, real experimental data were used to extract nonlinear properties of HRV time series. The chaotic features were discussed and compared in seven groups of patients with AF, PVC, LBBB, ISCH, SSS, CHB and VF and healthy subjects. The results are summarized in Table 3.3 and the corresponding distribution is shown using box plots in Figure 3.9.

Results show the non-integer D_2 values and the positive sign of λ_1 for all types of HRV time series. In the analysis of the ECG data, different chaotic measures such as

D_2 and λ_1 have been used in recent studies. It is known that the D_2 of the same person is different for different lead ECG signals [37], and also it depends on selecting the time delay and embedding dimension as discussed in Section 3.3.

Results show that D_2 is significantly different among the groups, and a normal signal has the highest value for D_2. These results show that the D_2 values increase from PVC, AF, and VF to Normal (2.29 to 2.58, to 2.90, and to 3.58). In the case of CHB, the estimated value of D_2 is 2.72 ±0.139. The range is low, indicating low variation in the heart rate data. In ISCH, the variation between the consecutive heart rates is low (D_2 = 3.3 ±0.142). For SSS, the D_2 is low (D_2 = 2.35 ±0.44) indicating the inherent periodicity, for AF has too much variation (D_2 =2.58 ±0.033). During PVC, the variation is high (D_2 = 2.29±0.099), finally, for the normal subjects the variation in their heart rates (D_2 =3.58±0.23) is high. In the case of LBBB (D_2 =3.2±0.41) and VF (D_2 =2.9±0.039). For the normal subjects, ectopic and AF, the D_2 is high and as the abnormality becomes more severe (CHB, SSS, ISCH) the D_2 will fall from the normal case. The reverse trend is observed with *H*. This is in agreement with the definition of *H*, when D_2 decreases *H* will increase. The results, obtained from clinical data, confirm the previous studies [20, 85]. From the median point of view, physiological function and control of the entire body is maintained by both the sympathetic and parasympathetic sections, which act in opposite directions. Thus, the observed heart rate variability is an indicator of the dynamic interaction and balance between these two branches of the

system. When the correlation dimension of HRV is decreased, the heart cannot react to unexpected changes [86].

TYPE	**NSR**	**PVC**	**LBBB**	**AF**	**VF**	**CHB**	**SSS**	**ISCHEMIC**	**p value**
α -slope	0.77 ± 0.076	0.27 ± 0.014	0.43 ± 0.11	0.13 ± 0.043	0.34 ± 0.022	0.54 ± 0.034	0.55 ± 0.013	0.97 ± 0.11	0.076
SD1/SD2	0.80 ± 0.16	1.42 ± 0.54	0.7 ± 0.20	2.98 ± 1.56	1.13 ± 0.47	0.64 ± 0.024	0.96 ± 0.32	0.59 ± 0.37	0.011
D_2	3.58 ± 0.23	2.29 ± 0.099	3.20 ± 0.415	2.58 ± 0.033	2.90 ± 0.039	2.72 ± 0.139	2.35 ± 0.448	3.30 ± 0.142	0.032
λ_1	0.50 ± 0.058	0.62 ± 0.003	0.47 ± 0.044	0.56 ± 0.112	0.42 ± 0..036	0.17 ± 0.011	0.82 ± 0.102	0.193 ± 0.066	0.056
H	0.611 ± 0.019	0.873 ± 0.032	0.643 ± 0.011	0.796 ± 0.043	0.706 ± 0.021	0.748 ± 0.011	0.821 ± 0.023	0.654 ± 0.021	0.081
SEN	1.63 ± 0.025	1.14 ± 0.057	1.24 ± 0.047	1.20 ± 0.037	1.06 ± 0.003	0.86 ± 0.054	1.27 ± 0.135	1.12 ± 0.11	0.064
REN	3.481 ± 0.221	2.46 ± 0.065	2.72 ± 0.237	2.63 ± 0.112	2.32 ± 0.713	2.19 ± 0.081	2.76 ± 0.089	2.42 ± 0.116	0.067
APEN	1.75 ± 0.077	1.51 ± 0.091	1.47 ± 0.137	1.57 ± 0.23	1.09 ± 0.173	0.97 ± 0.15	1.57 ± 0.097	0.76 ± 0.065	0.065
KSEN	0.573 ± 0.023	0.496 ± 0.002	0.429 ± 0.010	0.445 ± 0.022	0.409 ± 0.156	0.457 ± 0.052	0.278 ± 0.061	0.34 ± 0.115	0.061
$D^{Higuchi}$	1.36 ± 0.043	1.19 ± 0.043	1.31 ± 0.032	1.21 ± 0.036	1.27 ± 0.039	1.24 ± 0.042	1.21 ± 0.021	1.32 ± 0.024	0.072
D^{Katz}	1.58 ± 0.016	1.31 ± 0.019	1.53 ± 0.021	1.39 ± 0.023	1.46 ± 0.021	1.41 ± 0.033	1.36 ± 0.011	1.52 ± 0.017	0.046

Table 3.3 Results of HRV analysis.

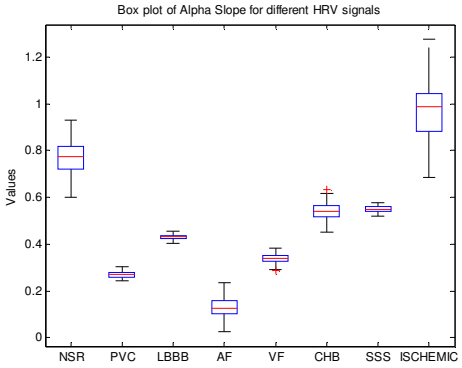
Box plot of Alpha Slope for different HRV signals
Values
NSR
PVC
LBBB
AF
VF
CHB
SSS
ISCHEMIC

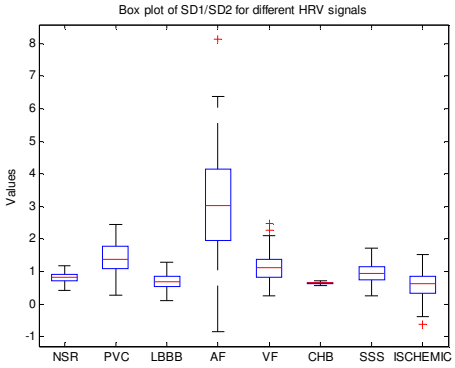
Box plot of SD1/SD2 for different HRV signals
Values
NSR
PVC
LBBB
AF
VF
CHB
SSS
ISCHEMIC

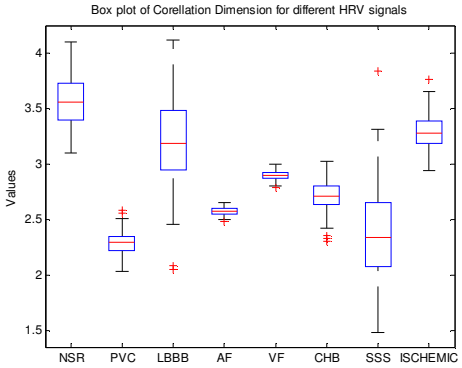
Box plot of Corellation Dimension for different HRV signals
Values
NSR
PVC
LBBB
AF
VF
CHB
SSS
ISCHEMIC

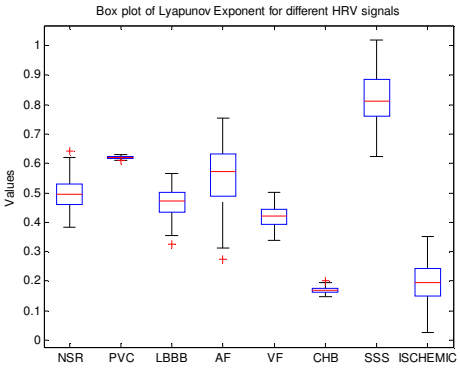
Box plot of Lyapunov Exponent for different HRV signals
Values
NSR
PVC
LBBB
AF
VF
CHB
SSS
ISCHEMIC

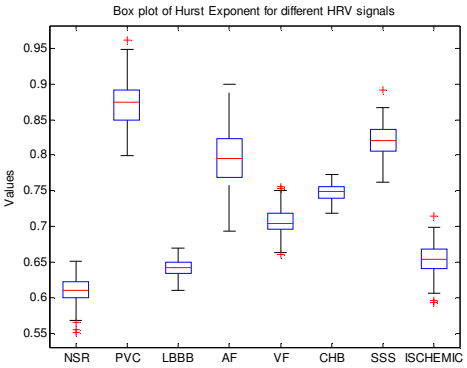
Box plot of Hurst Exponent for different HRV signals
Values
NSR
PVC
LBBB
AF
VF
CHB
SSS
ISCHEMIC

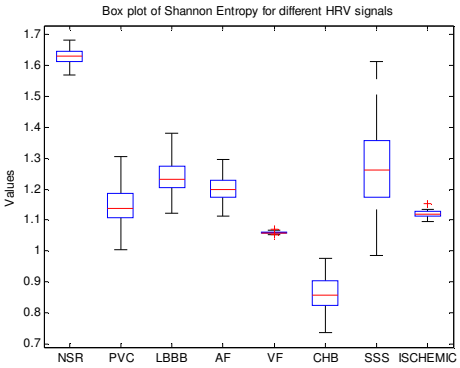
Box plot of Shannon Entropy for different HRV signals
Values
NSR
PVC
LBBB
AF
VF
CHB
SSS
ISCHEMIC

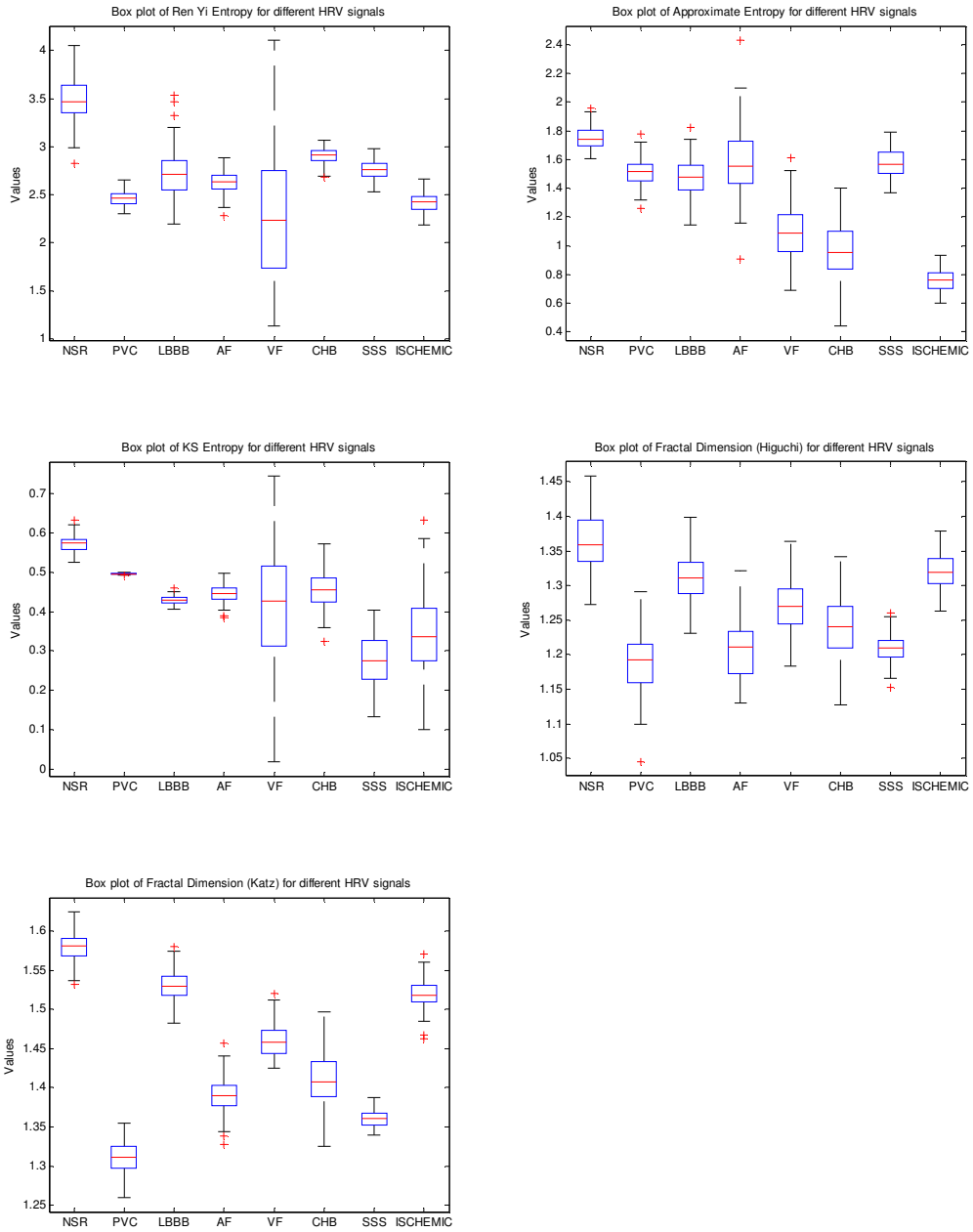

Figure 3.9 Variation of the chaotic measures of the HRV signals.

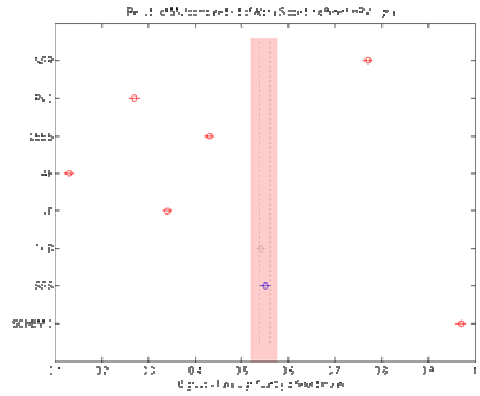

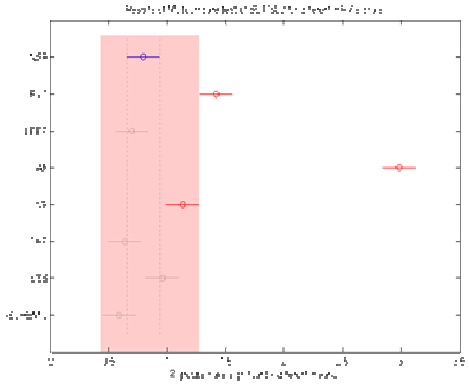

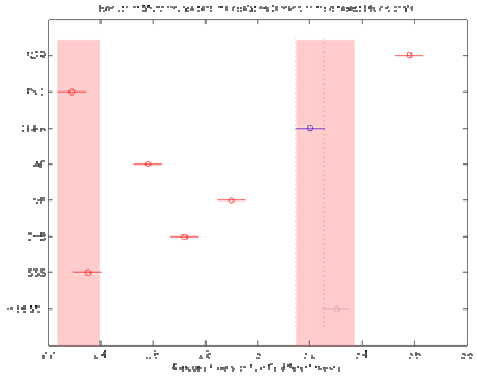

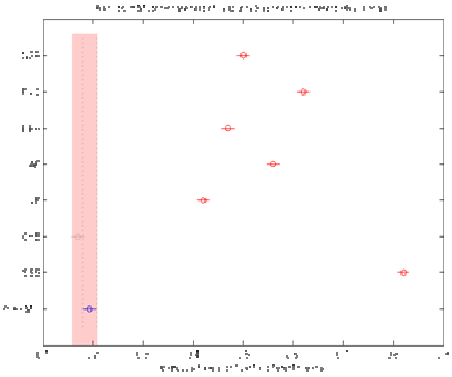

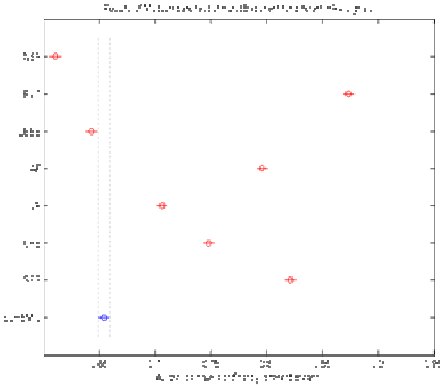

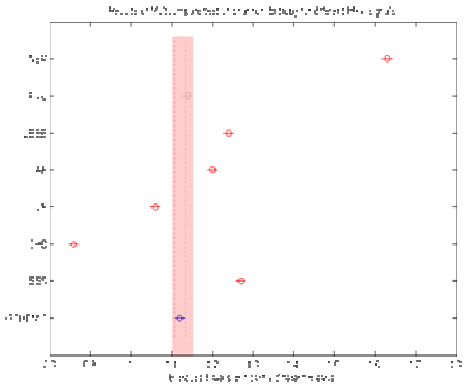

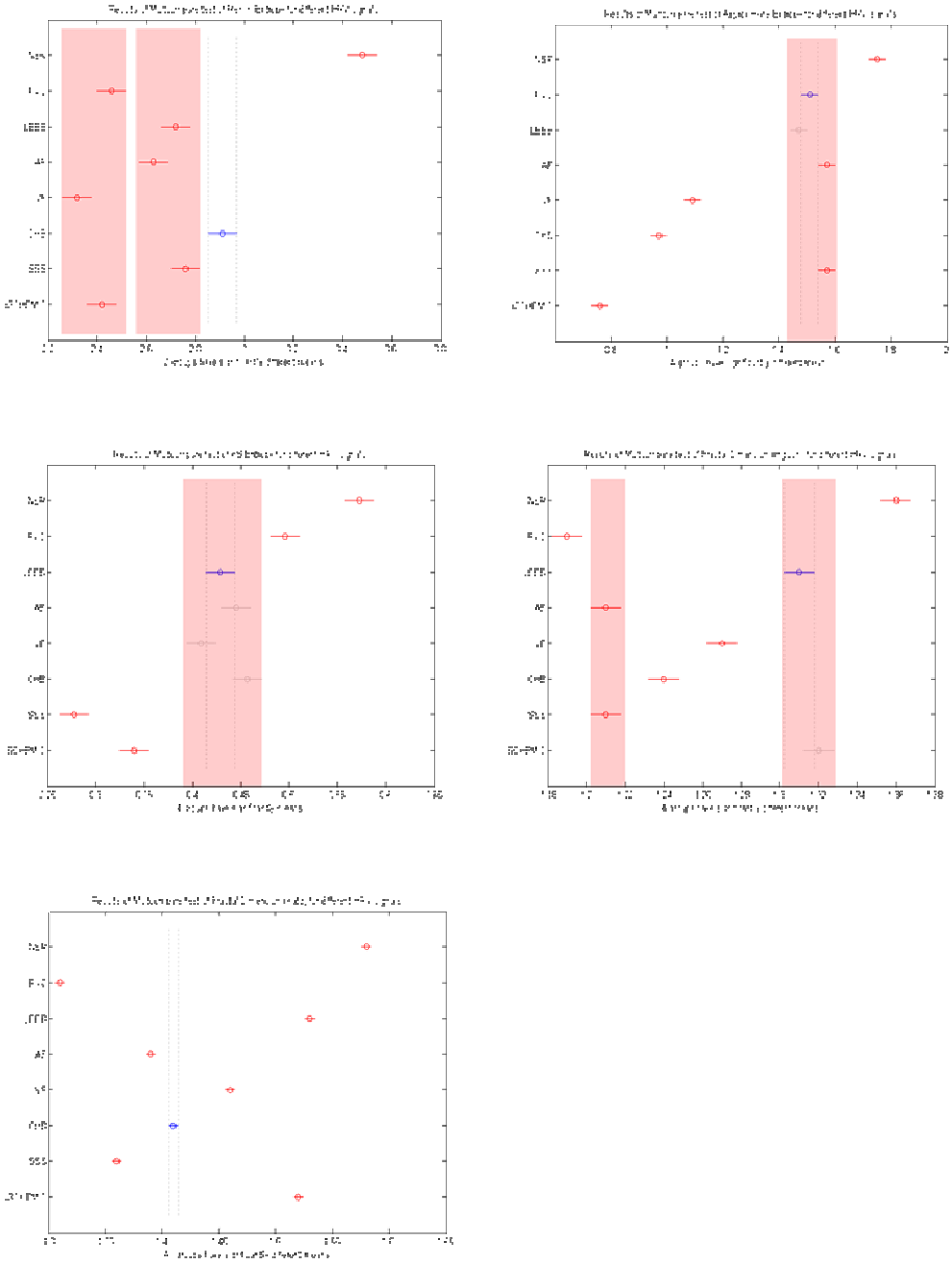

Figure 3.10 Results of multiple comparison test of the chaotic measures of the HRV signals.

The λ_1 was significantly higher in the patient groups, and the largest reported value has been reported for SSS groups. The Lyapunov exponent of the HRV signals can be considered as a complementary tool to improve diagnosis of heart diseases. By comparing the normal and patient groups, the result shows some differences in nonlinear properties of the HRV time series as shown in Table 3.3. The λ_1 for the normal subjects is higher (0.50±0.058), indicating the higher R-R variation. For PVC, it has still higher value (0.62±0.003) indicating higher R-R variation than normal subjects. In the case of LBBB, the λ_1 has sligtly lower value than normal subjcts due to the reduced R-R variation. For SSS (0.82±0.10), VF (0.56±0.11) and AF (0.42±0.036) the R-R variation is gradually decreases and as a result the λ_1 is also falls respectively. For ISCH cardiomyopathy (0.193± 0.06) and CHB (0.17±0.01), the λ_1 values are very low compared to normal subjects, because the R-R variation is negligible.

From Table 3.3, it can be seen that the fractal dimesions $D^{Higuchi}$ and D^{Katz} decreases for the various cardiac abnormalities with respect to the normal subject. This indicates that the irregularity or randomness of the HRV signal is lesser for cardiac abnormalities. Thus, FDs behave as a reliable indicator of heart diseases with a confidence of 90%.

The results of applying the entropy measures to the data sets are also presented in Table 3.3. The entropy values are always higher for normal subjects, so the healthy group can be distinguished from the patient groups. Entropy measures the degree of randomness or complexity of dynamical systems. As mentioned previously, *APEN* quantifies the

regularity of the time series. From another point of view, the more random the time series is, the higher the *APEN* values [82]. Therefore, this method quantifies the unpredictability of fluctuations in a time series such as the instantaneous HRV time series. Our results of *APEN* entropy has shown that the healthy group enjoys a higher *APEN* value, compared to that of the patient group. On the other hand, for the normal subjects the heart rate is more random Or has a higher variation (more chaotic). This range of values decreases as the beat to beat variation in the R-R interval decreases. It can be seen from the above results that, the range of values for the ISCH and CHB is small, due to their low variation in the R-R interval. For SSS, AF, PVC, LBBB, and VF, the R-R interval variation gradually decreases, hence the *APEN* range of values also falls respectively. The same trend is exhibited by the results of *KSEN, REN* and *SEN*.

From the results of DFA analysis, it canbe seen that the slope (α) for the normal subjects is found to be closer to 1, and it falls in different ranges for various types of cardiac abnormalities. This slope is very low for very highly varying signals like PVC, LBBB, AF and VF. But for rhythmically varying signals like SSS, CHB and ISCH this value is slightly higher. The value itself doesn't provide any conclusive results but it helps to observe the trend in HRV signals for different types of cardiac abnormalities.

Table 3.3 shows the Poincare plot indices, measured from Poincare plots reconstructed with a lag of one beat, recalling that both axes were greater in the healthy group than in the patient groups. The Poincare plot is formed through the long-term ECG recordings of R-R intervals, and it might be used as another diagnostic tool. The problem

regarding Poincare plot use has been the lack of obvious quantitative measures to characterize the salient features of the plot. The SD1/SD2 ratio reflects nonlinear information of HRV. One advantage of this selection is that the quantitative Poincare plot analysis does not require preprocessing or stationarity of the signal, and the parameters SD1 and SD2 can be computed very quickly. It is interesting to note that SD1 is connected to the vagal tone, while SD2 and the ratio SD1/SD2 are connected to the sympathetic tone [87]. SD1/SD2 did not significantly correlate with entropy measures. SD1/SD2 shows the ratio of short interval variation to long interval variation. This ratio is high in the case of PVC, AF, and VF due to more variation in the R-R interval; however the ratio falls for the slowly varying signals such as ISCHEMIC subjects. The results of extracted features are tested for statistical significance using ANOVA test and a p-value that is less than 0.1 is obtained in all cases. This indicates that atleast there is one group or class of the signals with mean significantly different from the other groups with 90% confidence. In this work, we have considered eight groups and eleven features and it is necessary to identify the groups that have distinct means and corresponding distinct features. To achieve this, multiple comparison test is performed and the results are given in Figure 3.10. It can be seen that Hurst exponent and the fractal dimension using had the significantly different means for all groups whereas Renyi entropy had only two groups with significant means. It can be noted that control group had significant means for all the features. It indicates that all the features are capable of significantly distinguishing the normal and abnormal group but within the abnormal group the features are distinct only

for few groups. As there are many cardiac abnormalities, it is necessary to evaluate a wide pool of features and identify the features for characterizing specific abnormalities.

3.9 Conclusion

The results from this study show that there is a clear separation between the time series of normal and patient groups, but it can be seen that there is no single feature that distinguishes all the seven cardiac abnormalities because the range of the values of patient groups overlapped considerably for few groups. From the results of the multi-comparison test (Figure 3.10), it can also be observed that each of these features can atleast distinguish any five of the eight classes and different features are predominant for different cardiac abnormalities. So it becomes clear that there is need for an intelligent system to identify the cardiac abnormalities by combining the information obtained from the features. Hence in Chapter 5 various classifier architectures are discussed to identify the cardiac states from the above mentioned features. A feature library with the above mentioned eleven features is developed for the eight classes of HRV signals. Features extracted are from different domains and it gives wide range to cover the different aspects of the underlying behavior of the system.

Chapter 4 Nonlinear Dynamics of Brain Signals

The brain is the most complex organ of the human body. Understanding the behavior and dynamics of billions of highly interconnected neurons involves a very difficult task that requires the fusion of several signal processing techniques, from the linear and nonlinear domains, and its correlation to the physiological events. An EEG is the measure and record of the electrical activity of the brain. Special sensors are attached on the scalp surface or sometimes subdural in the cerebral cortex and connected to a computer to record the brain's electrical activity. Certain conditions, such as seizures, are seen as the changes in the normal pattern of the brain's electrical activity.

An EEG measures primarily brain functions. The largest part of the brain is comprised of the cerebrum, which is split into right and left hemispheres. The cerebrum controls voluntary actions, thought, speech, and memory. In humans, the cerebrum comprises most of the brain, while in other mammals it is relatively small.

The outer layer of the cerebrum, called the cerebral cortex, is responsible for higher brain functions such as thought, reasoning, memory, and voluntary muscle movement. The cerebral cortex is mostly made up of neurons, which are nerve cells that carry messages throughout the body. In turn, the activity of the cerebral cortex is

regulated by two structures that are deeper in the brain: (i) the thalamus, which is located in the center of the brain and carries signals from the sensory organs to the brain, and (ii) the reticular activating system, which sends signals to tell us to go to sleep and to wake us up.

The electrical activity of all these structures is the primary focus of the EEG. The cerebral signal observed in the scalp EEG falls in the range of 1-30 Hz [88]. The EEG typically described in terms of (i) rhythmic activity and (ii) transients. The rhythmic activity is divided into bands by frequency. They are,

- Delta waves - frequency range up to 3 Hz. It tends to be the highest in amplitude and the slowest waves. It is seen normally in adults in slow wave sleep and also in babies.

- Theta waves - frequency range from 4 Hz to 7 Hz. It is seen normally in young children. It is seen in drowsiness or arousal in older children and adults and also during meditation. Excess theta represents abnormal activity.

- Alpha waves - frequency range from 8 Hz to 12 Hz. This activity is seen in the posterior regions of the head on both sides, being higher in amplitude on the dominant side. It is increased by closing the eyes and by relaxation. It will attenuate with eye opening or mental exertion.

- Beta waves - frequency range from 12 Hz to about 30 Hz. It is seen usually on both sides in symmetrical distribution and is most evident in frontal lobes. Low amplitude beta with multiple and varying frequencies is often associated with active, busy or anxious thinking and active concentration.

- Gamma waves - frequency range approximately 30–100 Hz. Due to the filtering properties of the skull and scalp, and due to contamination by EMG and minute eye movements, gamma rhythms are usually recorded using electrocorticography or possibly with magneto encephalography.

Some of the applications of EEG measurements are:

- Diagnose epilepsy and identify the type of seizures. EEG is the most useful and important test in confirming a diagnosis of epilepsy.
- Check for problems with loss of consciousness or dementia.
- To find out a person's chance of recovery after a change in consciousness.
- To find out if a person who is in a coma is brain-dead.
- Study sleep disorders, such as narcolepsy.
- Watch brain activity of the person receiving general anesthesia during brain surgery.
- To find out if a person has a physical problem (problems in the brain, spinal cord, or nervous system) or a mental health problem.

4.1 Description of the Data

The EEG data for our analysis were obtained from the EEG database available with the Bonn University [89]. Three sets each containing 30 single channel EEG segments of 23.6-sec duration, were composed for the study. These segments were selected and cut out from continuous multi-channel EEG recordings after visual inspection for artifacts, e.g., due to muscle activity or eye movements. Normal data sets consisted of segments taken from surface EEG recordings that were carried out on five healthy volunteers using a standard electrode placement scheme. Volunteers were relaxed in an awake state with eyes open. For epileptic data, EEG is obtained from five patients diagnosed with epilepsy and recorded during seizure activity. The background EEG data was recorded from the same five epilepsy patients when there is no seizure. All EEG signals were recorded with the same 128-channel amplifier system, digitized with a sampling rate of 173.61 Hz and 12 bit A/D resolution. The electrodes are placed as per the standard 10-20 electrode placement scheme for measuring EEG. The data was filtered using a band pass filter with settings 0.5340Hz~12 dB/octave. Sample recordings of normal, background and epileptic EEG are given in Figure 4.1.

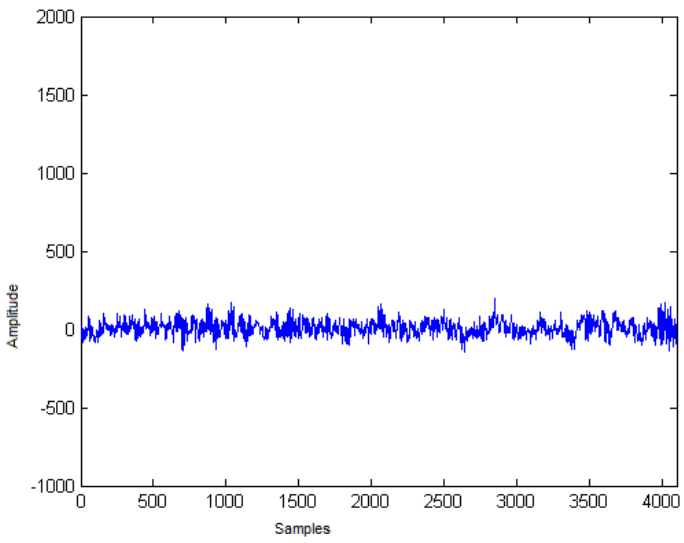
2000
1500
1000
500
0
-500
-1000
Amplitude
0
500
1000
1500
2000
2500
3000
3500
4000
Samples

(a)

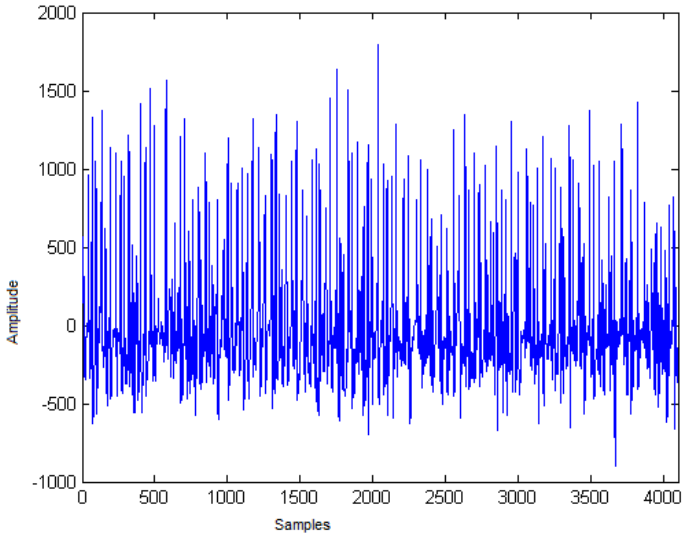
2000
1500
1000
500
0
-500
-1000
Amplitude
0
500
1000
1500
2000
2500
3000
3500
4000
Samples

(b)

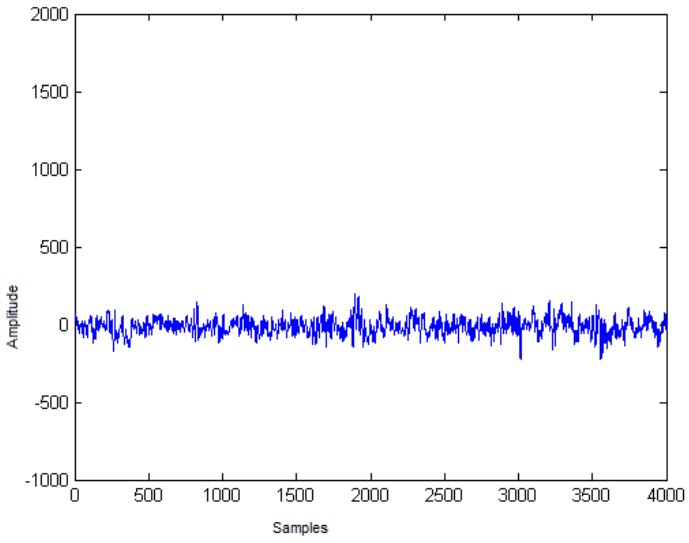

(c)

Figure 4.1 (a) Normal EEG signal (b) Epileptic EEG signal (c) Background EEG signal

In this work, we have analyzed the normal, background and epileptic EEGs using various nonlinear characteristic measures such as D_2, λ_1, H, D^{katz}, $D^{Higuchi}$, $KSEN$, $APEN$, REN and SEN. The characteristics measures are computed using a running window method, as given in Figure 4.2 and Figure 4.3. The shaded area is the sliding observation window, which moves through the data as the measures are computed. The data points inside this sliding window are used for feature generation as the window moves through the data. Therefore the observation window is continuously collapsed and the characteristic measure is computed for the data in new observation window. In our analysis, we have used the window size to be 200 samples with an overlap of 150 samples between consecutive windows. The window size of 200 samples corresponds to

more than one sec of the signal and we have used a overlap of 150 samples considering the nonstationarity of the signal. Hence there will be 80 such windows per dataset.

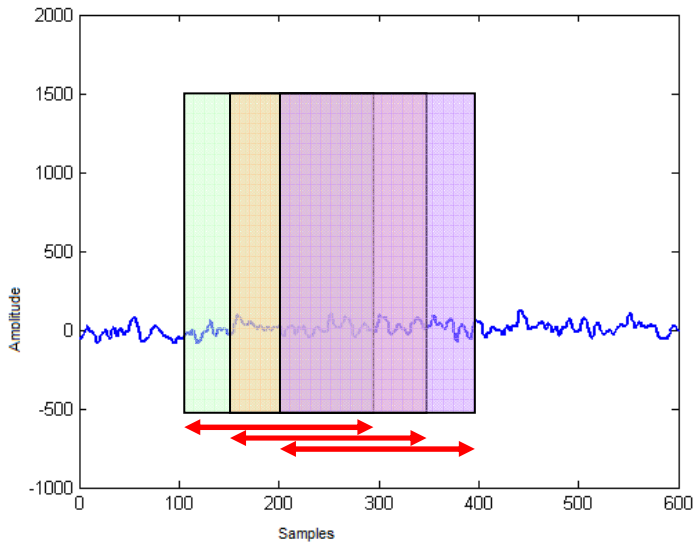

Figure 4.2 Sliding observation window (Normal EEG signal)

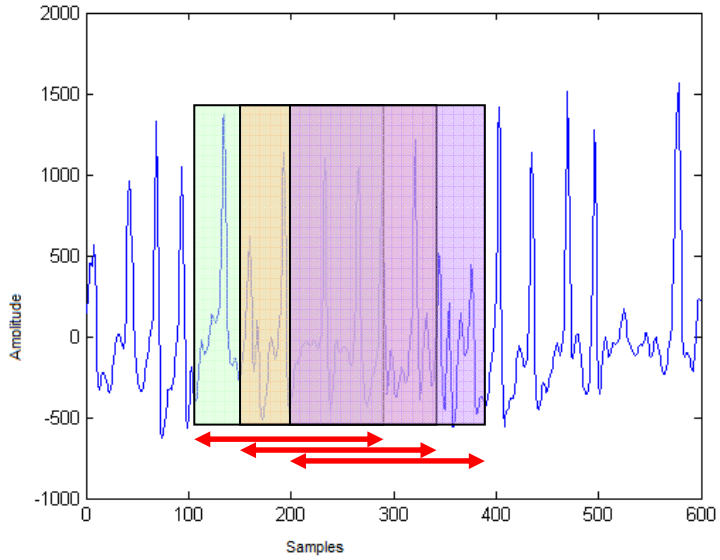

Figure 4.3 Sliding observation window (Epileptic EEG signal)

4.2 Test of Nonlinearity

Surrogate data analysis is used here to test the nonlinearity of the EEG signals. The complex phase values of the Fourier transformed input signal is used to produce the surrogate data set of the EEG data under consideration. Surrogate data sets are generated for 20 sets each of control, background and epileptic EEG signals. The 20 sets are selected randomly. The $APEN$ and D_2 measures are used as the discriminating statistics and the values for the original and the surrogate data are given in Table 4.1 . The discussion on calculation of APEN and D2 is given in Chapter 3. The calculation is done on 200 samples window and averaged. It can be seen that the $APEN$ values of the surrogate data and the original data are quite distinct and they differ by more than 60%. Similarly, in the case of using D_2, as the discriminating statistics as well, the surrogate data and original data are differing from each other by more than 50%. Thus, the null hypothesis that the data is generated from a linear process is rejected and hence the EEG data considered are nonlinear.

Type	**Normal EEG**	**Epileptic EEG**	**Background EEG**
$APEN(Original)$	0.7103	0.6542	0.6735
$APEN(Surrogate)$	0.2791	0.2411	0.2564
% Difference	60.7 %	63.1 %	61.9 %
$D_2(Original)$	4.8768	3.9407	4.2672
$D_2(Surrogate)$	2.2421	1.5429	1.987
% Difference	54.0 %	53.12 %	53.43%

Table 4.1 Results of surrogate data analysis

4.3 Chaotic Invariants Analysis

The optimum embedding parameters m and τ are determined using the method described in Chapter 3. The graph of D_2 vs m for normal, background and epileptic EEG is shown in Figure 4.4. D_2 saturates at $m_{sat} = 9$ and the optimum embedding dimension is chosen as $m = 10$ for the analysis of EEG signals.

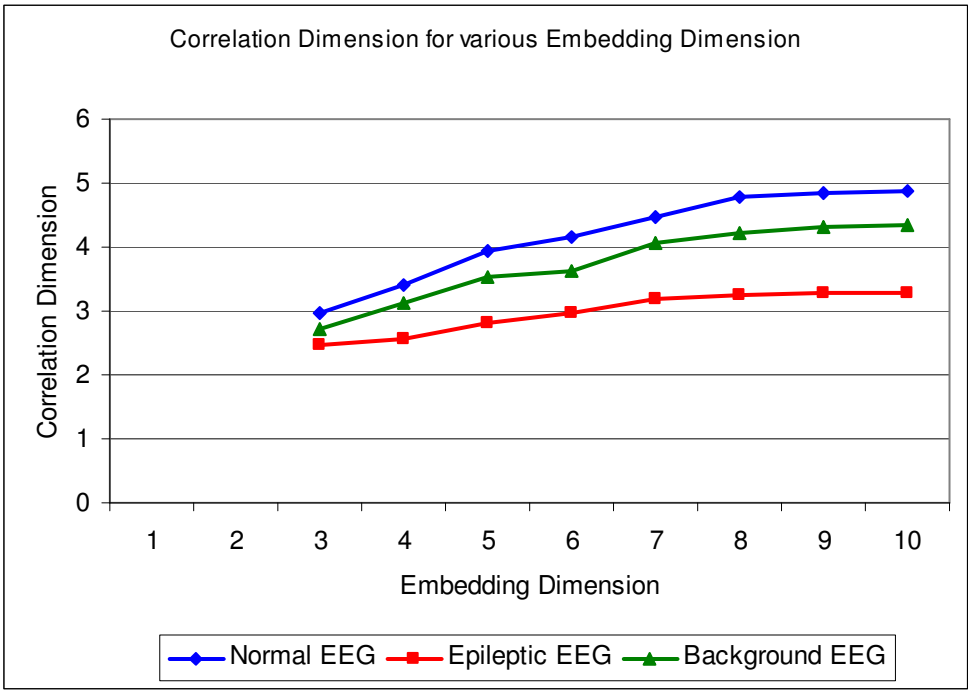

Figure 4.4 Variation of correlation dimension for different embedding dimension

Mutual information function for normal, epileptic and background EEG is given in Figure 4.5, Figure 4.6 and Figure 4.7 respectively. It can be clearly seen that the average mutual information reaches its first minimum at $\tau = 5$ for all the three types of EEG signals. Hence the optimal embedding delay τ is chosen as 5 for our analysis.

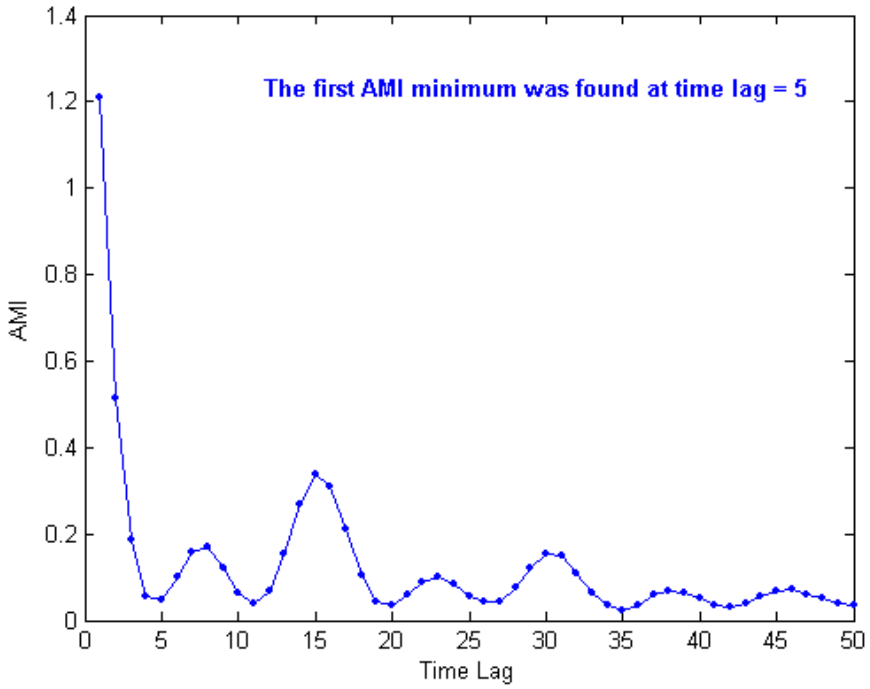

Figure 4.5 AMI of normal EEG signal

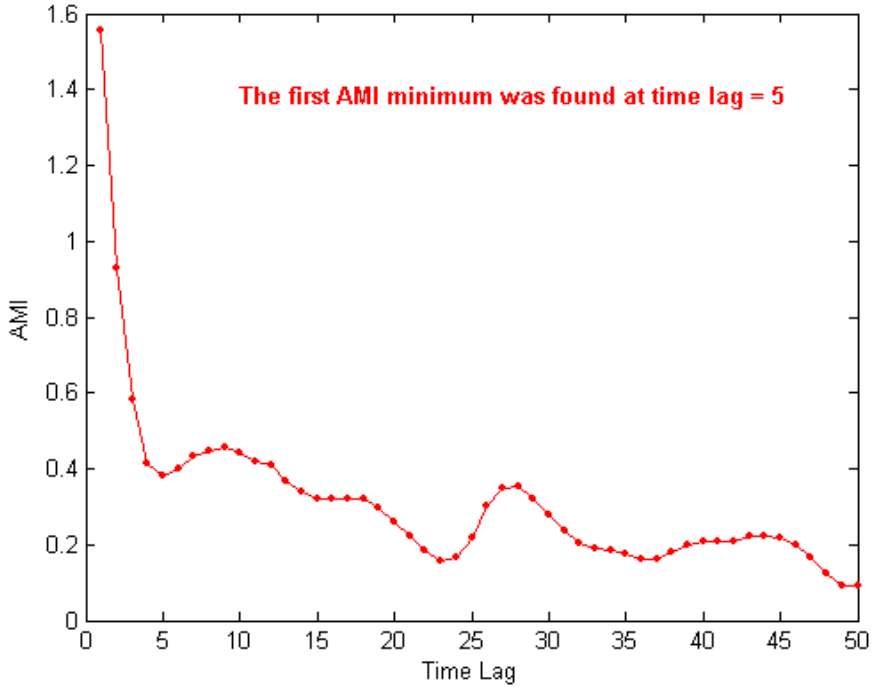

Figure 4.6 AMI of epileptic EEG signal

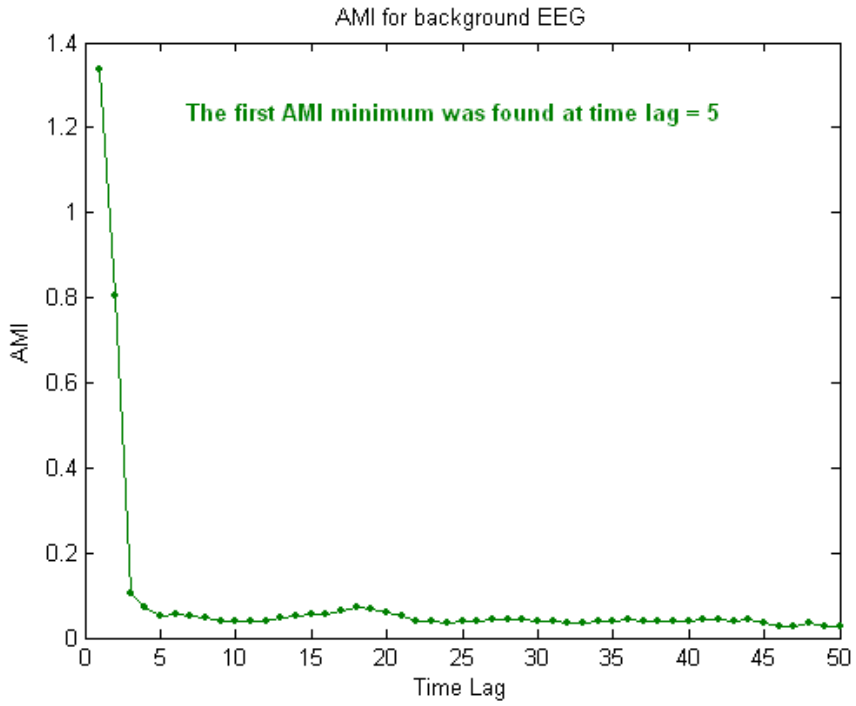

Figure 4.7 AMI of background EEG signal

Figure 4.8 shows the 3-D plot of the reconstructed attractor of the EEG signal from control subject with a time delay of $\tau = 5$, while the reconstructed attractor of the epileptic EEG is given in Figure 4.9 with the same conditions. Figure 4.10 shows the 3-D reconstruction of the background EEG. It can be seen from Figure 4.8 and Figure 4.9 that even in three dimensions, the attractor show clear differences in their structure between the epileptic EEG and that of control subject. The reconstructed attractor from an epileptic EEG shows more rhythmic activity and thus less chaotic. The attractor describes how the system trajectories are attracted as time tends to infinity.

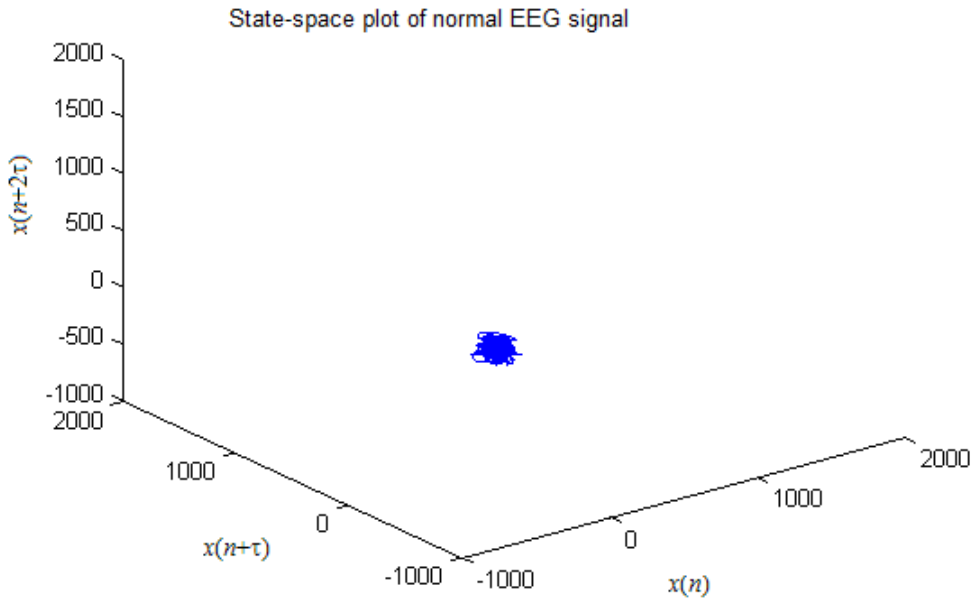

Figure 4.8 Phase-space plot of normal EEG signal

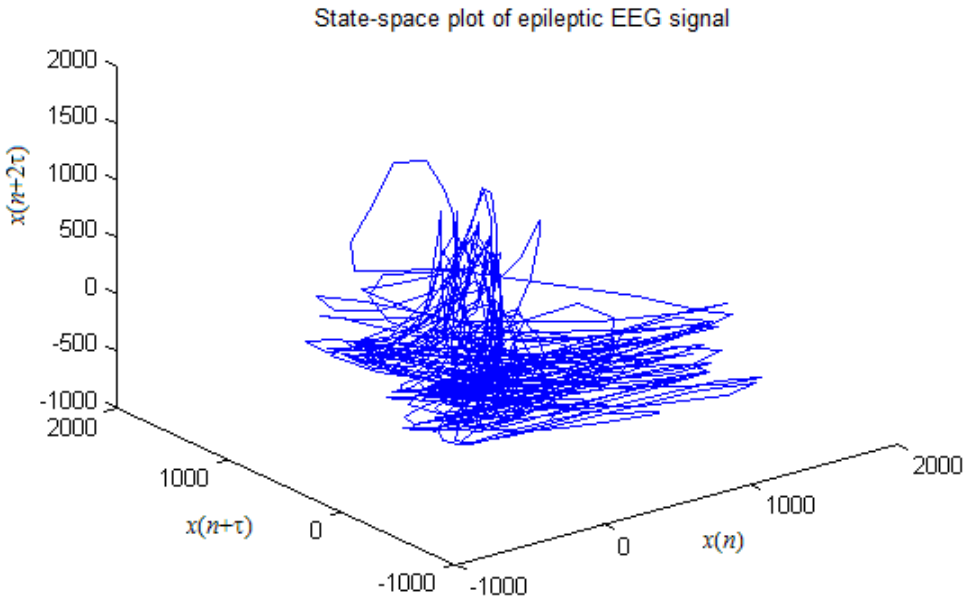

Figure 4.9 Phase-space plot of epileptic EEG signal

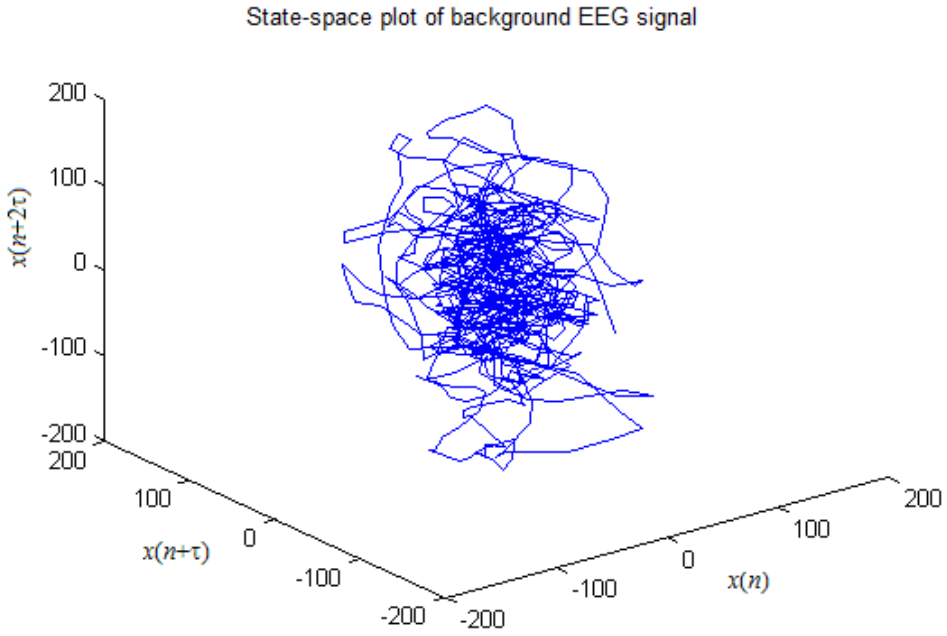

Figure 4.10 Phase-space plot of background EEG signal

Plot of the attractors serve as a descriptive representation of the signal and parametric representations of the reconstructed attractors are needed to quantify the signals. In this work, parameters such as D_2, λ_1, $KSEN$, SEN, $APEN$ and REN are used to quantitatively describe the attractor in multidimensional space. The measurements of these parameters are accurate only if the data under consideration are stationary. The stationarity of the normal, background and epileptic EEG signals used for analysis is tested using the recurrence plot method. The recurrence plots of normal, epileptic and background EEG signals are given in Figure 4.11, Figure 4.12 and Figure 4.13. It can be seen that the plots are symmetric along the diagonal and the overall pattern is fairly uniform. The uniform distribution of the pattern indicates that the process is a stationary process.

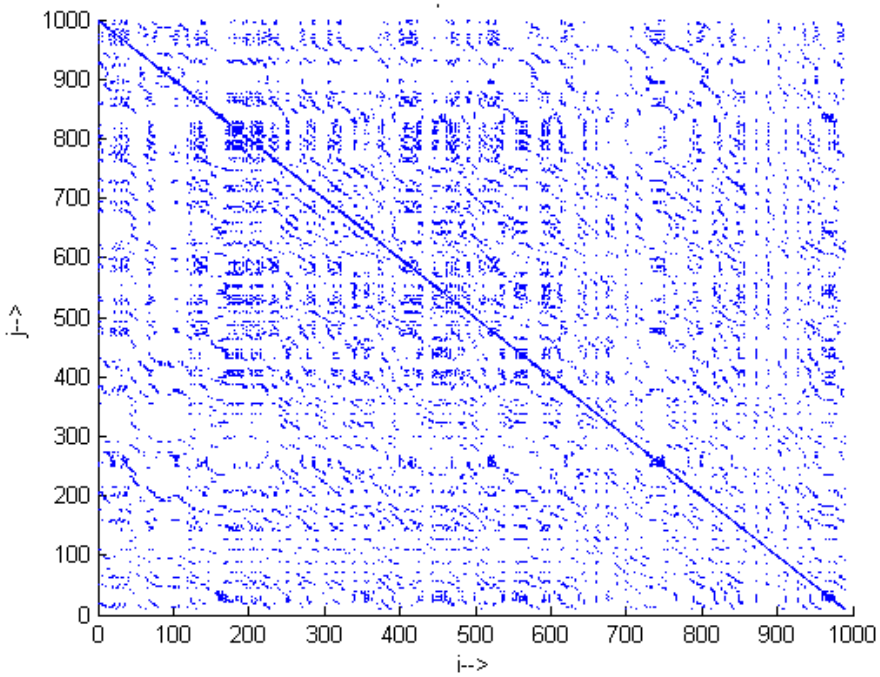

Figure 4.11 Recurrence plot of normal EEG signal.

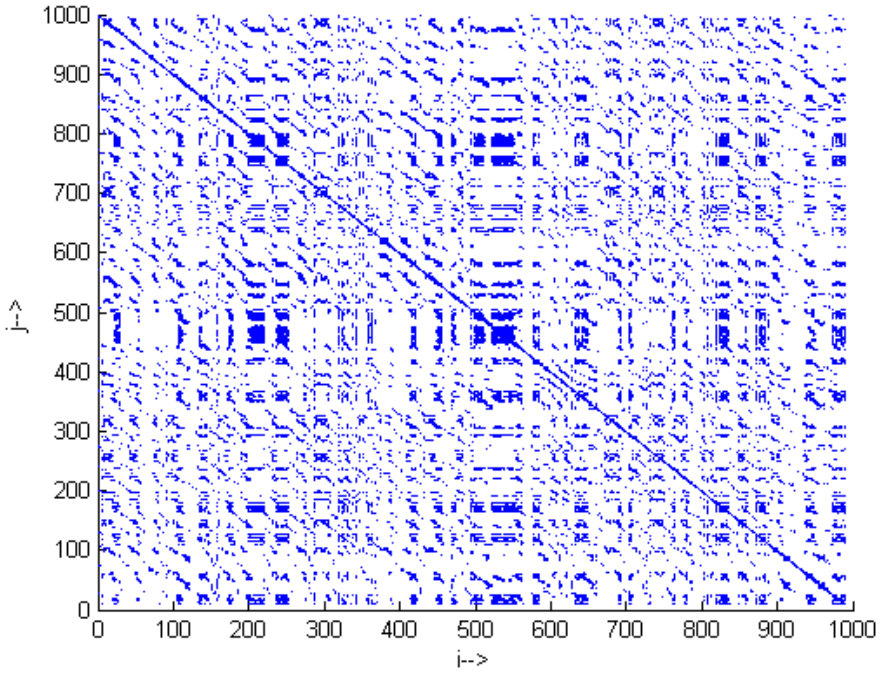

Figure 4.12 Recurrence plot of epileptic EEG signal.

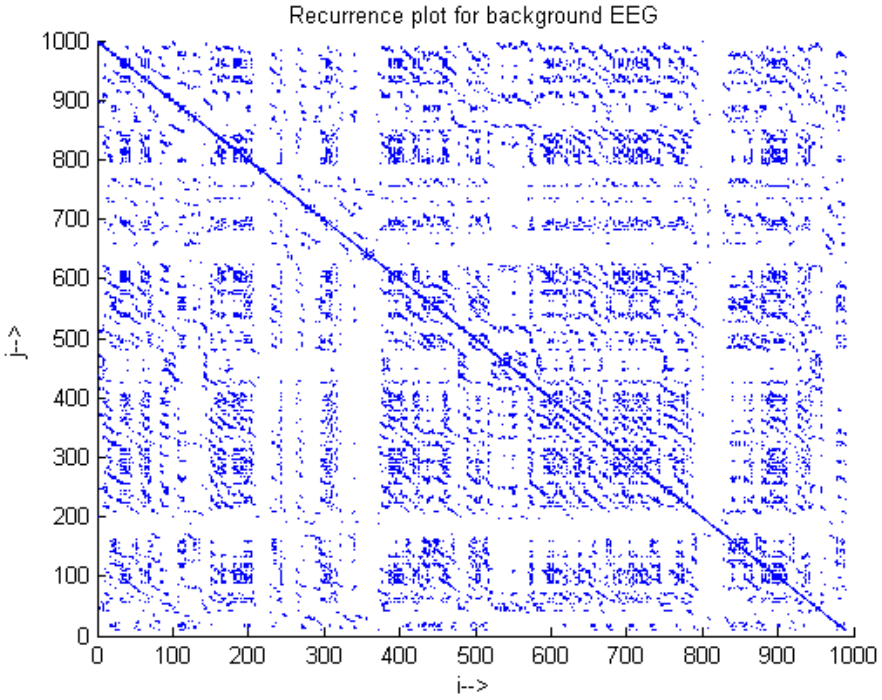

Figure 4.13 Recurrence plot of background EEG signal.

Table 4.2 shows results of nonlinear time series analysis of EEGs during seizures. From each EEG-recording, we have computed the chaotic invariants described in Chapter 3. D_2, the parameter that quantifies the variability of the time series is computed for embedding dimensions 3- 10 and the graph of D_2 for different values of *m* is shown in Figure 4.4. The results indicate that, the D_2 values are higher for normal subjects with mean and SD values of 4.8768 $\pm$ 0.3667, compared with the D_2 values of the background EEG signals of 4.3451 $\pm$ 0.182 and epileptic EEG's of 3.9407 $\pm$ 0.2582. This shows that the degree of complexity of epileptic EEG is less as compared to that of non-epileptic activity. This shows that the degree of complexity decreases gradually from the normal group, background and epileptic EEG signals in different stages respectively. The results are in agreement with the studies [36] on dimension analysis of EEG that epileptic seizures are emergent states with reduced dimensionality compared to non-epileptic activity. This concept finds support in the observations [42] that neuronal hyper-synchrony underlies seizures; a phenomenon during which the number of independent variables required to describe the system is smaller than at other times. The results are also supported by our statistical analysis using t-test ($p< 0.0001$) indicating extreme statistical significance. The intersubject variation of D_2 for normal, epileptic and background EEG is shown in Figure 4.14, 4.15 and 4.16., respectively. From these figures, it can be clearly seen that D_2 remains distinctly different for normal, background and epileptic states.

Chaotic measures	**Normal EEG**	**Epileptic EEG**	**Background EEG**	**p-value**
D_2	4.8768 $\pm$ 0.3667	3.9407 $\pm$ 0.2582	4.3451 $\pm$ 0.182	0.0001
λ_1	0.2036 $\pm$ 0.0156	0.1845 $\pm$ 0.0319	0.1912 $\pm$ 0.0114	0.0241
H	0.3248 + 0.0588	0.3563 + 0.0614	0.3411 $\pm$ 0.0181	0.0092
KSEN	0.6033 $\pm$ 0.0713	0.4926 $\pm$ 0.0474	0.5391 $\pm$ 0.0617	0.0001
APEN	0.7096 $\pm$ 0.0749	0.6484 $\pm$ 0.0117	0.6731 $\pm$ 0.0231	0.0001
SEN	-0.2215 $\pm$ 0.0139	-0.735 $\pm$ 0.0527	-0.513 $\pm$ 0.0312	0.0001
REN	-0.1897 $\pm$ 0.0172	-0.207 $\pm$ 0.0324	-0.194 $\pm$ 0.011	0.0365

Table 4.2 Chaotic measures of control, background and epileptic groups

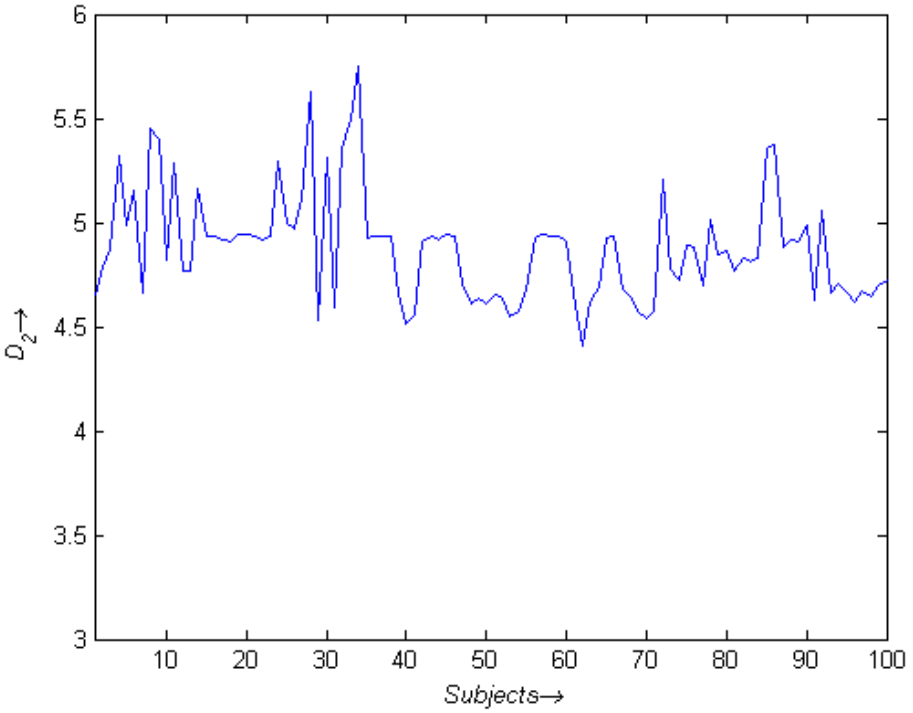

Figure 4.14 Inter subject variation of D_2 for normal EEG signal

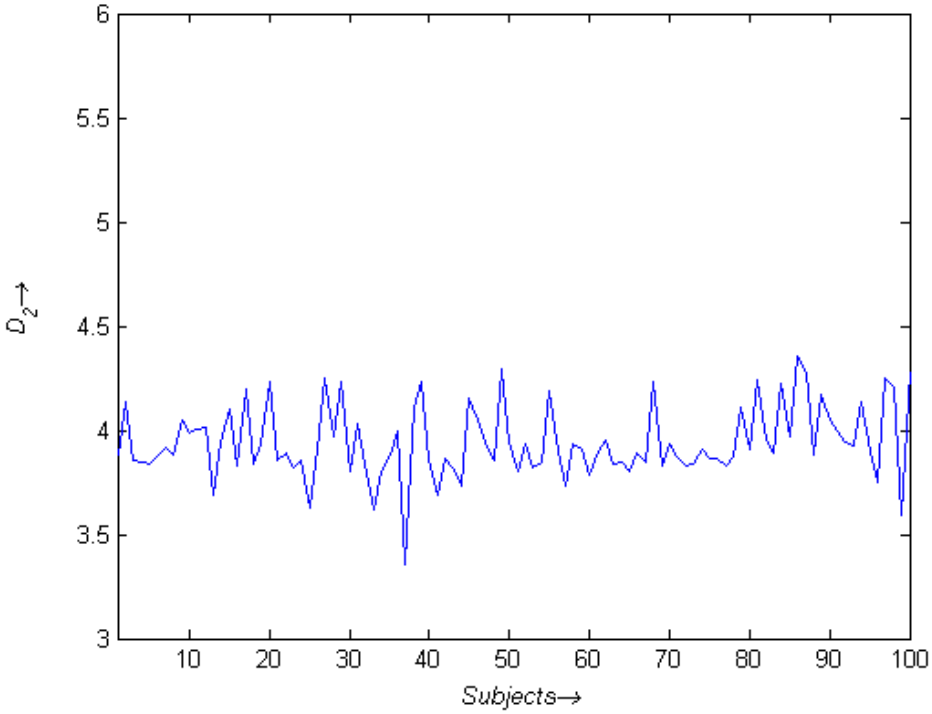

Figure 4.15 Inter subject variation of D_2 for epileptic EEG signal

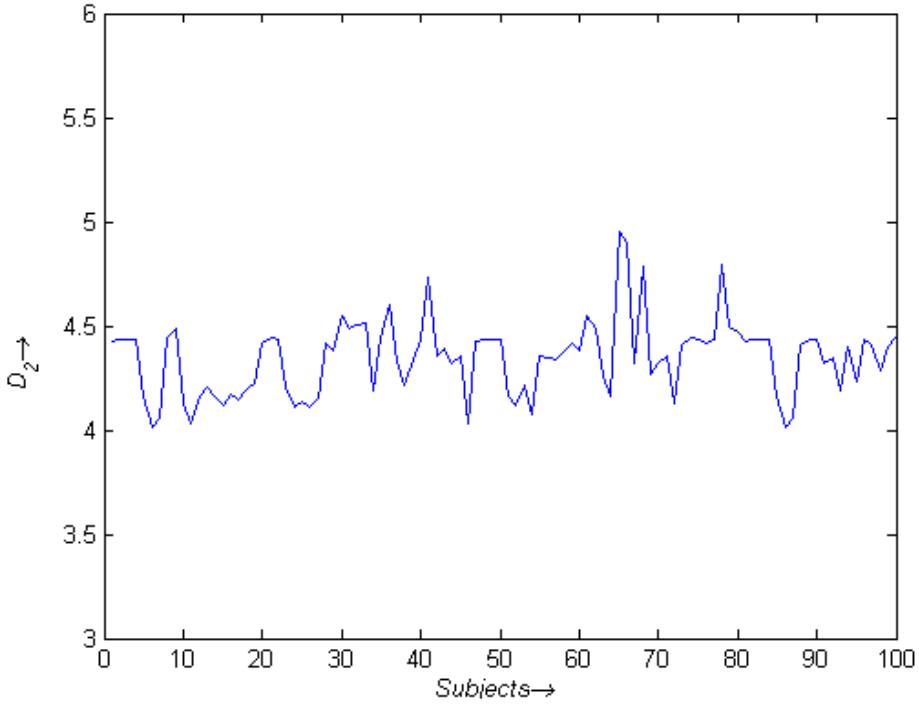

Figure 4.16 Inter subject variation of D_2 for background EEG signal

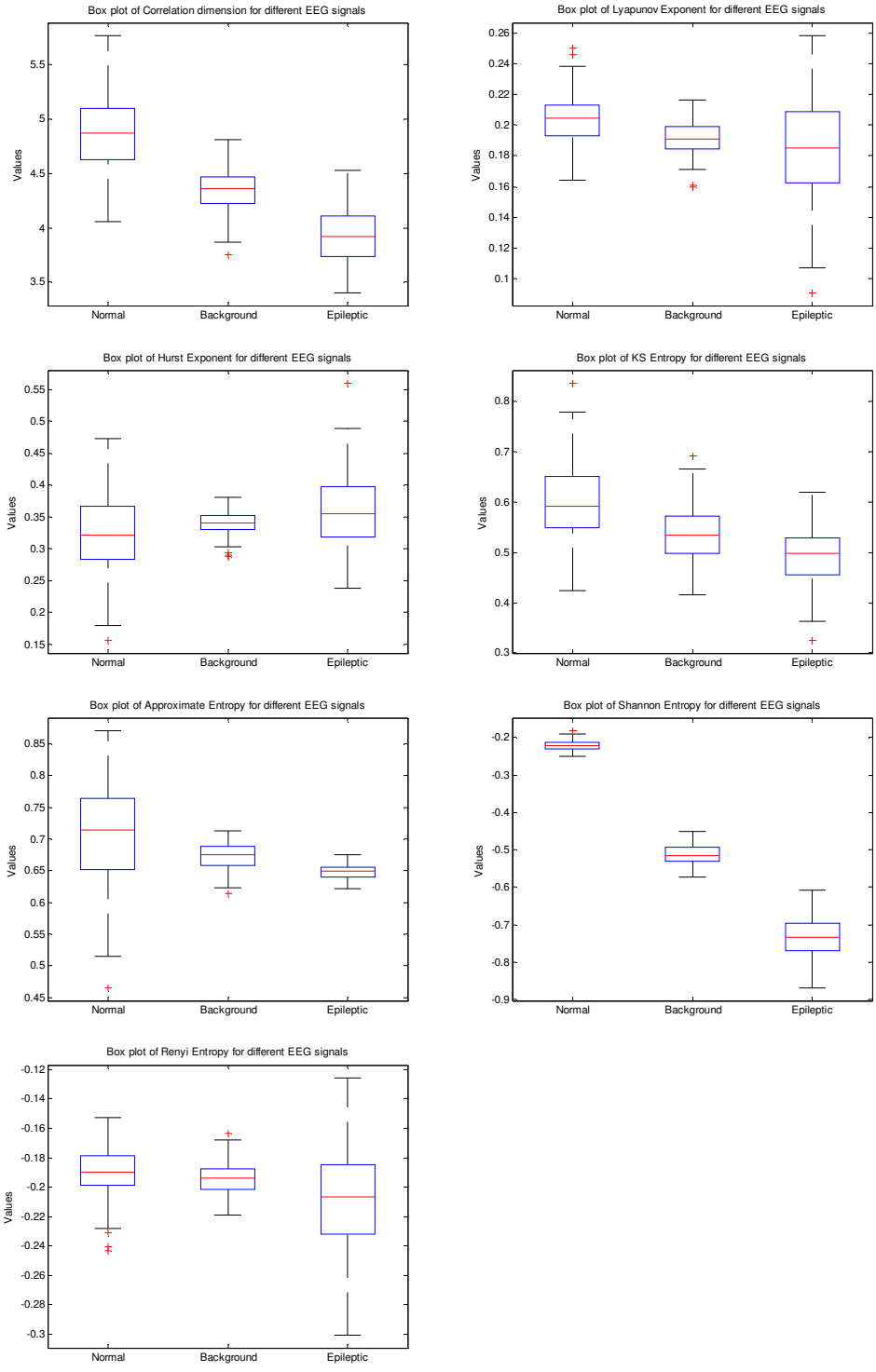

Figure 4.17 Variation of Chaotic measures for the EEG signal

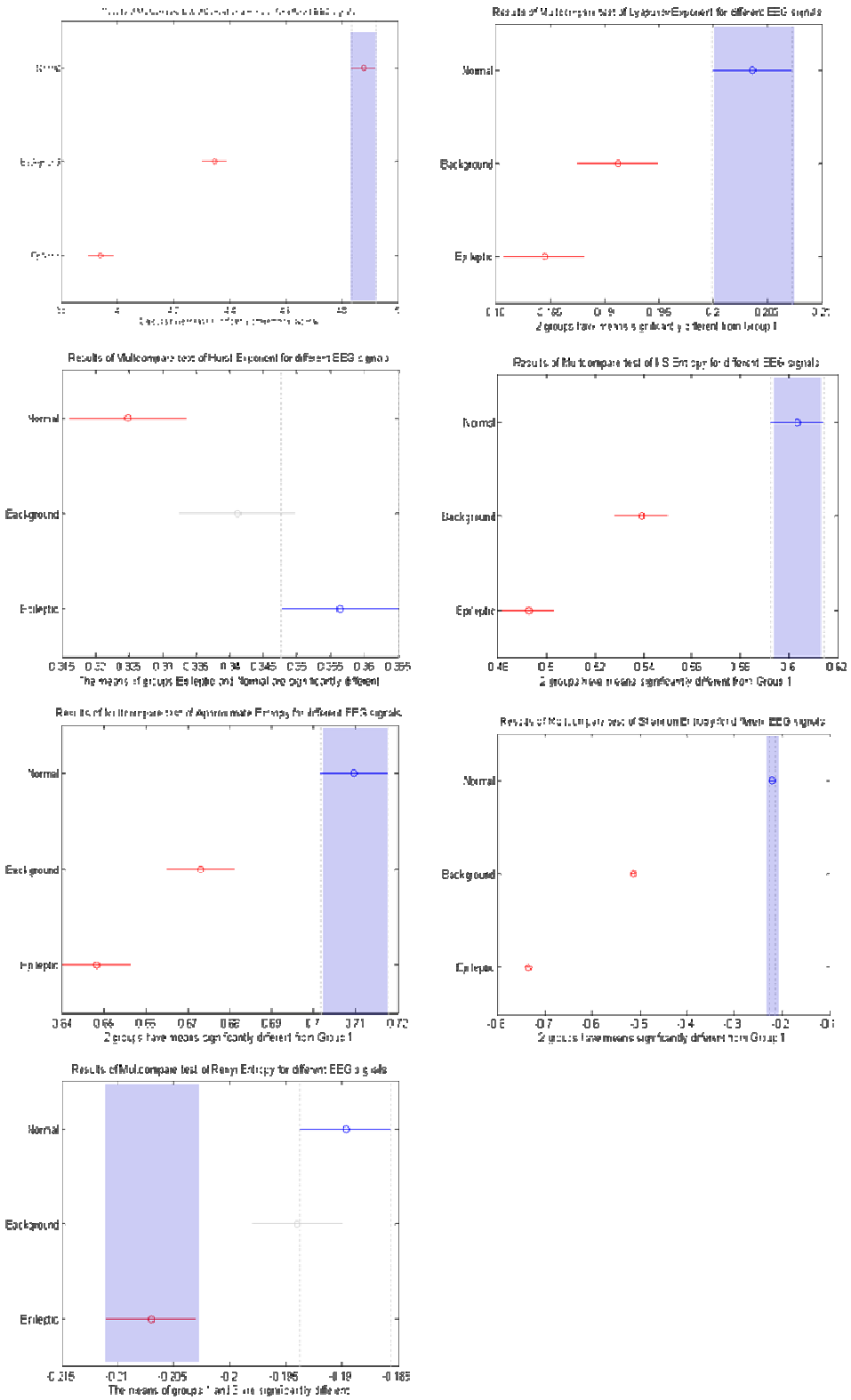

Figure 4.18 Results of Multiple comparison test of EEG chaotic measures

From the Figure 4.17 it can be seen that he results of λ_1 are similar to that observed for D_2. The positive values of λ_1 describes the divergence of trajectories starting at nearby initial states and corresponds to the flexibility of information processing in the brain [80]. In this context, flexibility refers to the ability of the central nervous system to reach different states of information processing from similar initial states. From the results in Table 4.2, it can be seen that the λ_1 of epileptic EEG (0.1845 ± 0.0319) is lesser than background and normal with mean and standard deviation value of (0.1912 ± 0.0114) and (0.2036 ± 0.0156), respectively. This means that, the brain during a seizure which has a smaller λ_1, indicate a drop in its flexibility of information processing. This result suggests a decreased complexity in the epileptic EEG and shows that there are less independent, parallel, functional brain processes active in the epileptic group than in the normal group. Also in our analysis, the λ_1 were positive in all cases giving an evidence of chaotic activity.

In time series analysis of EEG, H and D_2 were used by Dangel *et. al.* [75] for characterize the non-stationary behavior of the sleep EEG episodes. In their results they showed that there is a there is clearly a negative correlation between the values of D_2 and H and that is the expected behavior of a stochastic system with power-law spectra, $D_2 = \max(\frac{1}{H_2}, m)$, where m is the embedding dimension. From Table 4.2 it can be seen that our results also exhibited a similar trend and the H value increased for background and epileptic EEG compared to normal. Increase in the value of the Hurst

exponent indicates less complexity and more synchronization. The increasing trend of H as shown in the multiple comparison plot in Figure 4.18 indicates more synchronizing activity in the underlying phenomena of the brain as it changes form normal to inter-icatal and then ictal states. This is in accordance with our other results that the brain exhibit less chaotic behavior during a seizure.

According to Sleigh *et. al*. [90] the changes in entropy of the EEG are expected to indirectly coarsely measure changes in the entropy occurring within the cerebral cortex itself. $KSEN$ is one of the widely used measures of chaotic behavior and it describes the rate at which information about the state of the dynamics process is lost with time. $KSEN = 0$ implies an ordered system and $KSEN = \infty$ corresponds to a totally stochastic situation. The higher the $KSEN$, the more closer the system to be stochastic. From Table 4.2 it can be seen that $KSEN$ of normal EEG is greater than that of background and epileptic EEG indicating more mental activity in the brain for a normal subject.

$APEN$ gives a robust entropy estimate from short and noisy data sets and increasing values correspond to more irregularity or to increasing complexity in the time series [82]. Our results show that the epileptic EEG signals have significantly lower $APEN$ values (0.6484 ± 0.0117) than background (0.6731 ± 0.0231) and normal EEG (0.7096 ± 0.0749). This indicates that EEG during a seizure is more regular and less complex than the normal. This can be due to the dynamic processes underlying the EEG recording that are less complex for epileptic subjects than for normal subjects. This is in support of the studies that there will be decrease in brain complexity due to neuronal death, a general effect of neurotransmitter deficiency and loss of connectivity of local

neural networks as a result of nerve cell death [91, 92]. It can be seen from Table 4.2 that the results of SEN and REN also exhibit a similar trend like $APEN$ and $KSEN$.

From the results of analysis of various measures such as D_2, λ_1, H, $KSEN$, SEN, $APEN$ and REN, we can infer that the complexity or irregularity of the EEG signal is reduced during epilepsy. Also the values of these measures are distinct for normal and epileptic EEG signals. The results of the statistical analysis of these measures given in Table 4.2, also indicate extreme statistical significance with $p<0.01$ tested with ANOVA, for the chaotic measures such as D_2, λ_1, D^{katz}, $D^{Higuchi}$, $KSEN$ and SEN. Similar to HRV analysis, here also the multiple comparison tests are performed even though there are only three groups. The results are given in Figure 4.18. The results show most of the features considered have distinct mean for all the three groups expect for Hurst exponent and Renyi entropy. It can also be from the Figure 4.18, that the normal, background and epileptic EEG features values exhibit a increasing or decreasing trend. It indicates there is a gradual transition the brain activity from normal to seizure. This paves a way to look into feasibility of predicting the onset of the seizure.

4.4 Fractal Dimension Analysis

The FD of the EEG signals is computed using a sliding window approach. An overlapping sliding window with a size of 200 samples with 150 samples overlap is used. FD's are calculated for each set of data points that lay inside the window and the mean is taken to report the FD of the signal. Figure 4.19 and Figure 4.20 shows the variation of

FD of a normal EEG, epileptic EEG and background EEG with the sliding window determined by the two methods discussed earlier. Equivalent results were obtained for the all the records studied. It can be seen that Katz algorithm performs better compared to Higuchi's algorithm in discriminating epileptic EEG from normal EEG. In these cases, it appears that the actual value of the FD is not as important as the changes in FD associated with different brain states.

FD	**Normal EEG**	**Epileptic EEG**	**Background EEG**	p-value
$D^{Higuchi}$	1.5132 ± 0.0431	1.3546 ± 0.0724	1.4042 ± 0.0339	0.0001
D^{Katz}	1.8649 ± 0.0572	1.5139 ± 0.0970	1.5634 ± 0.0173	0.0001

Table 4.3 Results of Higuchi's and Katz FD algorithms

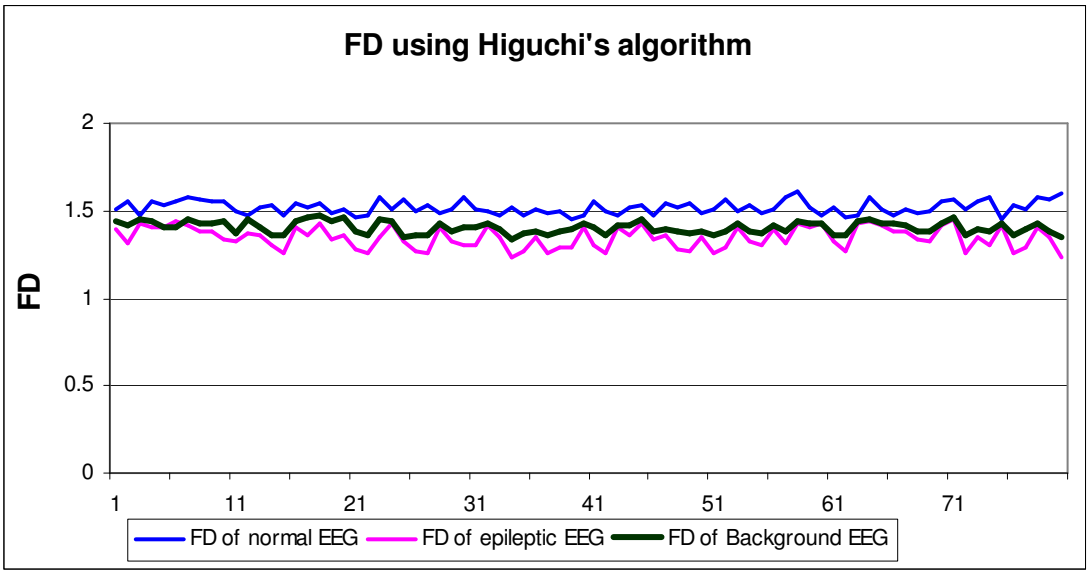

Figure 4.19 FD of EEG signals using Higuichi's algorithm

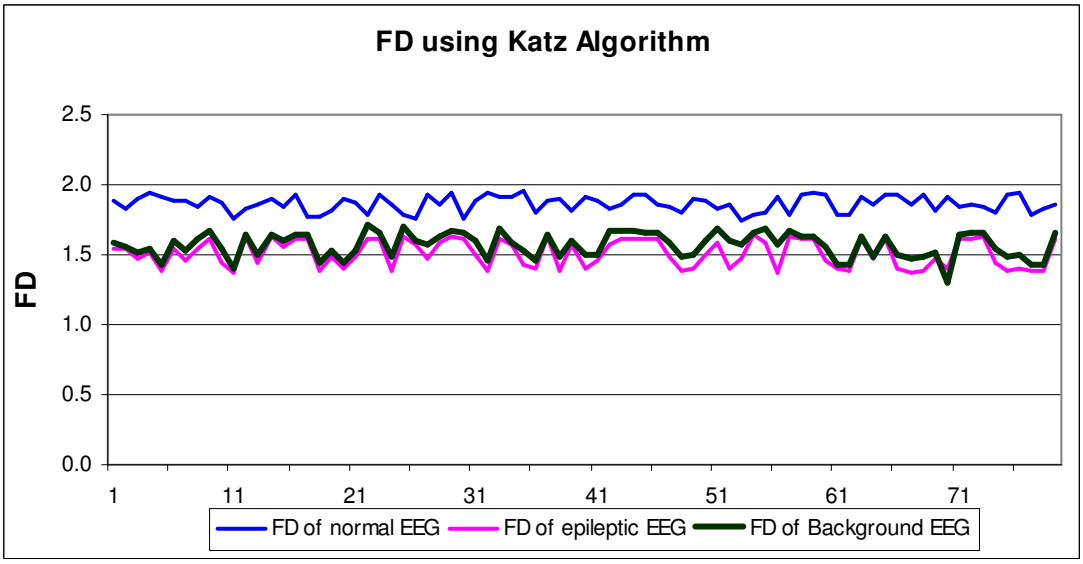

Figure 4.20 FD of EEG signals using Katz algorithm

The FD results obtained are given in Table 4.3 . It can be observed that both Higuchi's algorithm and Katz algorithm indicates similar trend of reduction in FD value for epileptic EEG as compared to background and normal EEG. The Katz algorithm reported a higher value of FD for both epileptic, background and normal EEG as compared to Higuchi's method. The reduction in FD values characterizes the reduction in brain system complexity for patients with epilepsy.

4.5 Conclusion

Epilepsy is one of the most frequently occurring malfunctions of the central nervous system and is characterized by a hyper-synchronous and hyper-excitable behavior of neuronal assemblies. Seizure activity is induced when the number of synchronized nerve cells exceeds a critical value. The EEG is the most important clinical

tool for the diagnosis of epileptic disorders. The study of EEG signals using techniques from nonlinear time series analysis is advantageous in gaining information about the dynamics of the system. The noninvasive nature and computational viability of these methods score above the more expensive imaging techniques used for diagnostics. In this study, we have analyzed the EEG signals of normal and epileptic subjects using a wide range of nonlinear time series analysis techniques expecting to extract quantitative measures that can reliably distinguish the EEG of an epileptic subject from that of a normal subject.

The results of our analysis demonstrated the potential of complexity measures such as D_2, λ_1, H, D^{katz}, $D^{Higuchi}$, $KSEN$, SEN, $APEN$ and REN in quantifying the regularity of EEG signal of normal and epileptic subjects. It is clearly shown that the values are higher for normal subject compared to that of epilepsy. The statistical results also support the discriminating ability of these measures in identifying epileptic and normal. These measures can serve as quantitative descriptors of EEG in automatic identification of normal and epileptic EEG signals. Also, the analysis of nonlinear dynamics in EEG signals can help in understanding the underlying physiological processes in the brain.

In Chapter 3 and Chapter 4, we discussed the extraction of nonlinear features from the ECG and EEG signals. In chapter 5, the detection of various abnormalities using the extracted feature set is discussed.

Chapter 5 Classifier Architectures for Cardiac Health and Mental Health Diagnosis

The HRV and EEG signals are used for monitoring the cardiac health and mental health diagnosis respectively. The abnormalities in the signals are detected using classifiers. The classifiers use the extracted features (discussed in Chapter 3 and Chapter 4) as inputs. In this work, we propose to use three different classifiers employing neural network (NN), fuzzy and ANFIS techniques. The performance of these classifiers are discussed and compared in this chapter.

A classifier can be viewed as a mapping operator that projects the M selected features contained in the feature vector onto a K^c-dimensional decision space, where K^c is the number of classes in the classification problem. The feature extraction and selection plays a crucial role in the classification results; however, it is highly important to select classifier architecture suitable to the underlying feature distribution in order to obtain a better recognition performance. In this work, emphasis is given to NN and fuzzy classifiers.

5.1 Neural Network Classifier

Artificial Neural Networks (ANN) are biologically inspired networks – inspired by the human brain in its organization of neurons and decision making process – which are useful in application areas such as pattern recognition, classification etc [93]. The decision making process of the ANN is more holistic, based on the aggregate of entire input patterns, whereas the conventional computer has to wade through the processing of individual data elements to arrive at a conclusion. The NNs derive their power due to their massively parallel structure, and an ability to learn from experience. They can be used for fairly accurate classification of fresh input data into categories, provided they are previously trained to do so. The accuracy of the classification depends on the efficacy of training, which in turn depends upon the rigor and depth of the training. The knowledge gained by the learning experience is stored in the form of connection weights, which are used to make decisions on the fresh input.

The characteristics of ANN are:

- *Adaptive learning*: An ability to learn how to do tasks based on the data given for training or initial experience.
- *Self-Organization*: An ANN can create its own organization or representation of the information it receives during the learning phase.

- *Real time operation*: ANN computations may be carried out in parallel, and special hardware devices are being designed and manufactured which take advantage of this capability.

In the human brain, a typical neuron (Figure 5.1) collects signals from others through a host of fine structures called *dendrites*. The neuron sends out spikes of electrical activity through a long, thin strand known as an *axon*, which splits into thousands of branches. At the end of each branch, a structure called a *synapse* converts the activity from the axon into electrical effects that inhibit or excite activity from the axon into electrical effects that inhibit or excite activity in the connected neurons. When a neuron receives excitatory input that is sufficiently large compared with its inhibitory input, it sends a spike of electrical activity down its axon. Learning occurs by changing the effectiveness of the synapses so that the influence of one neuron on another changes. ANN is a model (Figure 5.2) to simulate these features.

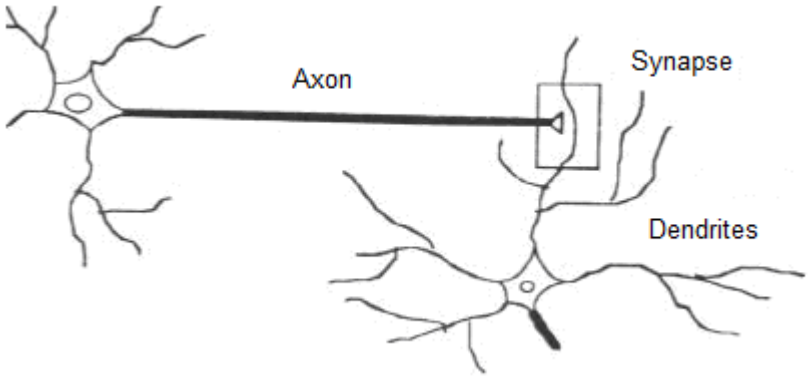

Figure 5.1 A typical neuron

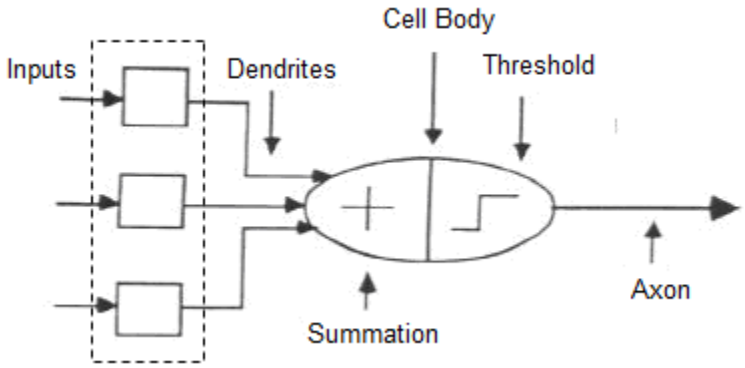

Figure 5.2 Neuron model

The common type of ANN consists of layers: a layer of "input" units is connected to a layer of "hidden" units, which is connected to a layer of "output" units. The inputs represent the raw information that is fed into the network. The activity of each hidden unit is determined by the inputs and the weights on the connections between the input and the hidden units. The behavior of the output units depends on the activity of the hidden units and the weights between the hidden and output units. The research on NNs has led to the development of different types of NNs to suit the purpose.

Three issues need to be settled in designing an ANN for a specific application: (i) topology of the network (ii) training algorithm and (iii) neuron activation function. The processing elements are organized into layers, and layers interconnected to form a network. The inputs to the processing unit are weighted signals derived from similar processing units of the previous layer. Usually, a processing element is linked to all the neurons of its immediate neighboring layers, which gives rise to a massive parallelism in architecture. The ANN can be organized into different topologies, such as feed forward and feedback networks. As noted above, to distinguish linearly separable classes, a single

layer perceptron classifier employing binary activation function is quite adequate. If the boundaries can be piecewise linear approximated, then two layer perceptron classifier with binary activation function can be used. If the nature of the classification is more complex, a three layer *feed forward* neural network, with sigmoid activation function is more suitable [94]. In the present case, the boundary between different classes for the chosen feature set is not linear and therefore NN classifier using radial basis functions techniques is adapted.

5.1.1 Radial Basis Function

A NN classifier is implemented using radial basis functions (RBF) [95] as shown in Figure 5.3. The net input to the radial basis transfer function is the vector distance between its weight vector **w** and the input feature vector **v** and multiplied with a bias *b*. The radial basis function has a maximum output of 1 when its input is 0. As the distance between **w** and **v** decreases, the output increases. Thus a radial basis neuron acts as a detector, which produces 1 whenever the input **v** is identical to its weight vector **w**. Probabilistic neural network, which is a variant of radial basis network is used for classification purpose. When an input is presented, the first layer computes distances from the input vector to the training vectors and produces a vector whose element indicate how close the input is to a training vector. The second layer sums these contributions for each class of inputs to produce as its net output vector probabilities. Finally, in the output layer, the maximum of these probabilities are chosen and a '1' is

produced for that class and a '0' for the other classes. The architecture for this system is shown in Figure 5.3.

For the input set of D training vector/target vector pairs associated with one of K^c classes, the first layer input weights **w** is set to the transpose of the matrix formed from the D training pairs. As the number of training vectors is 160 and input feature vector has M=3 inputs, the weight matrix formed is of dimension 3 x 160. When an input **v** of dimension 1 x 3 is presented, $\|\mathbf{w} - \mathbf{v}\|$ is calculated. $\|\mathbf{w} - \mathbf{v}\|$ indicates how close the input is to the vectors of the training set. These elements are multiplied, element-by-element, by the bias and sent to the radial basis transfer function. An input vector close to a training vector will be represented by a number close to 1 in the output vector **q**. The second layer weights **p** are set to the matrix **t** of target vectors. Each vector has a one only in the row associated with that particular class of input, and zeros elsewhere. At the competitive layer, sum of **qp** is obtained at each node. Finally, at the output layer maximum value of the outputs of competitive layer is detected and a '1' is generated corresponding to the maximum element and zeros elsewhere. Thus the network has classified the input vector into a specific one of K^c classes because that class had the maximum probability of being correct.

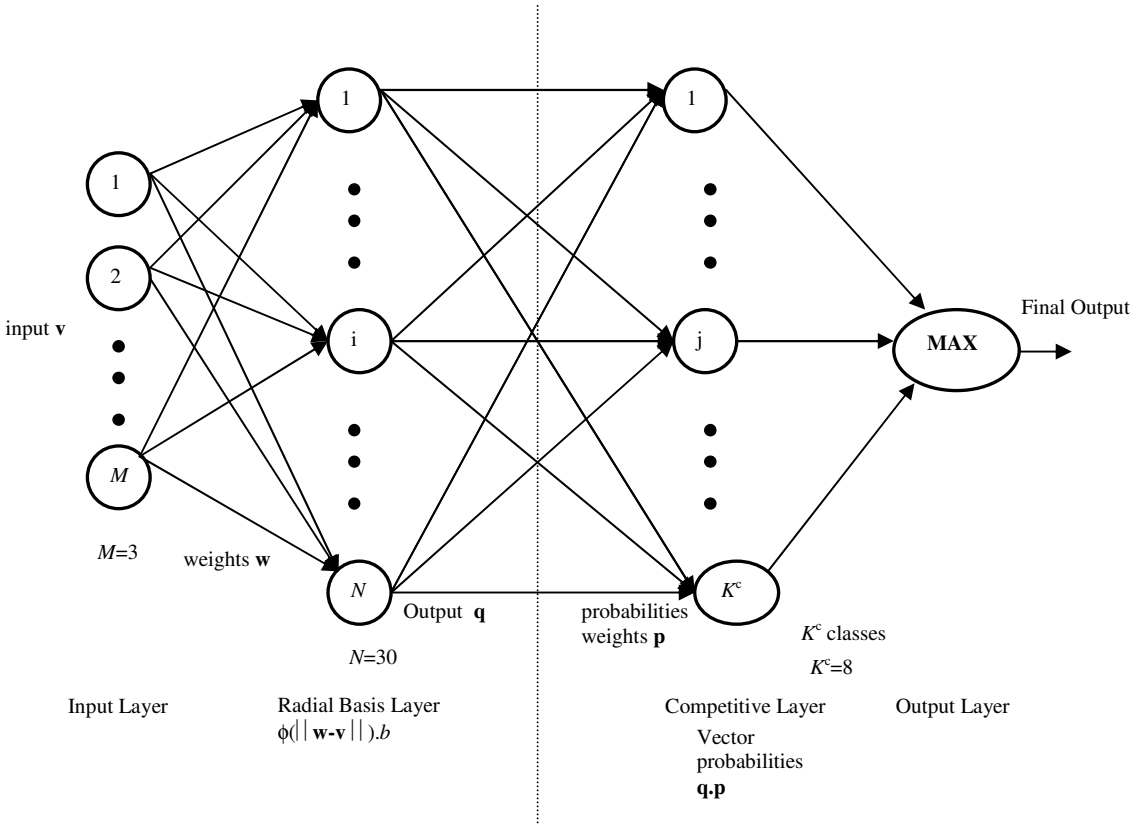

Figure 5.3 RBF network architecture

5.2 Fuzzy Classifier

In a fuzzy classification system, pattern space is divided into multiple subspaces. For each subspace, the relationships between the target patterns and their classes are described by if-then type fuzzy rules. The advantage of this system is that a nonlinear classification boundary can be easily implemented. Unknown patterns are classified by fuzzy inference, and patterns that belong to an unknown class which was not considered at learning can be easily rejected. Ishibuchi *et. al.*[96, 97] proposed methods to acquire a fuzzy classification system automatically by a simple learning procedure and a genetic

algorithm. With these methods, however, a pattern space is divided lattice-like. Therefore, many fuzzy rules corresponding to fine subspaces are required to implement a complicated classification boundary.

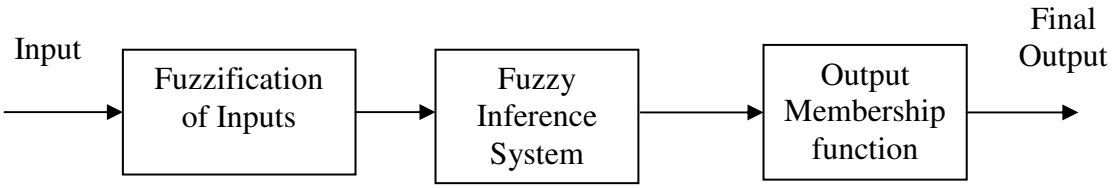

Figure 5.4 A fuzzy classification system

A fuzzy classifier [98] using subtractive clustering and Sugeno fuzzy inference system is implemented as a classifier as shown in Figure 5.4. The algorithm for implementation is as follows:

Step 1 - Fuzzify Inputs: The input is fuzzified using symmetric gaussian membership function given by

$$f(\mathbf{v};\sigma,\mu) = \frac{e^{-(\mathbf{v}-\mu)^2}}{2\sigma^2}, \tag{5.1}$$

where **v** is the input vector, σ and μ are variance and mean respectively.

Step 2 - Fuzzy inference: Fuzzy inference is the process of formulating the mapping from a given input to an output using fuzzy logic for making decisions. From the fuzzified inputs, the cluster centers are determined using subtractive clustering method. In this method,

- The data point with the highest potential to be the first cluster center is selected.

- All data points in the vicinity of the first cluster center (as determined by radii) is removed in order to determine the next data cluster and its center location.
- This process is iterated until all of the data is within the radii of a cluster center

Step 3 - Obtaining the output: Final output is obtained using the Sugeno fuzzy model. The output membership function is linear and is given by

$$r_i = ax + by + cz + d. \tag{5.2}$$

where a, b, c and d are membership parameters.

In the output layer, r_i of each rule is weighted by the firing strength w_i of the rule. The final output of the system is the weighted average of all rule outputs, computed as

$$\text{Final Output} = \frac{\sum_{i=1}^{N} w_i r_i}{\sum_{i=1}^{N} w_i}. \tag{5.3}$$

5.3 Adaptive Neuro Fuzzy Classifier

The Adaptive Neuro-Fuzzy Inference System (ANFIS) was first introduced by Jang [99] for classification purposes.

The neuro-adaptive learning techniques provide a method for the fuzzy modeling procedure to learn information about a data set, in order to compute the membership

function parameters that best allow the associated fuzzy inference system to track the given input/output data. This learning method works similarly to that of NNs. Using a given input/output data set, the MATLAB toolbox function "anfis" constructs a fuzzy inference system (FIS) whose membership function parameters are tuned (adjusted) using either a backpropagation algorithm alone, or in combination with a least squares type of method. This allows the fuzzy systems to learn from the data they are modeling. A network-type structure similar to that of a NN, which maps inputs through input membership functions and associated parameters, and then through output membership functions and associated parameters to outputs, is used to interpret the input/output map. The parameters associated with the membership functions will change through the learning process. The computation of these parameters (or their adjustment) is facilitated by a gradient vector, which provides a measure of how well the fuzzy inference system is modeling the input/output data for a given set of parameters.

The ANFIS network chosen is shown in Figure 5.5 with a first-order Sugeno model. For each input v_i, five fuzzy sets U_{ji}, with the corresponding membership functions $\mu_{ji}(v_i)$, were chosen for i =1 to 3 (inputs) and j = 1 to 5. Thus, the ANFIS network has a total of 125 (5^3) fuzzy rules and one output, *F*. The rule structure, for e.g, the *n*-th rule is of the form:

If v_1 is U_{i1} and v_2 is U_{j2} and v_3 is U_{k3} then $f_n = d_{i1}v_1 + d_{j2}v_2 + d_{k3}v_3 + d_n$,

where $(d_{i1}, d_{j2}, d_{k3}, d_n)$ are adaptable parameters and $n = k + 5(j-1) + 25(i-1)$ for *i, j, k* =1 to 5.

The architecture of the ANFIS system shown in Figure 5.5 is explained below:

- *Layer 1*: Every node *i* in this layer is square node (takes in one input) with the node function given by

$$U_{ji} = \mu_{ji}(v_i) \tag{5.4}$$

where v_i is the input and $\mu_{ji}(v_i)$ is the activation function for the input v_i given by,

$$\mu_{ji}(v_i) = \left(1 + \left[(v_i - c_{ji}) / a_{ji}\right]^{2b_{ji}}\right)^{-1} \tag{5.5}$$

where (a_{ji}, b_{ji}, c_{ji}) are adaptable parameters.

- *Layer 2*: Every node in this layer is a circle node (takes in multiple inputs) labeled Π which multiplies the incoming signals and send the product out. For example,

$$w_1 = \mu_{11}(v_1) \times \mu_{12}(v_2) \times \mu_{13}(v_3) \tag{5.6}$$

- *Layer 3*: Every node in this layer is a circle node labeled *N*. The i^{th} node calculates the ratio of the i^{th} rule firing strength to the sum of all the rules firing strengths. For example,

$$\overline{w}_1 = \frac{w_1}{\sum_{n=1}^{125} w_n} \tag{5.7}$$

- *Layer 4*: Every node in this layer is a square node that generates the node output $f_n \overline{w}_n$.

- *Layer 5*: This is the output layer with single node that generates the final output by adding all the outputs of Layer 4.

$$F = \sum_{n=1}^{125} f_n \overline{w}_n \tag{5.8}$$

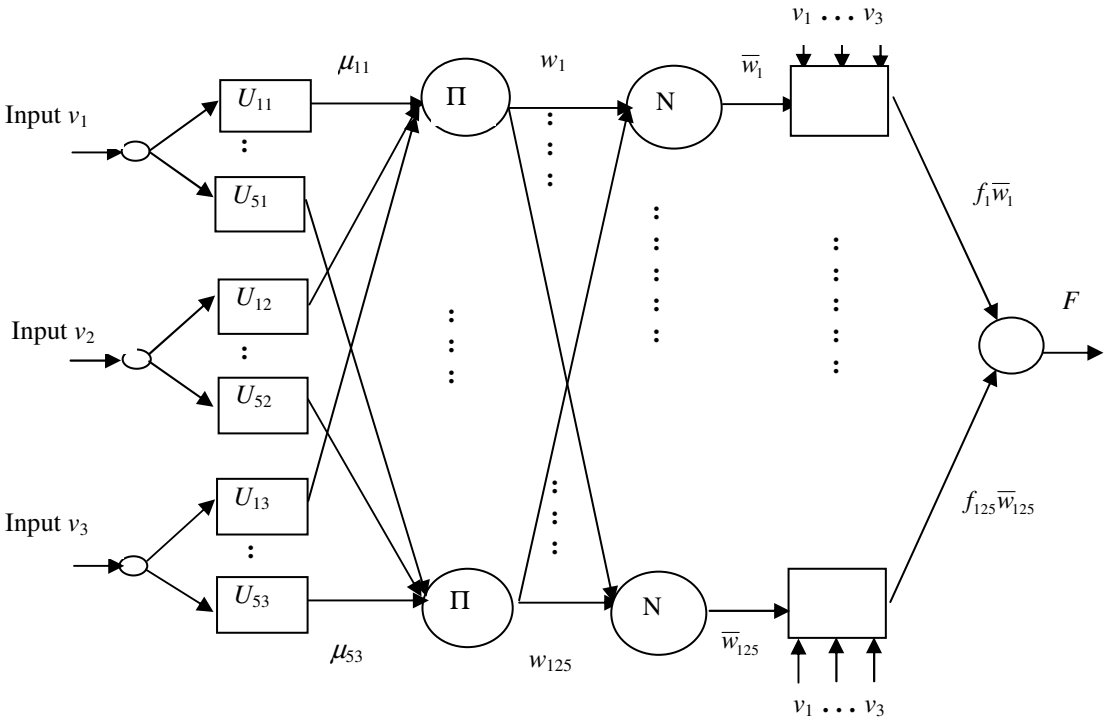

Figure 5.5 ANFIS architecture

5.4 Classification of HRV Signals

The characteristic measures are evaluated for their suitability for classification. The classification is done using three different classification techniques as discussed in the previous sections. Three features *SEN*, *SD1/SD2* and λ_1 extracted from the HRV signals are used for the proposed classification. These features are chosen based on trials for optimal performance in terms of better classification accuracy.

The NN classifier is implemented with 30 nodes in the radial basis layer and 8 nodes in the competitive layer. The classification results of the NN classifier is given in Table 5.1. The network is trained with 279 training vectors. The fuzzy classifier is implemented with Gaussian membership function. The classification results of the fuzzy classifier are given in Table 5.2. The ANFIS classifier is implemented with generalized bell-shaped membership. The network is trained with 279 datasets and back-propagation method is chosen for optimization. The initial and final (after training) input membership function for the input λ_1 is shown in Figure 5.6 and Figure 5.7. The "in1mf1" refers to the input1 membership function1. Each input is fuzzified with 5 membership functions. During the training phase the network converged at 100 epochs with a mean-squared-error of 9×10^{-3}. After training association, rules in the form of *if-then,* are generated and extracted. The final decision surfaces for input1 and input2, input1 and input3, and input3 and input2 are given in Figure 5.8, Figure 5.9 and Figure 5.10 respectively. The classification results of the ANFIS classifier is given in Table 5.3.

Fuzzy classifier works better than the NN classifier (Table 5.2). This classification is further improved using ANFIS classifier (Table 5.3). The classification accuracy is more than 90% for all disease classes in the neuro-fuzzy classifier. From Table 5.1, Table 5.2 and Table 5.3, it can be seen that there is a significant increase in the classification accuracy for cardiac abnormalities when ANFIS is used as classifier. The above results are compared with a simple IF-THEN-ELSE classifier using one input feature. The input feature value of the test data is compared with the range (mean $\pm$ standard deviation) of the feature values given in Table 3.3 and the correct class is identified. The classifier is tried with all the eleven features as input but with one at a time. Due to overlap in the range of values of some of the classes, the classification accuracy was about 60 to 70% as given in Table 5.4. For sake of fair comparison between different classifiers the same set of test data is used for all the classifiers including the simple classifier. When the simple classifier is tried with a combination of two or more inputs, the classification accuracies are poor. Even though the features are statistically significant for many groups but only intelligent classifiers using nonlinear techniques yield better accuracy and improved classification. These intelligent classifiers with fine tuning and training can yield better results and has to be evaluated for more cardiac abnormalities.

The neural network classifier, fuzzy classifier and ANFIS classifier are presented as diagnostic tools to aid the physician in the analysis of heart diseases. However, these tools generally do not yield results with 100% accuracy. The accuracy of the tools depend on several factors, such as the size and quality of the training set, the rigor of the training

imparted, and the inputs itself. However, from the analysis of the results listed in Table 5.1, Table 5.2 and Table 5.3, it is evident that the classifiers presented are effective to the tune of more than 80% accuracy.

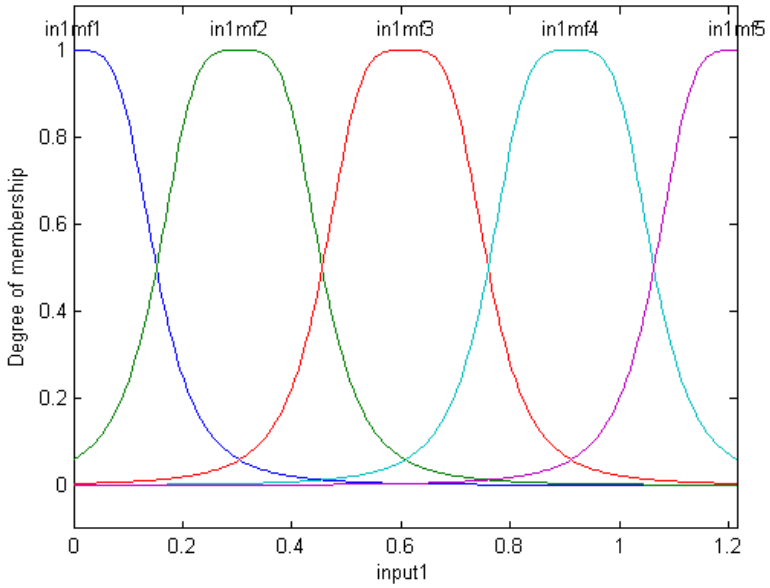

Figure 5.6 Initial membership function for input 1(λ_1)

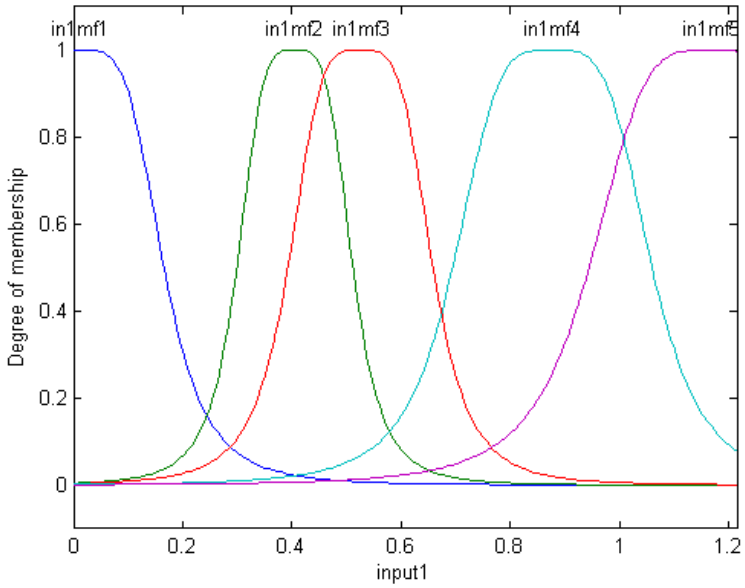

Figure 5.7 Final membership function for input 1(λ_1)

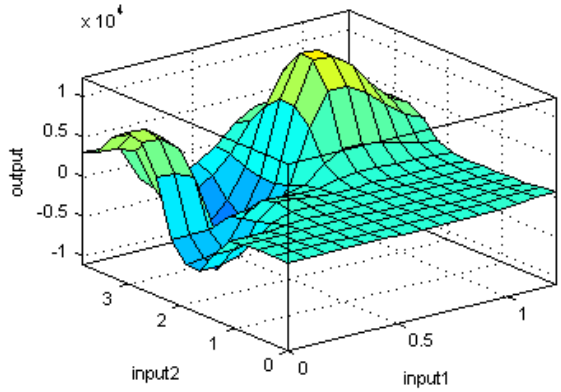

Figure 5.8 Final decision surface for input 1(λ_1) and input 2 (*SEN*)

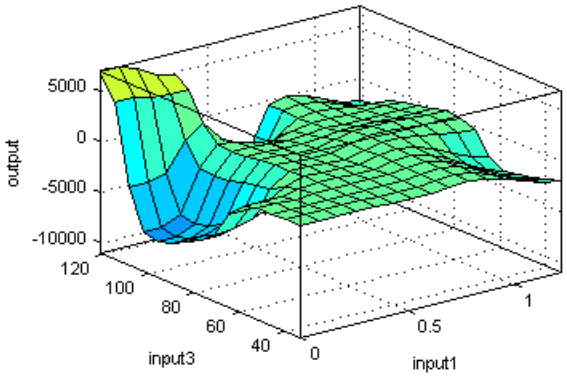

Figure 5.9 Final decision surface for input 1(λ_1) and input 3 (*SD1/SD2*)

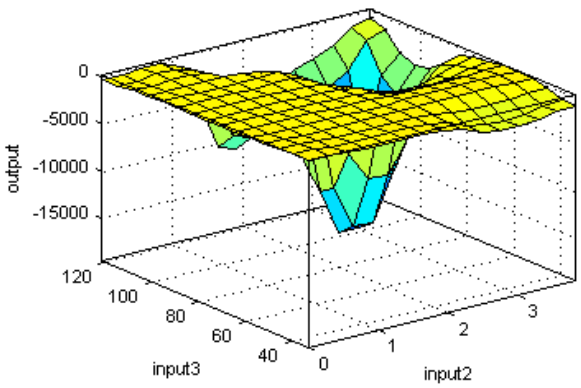

Figure 5.10 Final decision surface for input 3(*SD1/SD2*) and input 2 (*SEN*)

HRV signal types	No. of datasets (training)	No. of datasets (testing)	Classification accuracy
LBBB	28	18	88.88
NSR	60	40	87.5
PVC	45	30	86.66
AF	30	25	85
VF	28	25	92
CHB	28	25	84
ISCH	30	22	86.36
SSS	30	22	90.9

Table 5.1 Results of ANN classifier

HRV signal types	No. of datasets (training)	No. of datasets (testing)	Classification accuracy
LBBB	28	18	83.33
NSR	60	40	92.5
PVC	45	30	86.66
AF	30	25	88
VF	28	25	92
CHB	28	25	88
ISCH	30	22	86.36
SSS	30	22	90.9

Table 5.2 Results of fuzzy classifier

HRV signal types	No. of datasets (training)	No. of datasets (testing)	Classification accuracy
LBBB	28	18	88.88
NSR	60	40	95
PVC	45	30	93.33
AF	30	25	92
VF	28	25	88
CHB	28	25	92
ISCH	30	22	90.91
SSS	30	22	90.91

Table 5.3 Results of ANFIS classifier

Input Feature	Classification Accuracy
α -slope	67.3%
SD1/SD2	61.1%
D_2	77.1%
λ_1	70.9%
H	72.0%
SEN	75.6%
REN	61.1%
$APEN$	60.4%
$KSEN$	61.5%
$D^{Higuchi}$	61.8%
D^{Katz}	73.1%

Table 5.4 Results of a simple classifier implemented with one input feature

5.5 Classification of EEG Signals

The characteristic measures of the EEG signals discussed in Chapter 4 are evaluated for the suitability to do classification. The classification is done using three different classification techniques discussed in the sections 5.1, 5.2 and 5.3. The four entropy estimators SEN, REN, $KSEN$ and $APEN$ are used as inputs to the classifiers.

The NN classifier is implemented with 12 nodes in the radial basis layer and 3 nodes in the competitive layer. The classification results of the NN classifier is given in Table 5.5. The network is trained with 180 training vectors. The fuzzy classifier is implemented with Gaussian membership function. The classification results of the fuzzy

classifier are given in Table 5.6. The ANFIS classifier is implemented with generalized with generalized bell shaped membership function. The ANFIS network chosen with a first-order Sugeno model is used as given in Figure 5.11. For each input v_i, three fuzzy sets U_{ji}, with the corresponding membership functions $\mu_{ji}(v_i)$, were chosen for i =1 to 4 and j = 1 to 3.

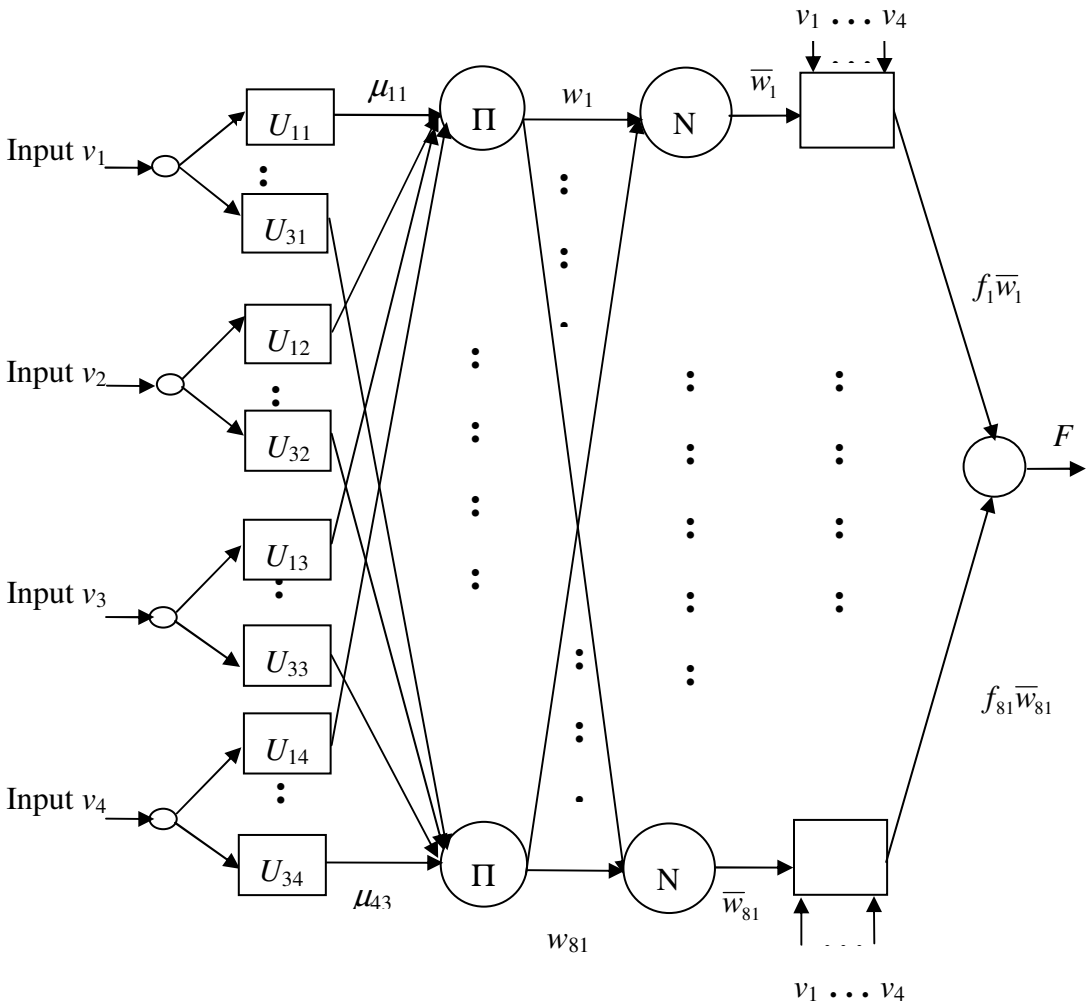

Figure 5.11 ANFIS architecture for classification of EEG signals

EEG signal types	No. of datasets (training)	No. of datasets (testing)	Classification accuracy
Normal	60	43	88.37
Epileptic	60	47	82.98
Background	60	47	85.11

Table 5.5 Results of ANN classifier for EEG signal classification

EEG signal types	No. of datasets (training)	No. of datasets (testing)	Classification accuracy
Normal	60	43	93.02
Epileptic	60	47	89.36
Background	60	47	85.11

Table 5.6 Results of FUZZY classifier for EEG signal classification

EEG signal types	No. of datasets (training)	No. of datasets (testing)	Classification accuracy
Normal	60	43	93.02
Epileptic	60	47	91.49
Background	60	47	91.49

Table 5.7 Results of ANFIS classifier for EEG signal classification

With one input		With two inputs	
Input feature	Classification Accuracy	Input features	Classification Accuracy
CD	83.3%	*CD & SEN*	86.7%
LE	62.5%	*CD & LE*	72.5%
H	41.7%	*CD & KSEN*	76.7%
KSEN	73.3%	*APEN & SEN*	77.5%
APEN	35.8%	*SEN & KSEN*	80.0%
SEN	93.3%	*REN & SEN*	76.7%
REN	59.2%	*SEN & H*	61.7%

Table 5.8 Results of simple classifier implemented with one/ two input features.

Table 5.5, Table 5.6 and Table 5.7 shows the results of EEG signal classification. The classification accuracy of more than 80% is achieved with the entropy estimators as input to the classifiers. ANFIS classifier gives a better classification accuracy of more than 90% when compared to the other classifiers. The above results are compared with the results of a simple IF-THEN-ELSE classifier using one / two input features given in Table 5.8. The simple classifier is implemented in the same way as it is implemented for classifying HRV signals. It can be seen that in certain cases the accuracy is even better than the intelligent classifiers. This may be due to the fact that the number of classes for identification is only three and that particular feature is completely significant for the three classes considered. The classification accuracy was about 70% when two features are used in combination for classification using the simple classifier. These classifiers may not perform well when more number of classes is considered as there will be some overlap in the features of different groups. In that scenario, intelligent classifiers are needed and need to be tuned for optimal performance. In this work, we evaluated three intelligent classifiers and ANFIS classifier performed better compared to the other two classifiers.

5.6 Conclusion

Three types of classifier architectures are described in this chapter. These classifier architectures classify the HRV and EEG signals with an accuracy of about 90%. The classifiers can identify the various abnormalities using the extracted feature set of

HRV and EEG signals. To further understand the characteristics of the signal, to predict the signal and to generate synthetic data, it is necessary to model the signals. The modeled signals are valid only if they exhibit similar characteristics as the original signal. Modeling of the HRV and EEG signals using linear and nonlinear modeling techniques are discussed in Chapter 6 and Chapter 7, respectively.

Chapter 6 Linear Modeling of Heart and Brain Signals

The nonlinear dynamics of the HRV and EEG signals presented in Chapter 3 and Chapter 4 aid to the diagnosis of various cardiac and mental health states discussed in Chapter 5. To further understand the characteristics and enhance the analysis of the signals, it is necessary to model these signals. The modeled signals are valid only if they exhibit similar characteristics as the original signal. In this work, first we propose linear techniques to model the HRV and EEG signals analyze the performance in detail.

6.1 Signal Modeling

Signal modeling is an important step in signal processing. Once the model of a signal is identified, characteristics of that signal can be easily controlled by changing the parameters of this model. The synthesized signal can then be used to validate and compare various signal processing algorithms. In addition, if the model does faithfully reflect the physiological process of the signal, it can be used to study the physiological mechanism of this signal as well.

Extracting useful clinical information from the experimental (noisy) ECG requires the application of reliable signal processing techniques. These include R-peak detection, QT-interval detection, and the derivation of heart rate and respiration rate from the ECG. The variability of the R-R intervals reveals important information about the physiological state of the subject.

At present, new biomedical signal processing algorithms are usually evaluated by applying them to ECGs acquired from real patients. Usually it will be of short duration not sufficiently long enough for the evaluator to decide on the accuracy and reliability of a given algorithm. To facilitate this evaluation, it is required to generate longer duration signals from these short duration signals while preserving the characteristics of the signal in time domain and as well as in frequency domain. A realistic artificial biomedical signal generator that is able to encompass the range of signals observed for both normal and abnormal subjects is therefore a useful tool. Furthermore, the ability to rapidly create a re-generable time series enables a researcher to quickly prototype applications and test theories on both normal and abnormal signals. The linear models for generating a synthetic HRV and EEG signals with realistic and prescribed dynamical characteristics is discussed in this chapter.

In this chapter, a detailed discussion on the prediction of HRV and EEG signals using linear techniques is presented. The simulated signal is validated using the frequency domain measures of LF and HF components. The time-domain performance

measures such as normalized root mean square error (NRMSE) and the signal to noise ratio (SNR) are also used for comparison.

The NRMSE is the most popular measure of the differences between the values predicted by a model and the actual values. NRMSE is given by

$$NRMSE = \frac{\sqrt{E(\hat{\mathbf{x}} - \mathbf{x})^2}}{x_{\max} - x_{\min}} \tag{6.1}$$

where $E(\hat{\mathbf{x}} - \mathbf{x})^2$ is the mean of the square of the error, $\hat{\mathbf{x}}$ is the predicted signal, $\mathbf{x}$ is the actual signal, $x_{\max}$ is the maximum value of the signal $\mathbf{x}$ and $x_{\min}$ is the minimum value of the signal $\mathbf{x}$.

The SNR is defined as the ratio of signal power to the noise power present in the signal under consideration. It is given by

$$SNR = \frac{P_{signal}}{P_{noise}} = \left(\frac{A_{signal}}{A_{noise}} \right)^2 \tag{6.2}$$

where P is the average power and A is the amplitude. Usually SNR is expressed in dB and is given by

$$SNR(dB) = 10\log_{10}\left(\frac{P_{signal}}{P_{noise}} \right) = 20\log_{10}\left(\frac{A_{signal}}{A_{noise}} \right) \tag{6.3}$$

6.2 Modeling Techniques

Signal modeling is concerned with the representation of signals in an efficient manner. In general, there are two steps in the modeling process. The first is to choose an appropriate parametric form for the model. Once the form of the model has been selected, the next step is to find the model parameters that provide the *best* approximation to the given signal. There are, however, many different ways to define what is meant by the best approximation. Based on the definition that is used, there will be different solutions to the modeling problem along with different techniques for finding the model parameters. Therefore, in developing an approach to signal modeling, it is important not only to find a model that is useful, i.e., works well, but one that has a computationally efficient procedure for deriving the model parameters from the given data.

6.3 Linear Models

Linear modeling techniques are based on the estimation of a linear time-invariant model that has white noise as input and the signal to be analyzed as output. There are power spectrum estimate methods that use models without zeros (AR) and models without poles (MA). AR models lead to power spectrum with sharp peaks. Moreover the linear equations, to find the coefficients of AR models, are simpler to be solved. The various AR modeling techniques are Yule-Walker, Burg, covariance, and modified covariance methods. The Yule-Walker and covariance methods solve the set of linear

equations by minimizing the forward prediction error in the least squares sense. The Burg and modified covariance methods solve the set of linear equations by minimizing the forward and backward prediction errors in the least squares sense. The Yule-Walker and Burg approaches always guarantee a stable model. Unfortunately, the performance of the Yule-Walker approach degrades when the number of samples decreases. The covariance-based approaches perform well also when the model order p is chosen smaller than the number of sinusoids actually present in the analyzed signal. The Burg's approach yields a more stable and robust to estimate of the AR model parameters [100].

6.3.1 Parametric Model

The AR model [100, 101] is one of the linear prediction techniques that attempt to predict an output $\hat{x}(n+1)$ of a system based on the previous inputs $(x(n), x(n-1), x(n-2), ..., x(n-p))$, where p is the order of the predictor. It is also known in the filter design industry as an infinite impulse response filter (IIR) or an all pole filter, and is sometimes known as a maximum entropy model in physics applications. The definition used here is as follows:

$$\hat{x}(n+1) = \sum_{i=1}^{p} a_i . x(n-i) + \varepsilon(t) \tag{6.4}$$

where $a_i, i = 1,2,\cdots, p$ are the AR coefficients. The noise term or residue, $\varepsilon(t)$ in the equation (6.4), is almost always assumed to be Gaussian white noise. The current term of the series can be estimated by a linear weighted sum of previous terms in the series. The

weights are the autoregression coefficients. The problem in AR analysis is to derive the "best" values for a_i given a series $\{x(i); i = 1,2,\ldots,N\}$. The majority of methods assume the series $\mathbf{x}$ is linear and stationary. By convention the series $\mathbf{x}$ is assumed to be zero mean, if not this is simply another term a_0 in front of the summation in the equation above.

The power spectrum of a p^{th} order AR process is

$$P_{xx}^{BU}(f) = \frac{\sigma^2}{\left|1 + \sum_{k=1}^{p} a_k \, e^{-j2\pi fk}\right|^2} \tag{6.5}$$

where σ^2 is the driving white noise variance. The Burg method results in high resolution and yields a stable AR model.

It is essential to choose the appropriate model order. The order of the AR model has a major effect on the spectral estimate for the time series. Too low order will result in a smoothed spectrum and too high order will increase the resolution of the spectrum and introduce spurious peaks. The estimate for the power associated with the single component is also dependent on the order that is selected. The orders p=15-20 are often satisfactory for heart rate signal prediction. Several penalty function methods for model order selection exist that utilize the prediction error variance such as FPE (final prediction error) and AIC (Akaike information criteria) [102, 103].

6.4 Modeling of HRV Signals

The model is to provide a standard realistic HRV signal with known characteristics. The main characteristics of an HRV signal are discussed in Chapter 3. In the time domain, the signal is neither periodic nor completely random and in the frequency domain, the signal consists mainly of three spectral peaks, i.e., a high frequency (HF) peak around 0.20 Hz**,** a low frequency (LF) peak around 0.10 Hz, and a very low frequency (VLF) peak, which is also called the l/f component because its spectral magnitude increases with the decrease of frequency. Thus, the simulated HRV signal must atleast be able to reveal the following characteristic parameters: the HF component frequency, the LF component frequency, and the parameters governing the l/f spectrum of the VLF component.

Generating a long duration HRV signal from the given short duration signal facilitates a comparison of different signal processing techniques. The HRV signal generated with the prescribed time domain and frequency domain characteristics can be used for diagnostic purposes by predicting the nature of the HRV signals. The model also can be used for numerous applications such as (i) the synthetic HRV could be used to assess the effectiveness of different techniques for noise and artifact removal. These could be evaluated by adding noise and/or artifact onto the synthetic signal and then comparing the original with the processed signal. (ii) Abnormal morphological changes could be introduced to the lead II signal and the long term changes could be observed and (iii) Abnormal beats can be predicted on a long run and used for diagnostic purposes. The

linear modeling techniques discussed in Section 6.3 are applied to eight different types of HRV signals. The original NSR, VF, AF, ISCH, CHB, LBBB, PVC and SSS segments, the corresponding AR modeled segments reconstructed using Burg's method and the error signals are shown in Figure 6.1. The error signal obtained by comparing the original and the reconstructed signal.

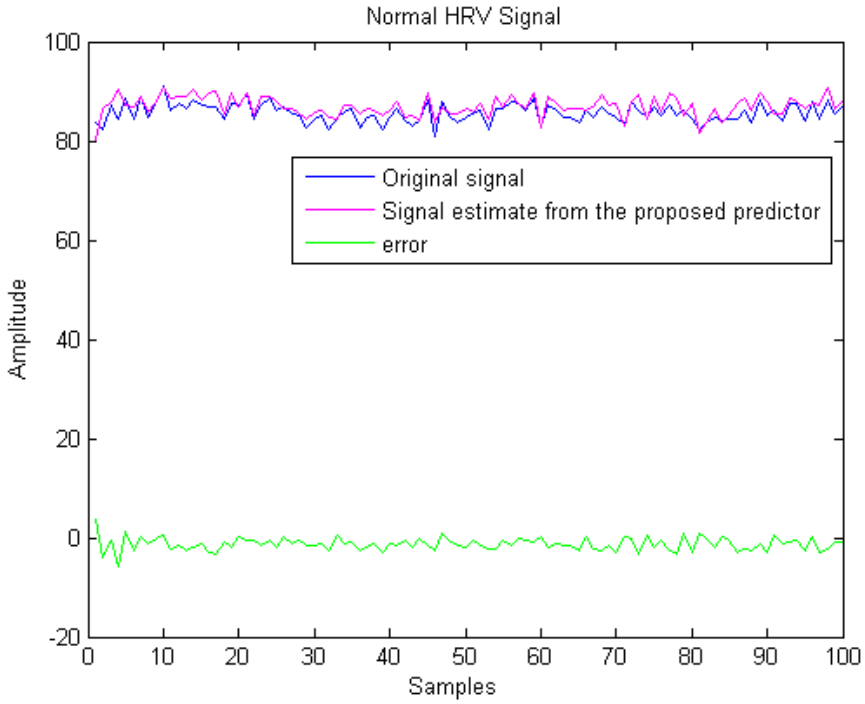

(a)

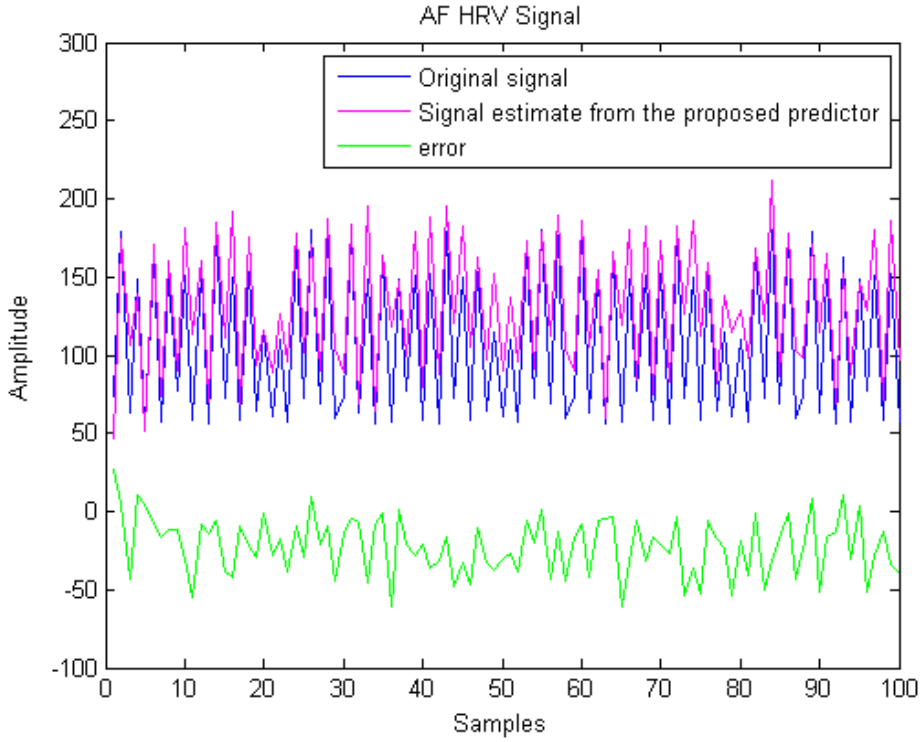
AF HRV Signal
Original signal
Signal estimate from the proposed predictor
error
Amplitude
Samples
300
250
200
150
100
50
0
-50
-100
0
10
20
30
40
50
60
70
80
90
100

(b)

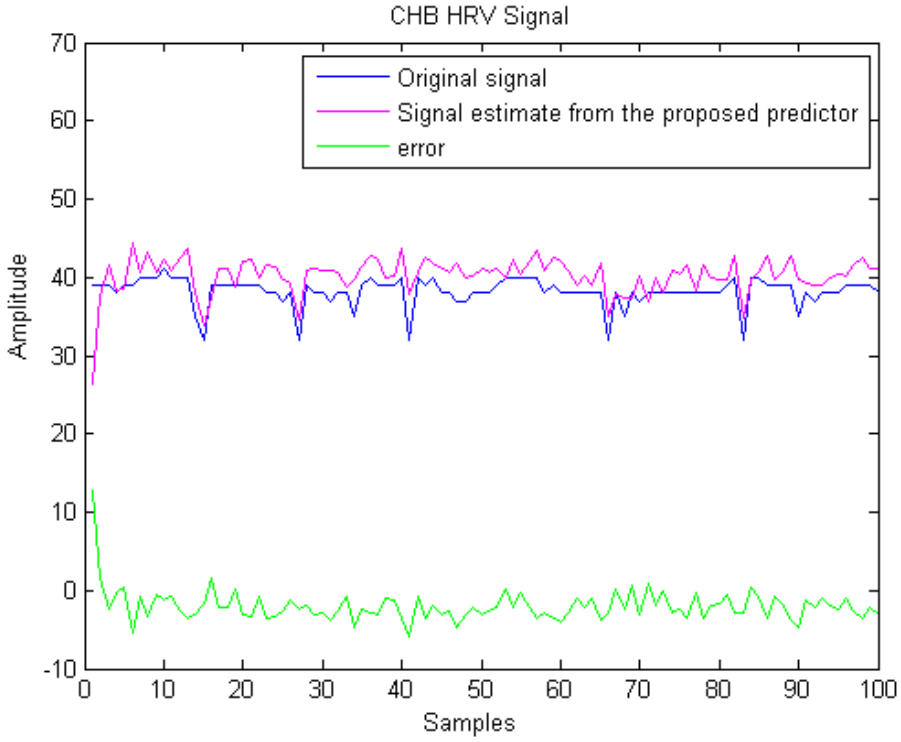
CHB HRV Signal
Original signal
Signal estimate from the proposed predictor
error
Amplitude
Samples
70
60
50
40
30
20
10
0
-10
0
10
20
30
40
50
60
70
80
90
100

(c)

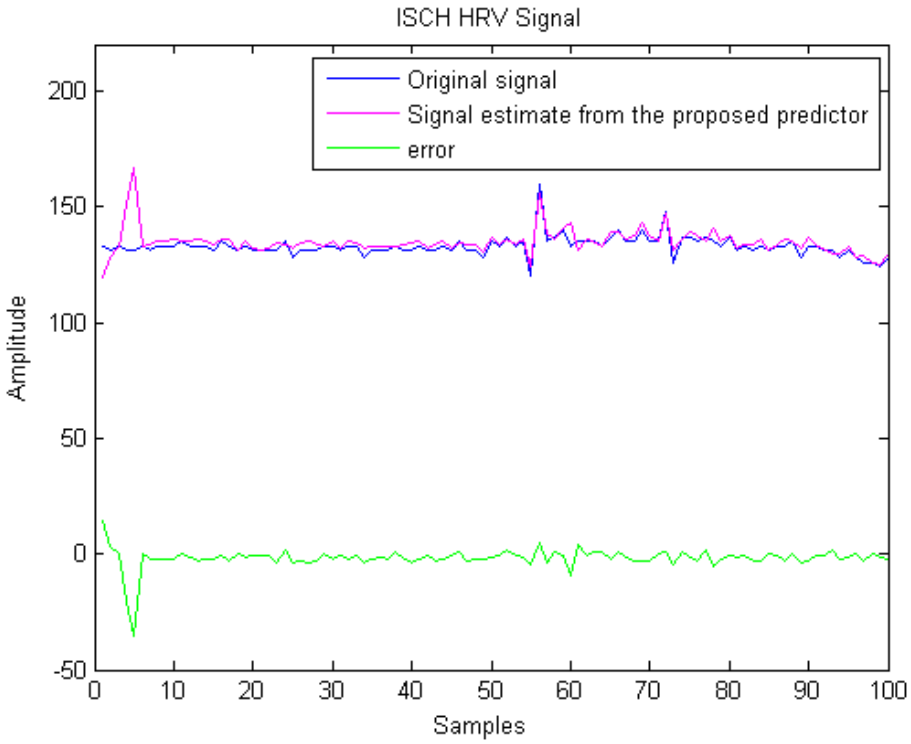
ISCH HRV Signal
Original signal
Signal estimate from the proposed predictor
error
Amplitude
Samples
200
150
100
50
0
-50
0
10
20
30
40
50
60
70
80
90
100

(d)

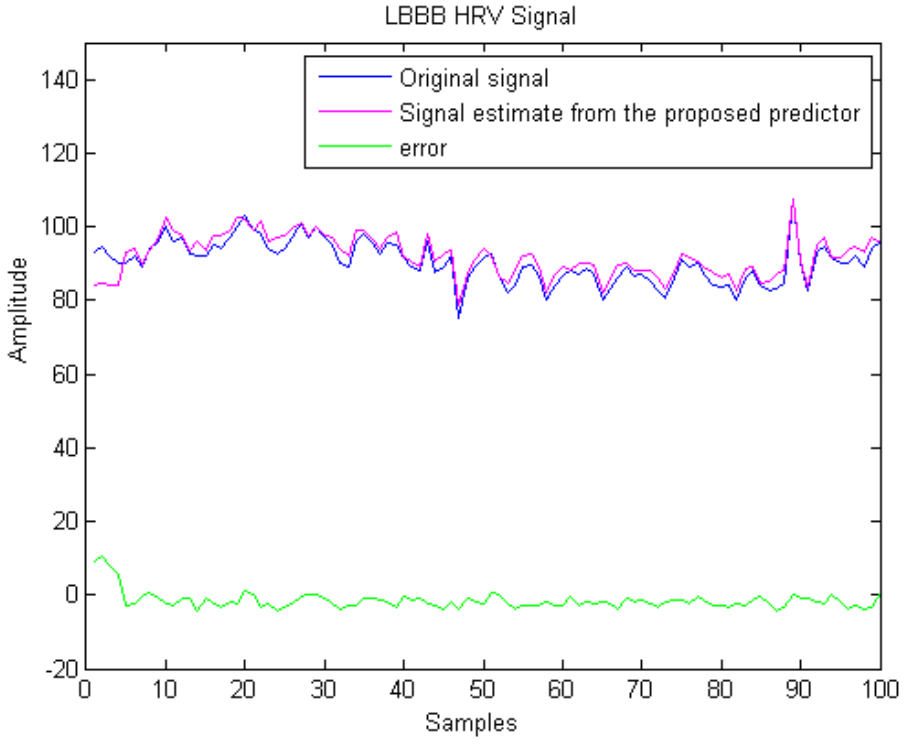
LBBB HRV Signal
Original signal
Signal estimate from the proposed predictor
error
Amplitude
Samples
140
120
100
80
60
40
20
0
-20
0
10
20
30
40
50
60
70
80
90
100

(e)

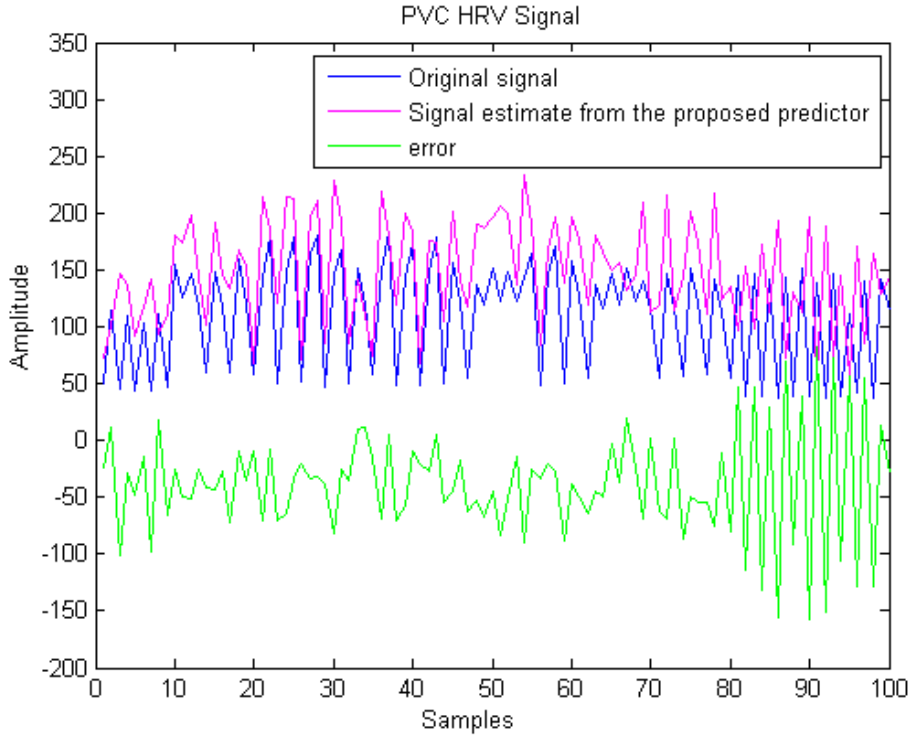
PVC HRV Signal
Original signal
Signal estimate from the proposed predictor
error
Amplitude
Samples
350
300
250
200
150
100
50
0
-50
-100
-150
-200
0
10
20
30
40
50
60
70
80
90
100

(f)

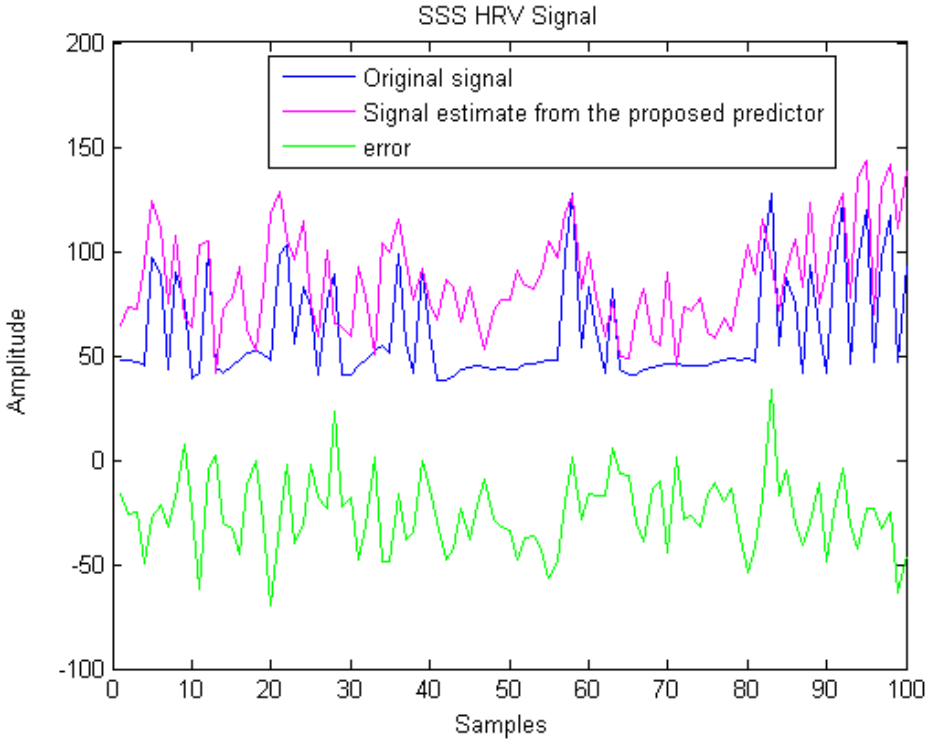
SSS HRV Signal
Original signal
Signal estimate from the proposed predictor
error
Amplitude
Samples
200
150
100
50
0
-50
-100
0
10
20
30
40
50
60
70
80
90
100

(g)

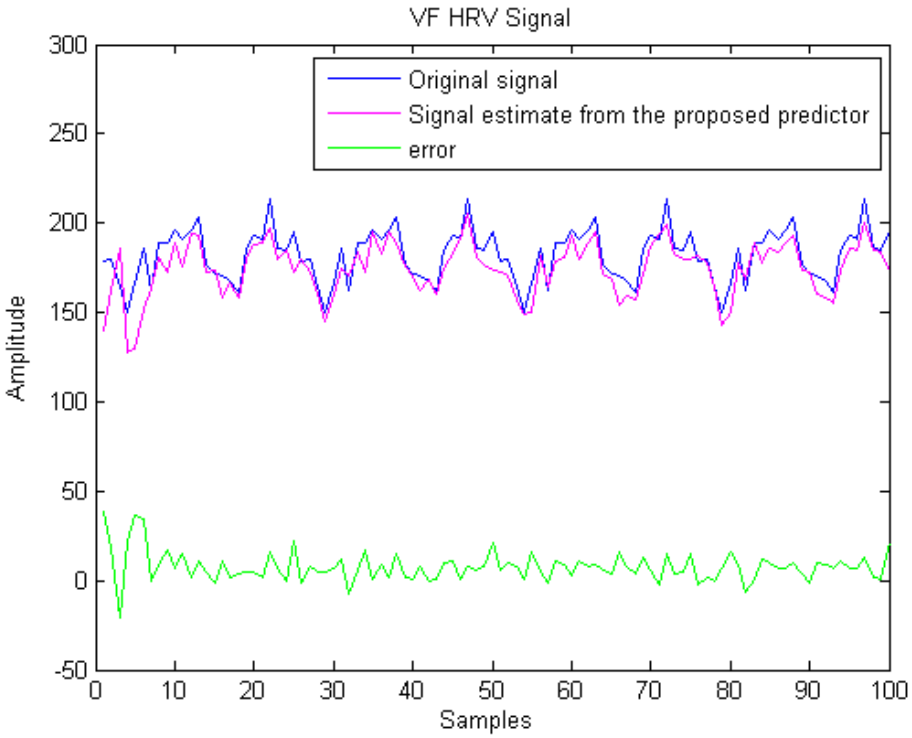

(h)

Figure 6.1 Original, reconstructed and error signals for various HRV signals using the AR modeling technique.

The signals are reconstructed using an All-Pole Filter with White Noise as Input. Thirty datasets are reconstructed for each class of the HRV signal with each dataset having 200 samples. Two main criteria, SNR and NRMSE are used to evaluate the performance of the linear model. The SNR was calculated to be from 15 dB to 35 dB. Table 6.1 shows the SNR and the NRMSE of the predicted HRV signals.

HRV signal types	SNR	NRMSE
NSR	21	0.49±0.13
AF	30	21.63±1.31
VF	30	10.68±0.53
CHB	26	7.32±1.11
ISCH	24	10.54±1.63
PVC	30	31.33±1.91
SSS	30	26.69±3.12
LBBB	21	2.61±1.22

Table 6.1 SNR and NRMSE (%) values of the predicted signals using Burg's method.

6.4.1 Validation of the Signal Model

The generated HRV signals are validated using LF/HF ratio and the chaotic invariant measures. The commonly used frequency domain measure for HRV signal is the low frequency/ high frequency (LF/HF) ratio, defined as the ratio of power between 0.015–0.15 Hz and 0.15–0.4 Hz in the R-R tachogram. The LF/HF power ratio of the HRV signals varies for various cardiac abnormalities and aids in the assessment of cardiovascular disease. The heart rate may be increased by slow acting sympathetic activity or decreased by fast acting parasympathetic (vagal) activity. The balance between the effects of the sympathetic and parasympathetic systems, the two opposite acting branches of the autonomic nervous system, is referred to as the sympathovagal balance and is believed to be reflected in the beat-to-beat changes of the cardiac cycle. The heart rate is given by the reciprocal of the R-R interval in units of beats per minute. Spectral

analysis of the R-R tachogram is typically used to estimate the effect of the sympathetic and parasympathetic modulation of the R-R intervals. The two main frequency bands of interest are referred to as the LF band (0.04–0.15 Hz) and the HF band (0.15–0.4 Hz). Sympathetic tone is believed to influence the LF component whereas both sympathetic and parasympathetic activity has an effect on the HF component. The ratio of the power contained in the LF and HF components has been used as a measure of the sympathovagal balance.

From the Figure 6.1, it can be that the modeled signal closely follows the original signal in the time domain. In frequency domain, the results of LF/HF ratio given in Table 6.2 measure indicate the preservance of the frequency domain features in the predicted signal. The % difference of the ratio between the modeled and actual signal is less than 10% for modeled signal using Burg's method. The modeled signals are also validated using the chaotic measures discussed in Chapter 3. The results of the chaotic measures of the synthesized HRV signals modeled using the Burg's method is given in Table 6.4. By comparing the results with the results of the actual signal given in Table 6.3, it can be seen that the Burg's method results closely follows the actual signal results. It can be seen that the results of the FDs and *H* are not significant for each class. The variation of the characteristic features is more than 10% for the synthesized signals as compared to the actual signal.

HRV SIGNAL TYPES	LF/HF RATIO		
		BURG	
	ORIGINAL SIGNAL	PREDICTED SIGNAL	% difference
NSR	0.8635	0.8861	2.6141
LBBB	0.2441	0.2642	8.2516
PVC	1.3453	1.2122	9.8938
AF	0.5498	0.5581	1.5010
VF	0.2853	0.3011	5.5316
CHB	1.1532	1.2529	8.6417
ISCH	2.9948	3.2674	9.1041
SSS	0.4185	0.4378	4.6202

Table 6.2 Comparison of LF/HF Ratio of the predicted signals with the original signal.

Chaotic measures	NSR	PVC	LBBB	AF	VF	CHB	SSS	ISCH
D_2	3.58	2.29	3.2	2.58	2.9	2.72	2.35	3.3
λ_1	0.5	0.62	0.47	0.56	0.42	0.17	0.82	0.193
H	0.611	0.873	0.643	0.796	0.706	0.748	0.821	0.654
KSEN	0.573	0.496	0.429	0.445	0.409	0.457	0.278	0.34
APEN	1.75	1.51	1.47	1.57	1.09	0.97	1.57	0.76
SEN	1.63	1.14	1.24	1.2	1.06	0.86	1.27	1.12
REN	3.481	2.46	2.72	2.63	2.32	2.19	2.76	2.42
$D^{Higuchi}$	1.36	1.19	1.31	1.21	1.27	1.24	1.21	1.32
D^{Katz}	1.58	1.31	1.53	1.39	1.46	1.41	1.36	1.52

Table 6.3 Chaotic measures of HRV signal - Actual.

Chaotic measures	**NSR**	**PVC**	**LBBB**	**AF**	**VF**	**CHB**	**SSS**	**ISCH**
D_2	3.513	2.268	3.17	2.578	2.85	2.641	2.329	3.299
λ_1	0.475	0.538	0.465	0.525	0.389	0.138	0.795	0.13
H	0.527	0.789	0.612	0.752	0.608	0.71	0.721	0.599
KSEN	0.492	0.458	0.402	0.372	0.354	0.434	0.215	0.314
APEN	1.705	1.438	1.404	1.56	1.049	0.966	1.542	0.734
SEN	1.544	1.101	1.228	1.144	0.974	0.797	1.187	1.021
REN	3.471	2.439	2.706	2.626	2.26	2.103	2.737	2.34
$D^{Higuchi}$	1.301	1.111	1.257	1.159	1.259	1.151	1.123	1.232
D^{Katz}	1.533	1.309	1.493	1.348	1.368	1.387	1.334	1.519

Table 6.4 Chaotic measures of modeled HRV signal – Burg's method.

6.5 Modeling of EEG Signals

The linear modeling techniques discussed in Section 6.3 are used to model the three categories of the EEG signals – normal, background and epileptic. The AR model is implemented with the model order p=16. The original EEG signals and the corresponding reconstructed signal using Burgs method along with the error is given in Figure 6.2. Two main criteria, NRMSE and SNR are used to evaluate the performance of the linear model. The results are given in Table 6.5.

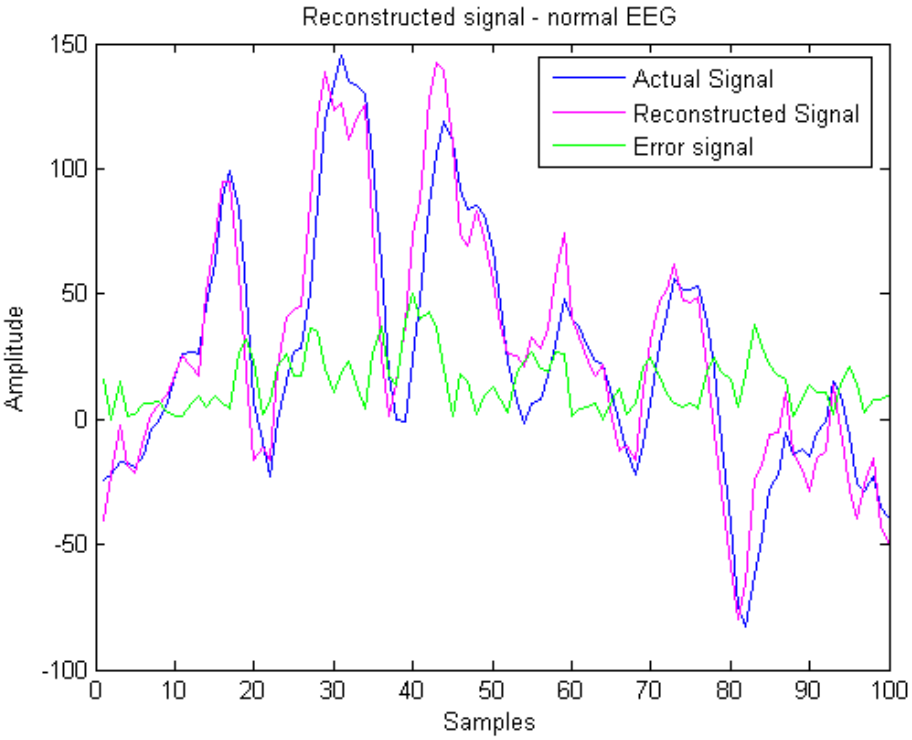
Reconstructed signal - normal EEG
Actual Signal
Reconstructed Signal
Error signal
Amplitude
Samples
150
100
50
0
-50
-100
0
10
20
30
40
50
60
70
80
90
100

(a)

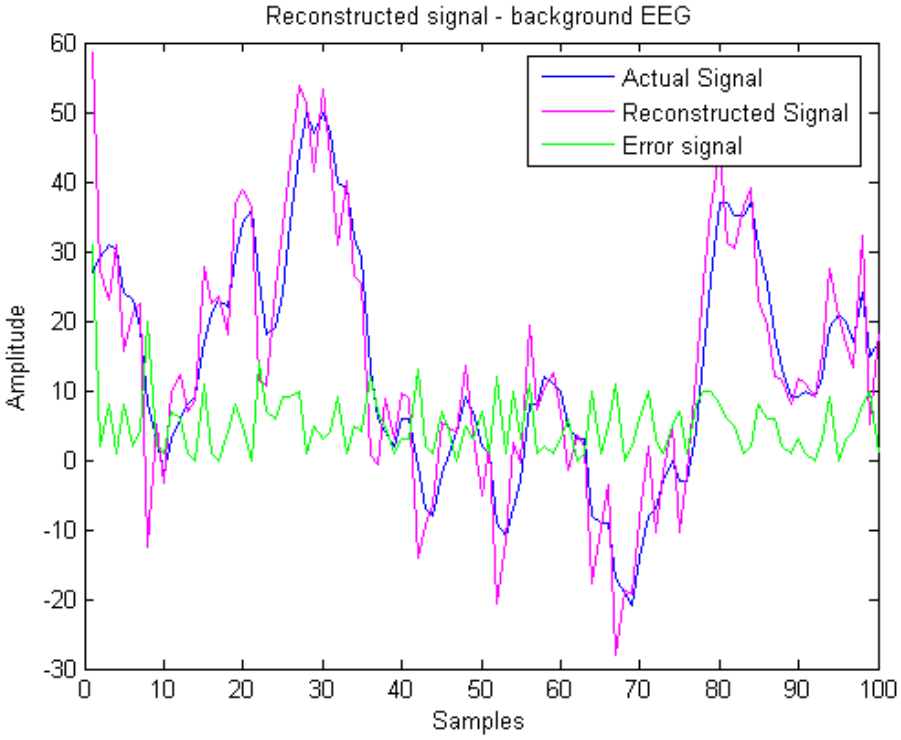
Reconstructed signal - background EEG
Actual Signal
Reconstructed Signal
Error signal
Amplitude
Samples
60
50
40
30
20
10
0
-10
-20
-30
0
10
20
30
40
50
60
70
80
90
100

(b)

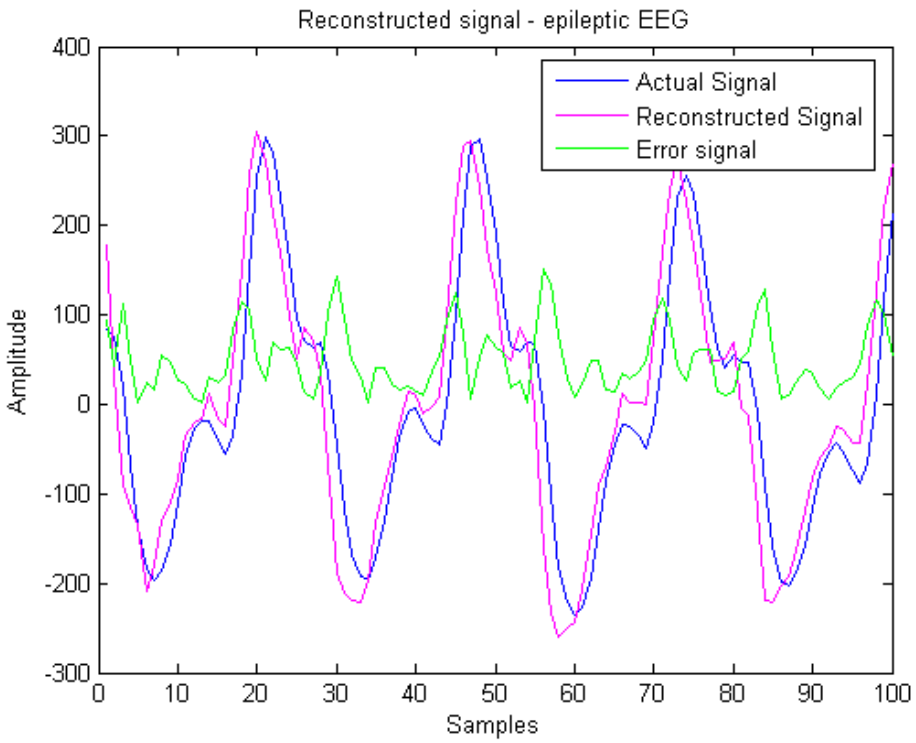

(c)

Figure 6.2 Actual and reconstructed EEG signals using Burg's method

EEG signal Types	**SNR**	**NRMSE**
Normal	16	8.691±1.121
Background	18	6.621±1.561
Epileptic	15	14.368±1.253

Table 6.5 SNR and NRMSE (%) values of the predicted signals from the model.

6.5.1 Validation of the Signal Model

The synthesized EEG signals are validated using the nonlinear characteristic measures discussed in Chapter 4. The results of the synthesized normal, background and epileptic EEG signals are given in Table 6.6, Table 6.7 and Table 6.8 respectively. The characteristics measures are calculated for all the categories of the EEG signals reconstructed using the Burg's method. It can also be seen that the characteristic measures are not distinct for the three categories. This may be due to the fact that the linear models are unsuccessful in capturing the nonlinear features of the signal.

Chaotic measures	**Actual**	**Burg**
D_2	4.8768	4.5672
λ_1	0.2036	0.1876
H	0.3248	0.2974
KSEN	0.6033	0.5788
APEN	0.7096	0.6933
SEN	-0.2215	-0.2341
REN	-0.1927	-0.2109
$D^{Higuchi}$	1.5132	1.4874
D^{Katz}	1.8649	1.7991

Table 6.6 Chaotic measures of the modeled normal EEG signal

Chaotic measures	**Actual**	**Burg**
D_2	4.3451	4.1141
λ_1	0.1912	0.1832
H	0.3411	0.3121
$KSEN$	0.5391	0.5121
$APEN$	0.6731	0.6534
SEN	-0.4818	-0.5121
REN	-0.183	-0.2012
$D^{Higuchi}$	1.4051	1.2987
D^{Katz}	1.5634	1.4521

Table 6.7 Chaotic measures of the modeled background EEG signal

Chaotic measures	**Actual**	**Burg**
D_2	3.9407	3.7534
λ_1	0.1845	0.1564
H	0.3563	0.3231
$KSEN$	0.4926	0.4571
$APEN$	0.6484	0.6153
SEN	-0.735	-0.7561
REN	-0.195	-0.2111
$D^{Higuchi}$	1.3546	1.2567
D^{Katz}	1.5139	1.3967

Table 6.8 Chaotic measures of the modeled epileptic EEG signal

6.6 Conclusion

In this chapter, we discussed the modeling of the HRV and EEG signals using linear techniques. The parametric modeling using Burg's method is implemented. The modeled signals are given and the performances of the models are evaluated using NRMSE and SNR as the performance measures. The signals are validated using the characteristic measures as well. From the results it can be seen that the nonlinear and chaotic measures are not significant for each case using the modeled signals. This may be because the linear models are unable to completely capture the nonlinearity in the signal being modeled. This necessitates the need for the nonlinear models which is discussed in Chapter 7.

Chapter 7 Nonlinear Modeling of Heart and Brain Signals

7.1 Nonlinear Modeling

In conventional modeling, it is assumed that the signal is the output of a linear system driven by random noise. In other words, signals are treated as realizations of some random process and the underlying systems are modeled as linear [100, 104]. After the discovery of chaos, deterministic systems with few degrees of freedom can produce signals that exhibit uncertainty and possess noise like spectra [105]. A chaotic system is a nonlinear dynamical system and the uncertainty existing in its output is originated from the system dynamics instead of an external driving force. Therefore, it is appropriate to apply nonlinear methods to model the underlying dynamics of the chaotic signal such as the HRV signal and EEG signal and is discussed in detail in this chapter.

ANN, regarded as a dynamical system, is a powerful tool for modeling nonlinearity [106]. The relaxation of the neural networks can exhibit a rich variety of dynamical behavior [107, 108]. This property is highly desirable in dynamic modeling to preserve the dynamics of the original system. The advantage of ANN is their ability to

generalize what they learn during training to new situations. If the signal to be modeled is noisy and has finite length, it is desirable that a model is able to interpolate and extrapolate the mapping from the training examples in a sensible way. Due to their plasticity, function approximation capability, wide spectrum of possible dynamics and generalization capability, ANNs are often used as a tool in modeling nonlinear signals.

7.2 Modeling Techniques

There are several ANN architectures that are used for modeling signals. Recurrent neural networks (RNN) involving dynamic elements and internal feedback connections have been considered to be more suitable for nonlinear modeling purposes [109]. In the last few years, various works have been presented showing that the recurrent neural networks are quite effective in modeling nonlinear dynamical systems. [110,111]. The critical issue in the application of RNN is the choice of network architecture and the training (suitable) algorithm. For the application of modeling HRV and EEG signals, a recurrent Elman network using back propagation algorithm is chosen [112].

7.2.1 Recurrent Neural Network (Elman Method)

Feed-forward neural networks have been successfully used to solve problems that require the computation of a static function *i.e* a function whose output depends only on the current input, and not on any previous inputs. In the real world however, one encounters many problems which cannot be solved by learning a static function because

the function being computed changes with each input received. In such cases, system needs to predict the outputs with some knowledge of how the past inputs affect the processing of the present input, as well as a way of storing the past inputs. In other words such a system must have a memory of the past input and a way to use that memory to process the current input. It should be clear from the architecture of feed-forward neural networks that past inputs have no way of influencing the processing of future inputs. This situation can be rectified by the introduction of feedback connections in the network. This way the network activation produced by past inputs can cycle back and affect the processing of future inputs. The classes of neural networks which contain cycles or feedback connections are called RNNs. While the set of topologies of feed-forward networks is fairly constrained, an RNN can take on any arbitrary topology as any node in the network may be linked with any other node (including itself). The only requirement we make is that the network have clearly defined input and output nodes.

Recurrent networks are the state of the art in nonlinear time series prediction, system identification, and temporal pattern classification. As the output of the network at time t is used along with a new input to compute the output of the network at time $n + 1$, the response of the network is dynamic. There are few RNN architectures proposed by Frasconi, Gori-Soda, Narendra-Parthasarathy , Williams and Zipser, and Elman[113].

Elman networks [112, 114 - 115] are a form of RNNs which have connections from their hidden layer back to a special copy layer. This means that the function learnt by the network can be based on the current inputs plus a record of the previous state(s)

and outputs of the network. In other words, the Elman network is a finite state machine that learns what state to remember (i.e., what is relevant). The special copy layer is treated as just another set of inputs and hence the standard back-propagation learning techniques can be used (something which is not generally possible with recurrent networks).

7.2.1.1 Architecture of a Simple Elman Network

An Elman network is a general feed-forward NN extended with a context layer. The context layer acts as another input to the network. It is added to provide the network with memory. The architecture of the Elman network is shown in Figure 7.1. The network contains p nodes in the input layer, J nodes both in the hidden and the context layers and one node in the output layer. The context layer provides the recurrent connection to the feed-forward network.

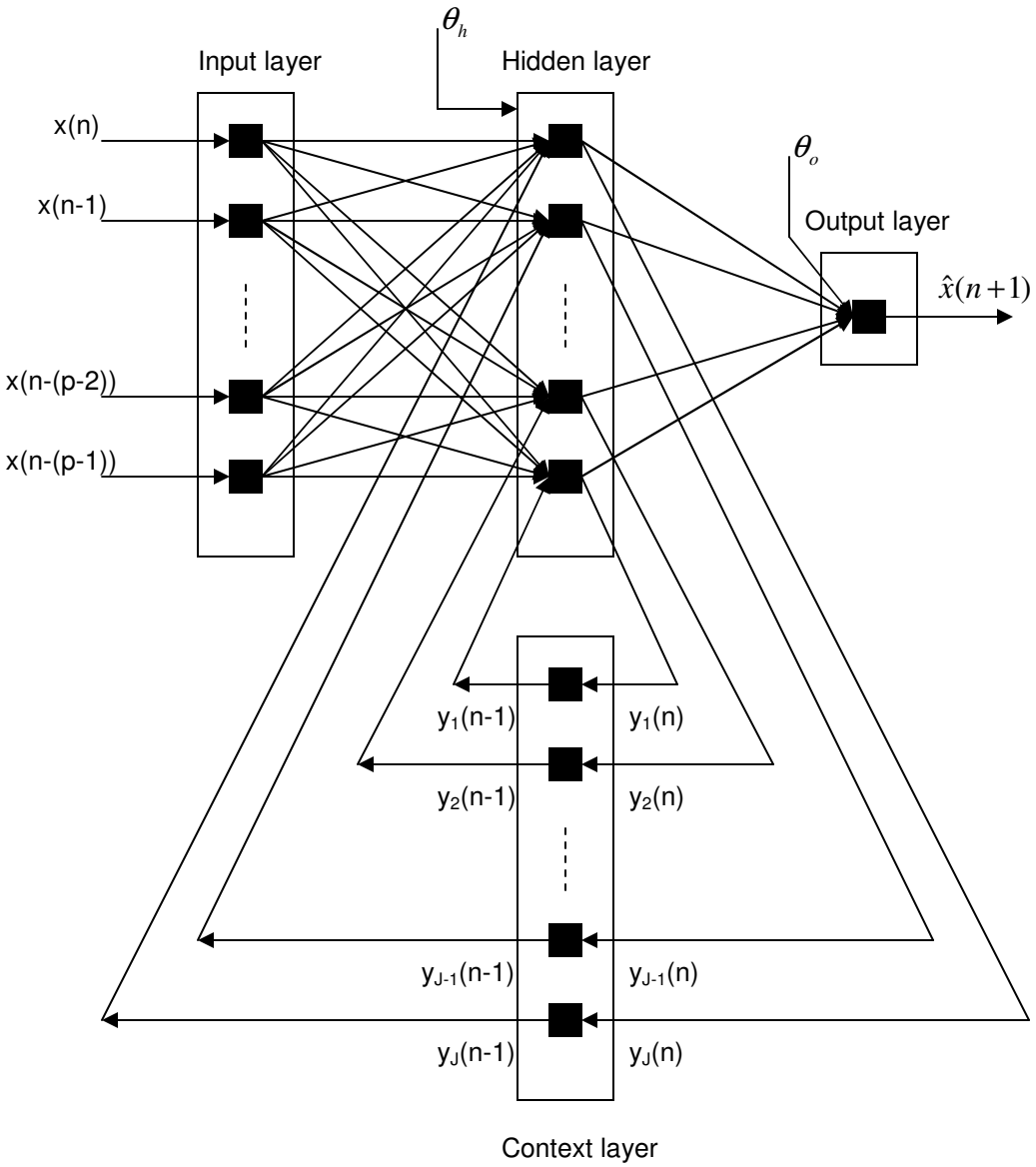

Figure 7.1 Elman network architecture

Recurrent connections in this network are implemented as follows: At any time instant *n*, the values in the hidden nodes are stored one-to-one in context nodes. The context nodes are connected in the forward direction to the hidden nodes in the one-to-

one fashion. The presence of this simple loop implies that the activations of the hidden units at time n can influence the activations of the hidden units at instant n+1. There are same numbers of context units as hidden units and the connections from the latter to the former are one-to-one and have weights fixed at 1. The context units can be connected to the hidden units in a one-to-many fashion. In our implementation, the context units are connected to the hidden units in the forward direction in a one-to-one fashion with fixed weights of 1. For HRV signal and EEG signal modeling, the Elman network is implemented with p = 16 and J = 8. The parameters are chosen such that the given network produces optimal results i.e with minimum NRMSE. There is signal extrapolation. The reconstructed signals shown in Figure 7.5 and Figure 7.7 are the extrapolated signals based on the previous values of the actual signals.

7.2.1.2 Training Elman Networks

At each time step, a copy of the hidden layer units is made to a copy layer. Training the Elman network consisted of the following steps:

1. Initialize the context layer with random weights.

2. Present the first set of inputs to the input layer.

3. Calculate the hidden layer output with the inputs from input layer and the context layer.

4. Calculate the predicted output.

5. Compare the predicted output with the expected output.

6. Backpropagate the error by adjusting the weights of the hidden layer and the output layer.

7. Copy the hidden layer output to the context layer.

8. Repeat steps 3-7, this time by presenting the next set of inputs. Repeat until the end of the data sequence is reached.

9. Repeat steps 1-8 until the training error is sufficiently small.

The output of the hidden layer $y_j(n)$ is given by

$$y_j(n) = f(net_j(n)) \tag{7.1}$$

$$net_j(n) = \sum_i w_{ji} x_i(n-i) + \sum_l u_{jl} y_l(n-1) + \theta_h \tag{7.2}$$

where w_{ji} is the weight between the j^{th} hidden node and the i^{th} input node, u_{jl} is the weight between the j^{th} hidden node and the l^{th} context node, $f(.)$ is the activation function at the hidden layer. The final output $\hat{x}(n+1)$ is given by

$$\hat{x}(n+1) = g(net_k(n)) \tag{7.3}$$

$$net_k(n) = \sum_j v_{kj} y_j(n) + \theta_o \tag{7.4}$$

where θ_h is the bias input to the hidden layer, θ_o is the bias input to the output layer, v_{kj} is the output layer weights and $g(.)$ is the activation function at the output layer.

As all of the trainable weights are in the forward direction, the standard back propagation algorithm is used to train this network. In the generalized version of the Elman network, the activations of hidden units and input units of many previous time steps are stored and a specialized version of the back propagation algorithm called back propagation through time (BPTT) is used.

7.2.2 Pipelined - Recurrent Neural Network (PRNN)

A neural network is well suited for the nonlinear prediction of signals by virtue of the distributed nonlinearity built into its design and the ability of the network to learn from its environment. The recurrent time recurrent learning (RTRL) architecture is capable of continuously learning which is required in bio-signals such as heart and brain signals. In large scale, the computational complexity of the RTRL algorithm increases. To address this problem, a *pipelined recurrent neural network* (PRNN) is proposed that uses RTRL learning algorithm with a modular and recurrent architecture [113]. The PRNN consists of *T* nonlinear subsections or modules connected in a linear fashion. Each nonlinear subsection by itself is a simple recurrent architecture. By combining nonlinear sections in a linear fashion, the architecture can model the signals with its both linear and nonlinear characteristics. The modeled signal is expected to preserve both the linear and

nonlinear characteristics of the signal. The block diagram of the PRNN is given in Figure 7.2.

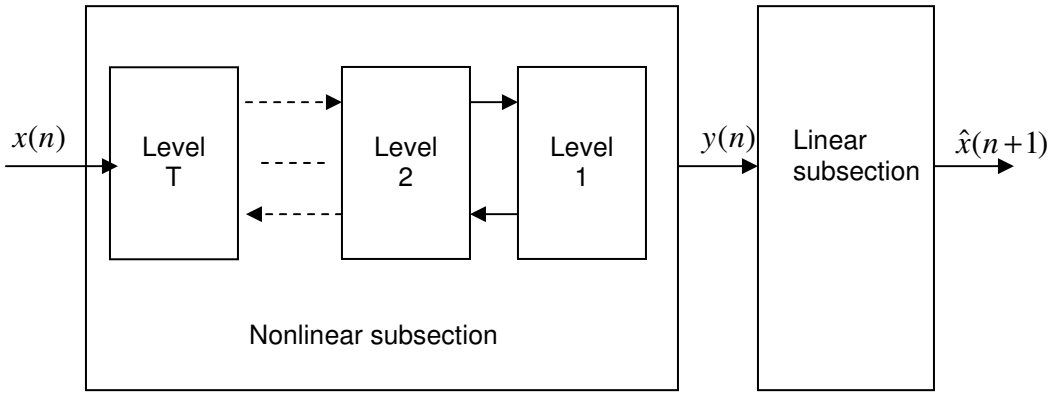

Figure 7.2 Block diagram of the PRNN model

7.2.2.1 Architecture of a PRNN Network

The detailed architecture of the PRNN is shown in Figure 7.3 and the architecture for the i^{th} module is shown in Figure 7.4. The nonlinear subsection consists of *T* modules as given in Figure 7.3a. Each module has a neural network module and a comparator. The neural network module at each level is a RNN with *p* external inputs, *Q-1* inputs from the current network output, one input from the previous level output and one bias input. All the modules operate in the same fashion and have exactly same number of inputs, outputs, layers and neurons. For computational simplicity, all the modules are designed to have same synaptic weight matrix. The comparator compares the output of each module to generate the error signal. The linear subsection given in Figure 7.3b has an order of *q* and generates the predicted output $\hat{x}(n+1)$ from the nonlinear subsection output, $y(n)$.

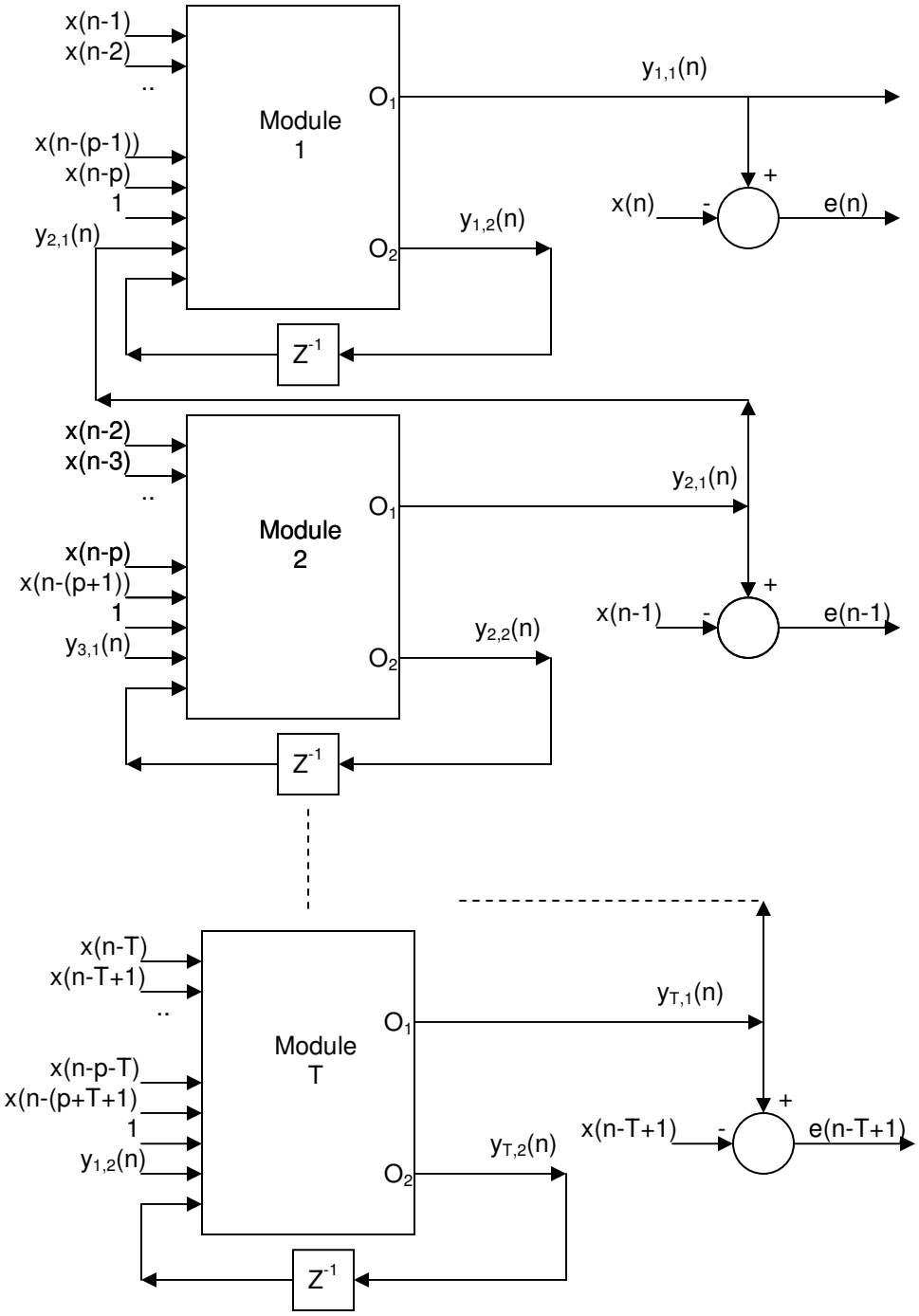
x(n-1)
x(n-2)
..
x(n-(p-1))
x(n-p)
1
y2,1(n)
Module 1
O1
O2
y1,1(n)
y1,2(n)
x(n)
-
+
e(n)
Z-1
x(n-2)
x(n-3)
..
x(n-p)
x(n-(p+1))
1
y3,1(n)
Module 2
O1
O2
y2,1(n)
y2,2(n)
x(n-1)
-
+
e(n-1)
Z-1
x(n-T)
x(n-T+1)
..
x(n-p-T)
x(n-(p+T+1)
1
y1,2(n)
Module T
O1
O2
yT,1(n)
yT,2(n)
x(n-T+1)
-
+
e(n-T+1)
Z-1

(a)

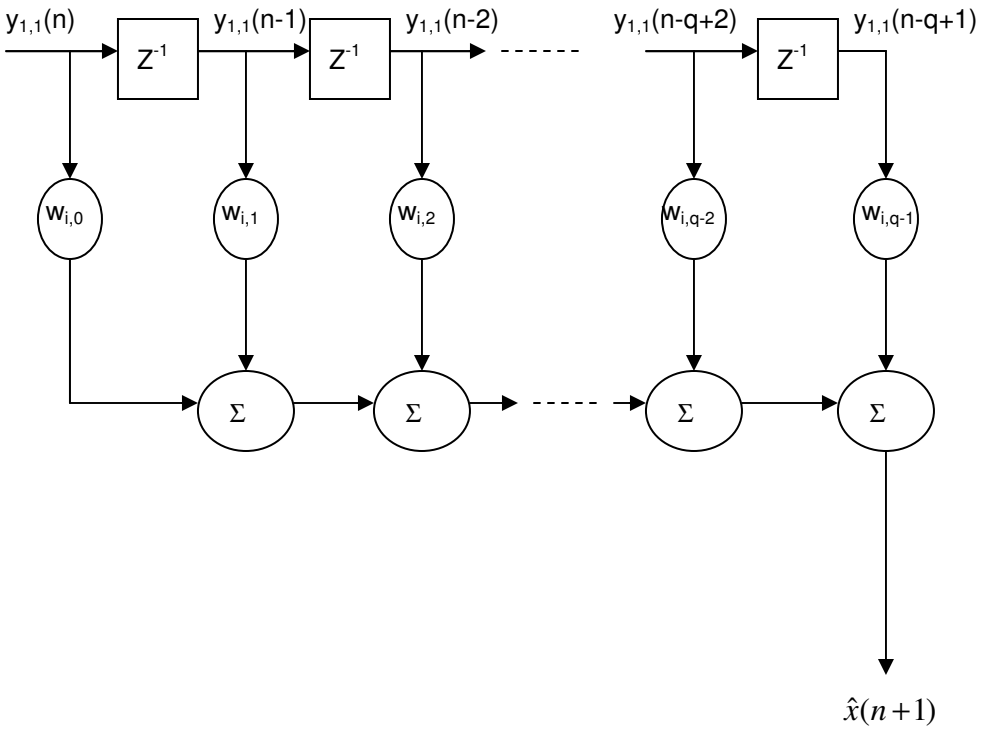

(b)

Figure 7.3 PRNN Network architecture (a) Nonlinear subsection (b) Linear subsection

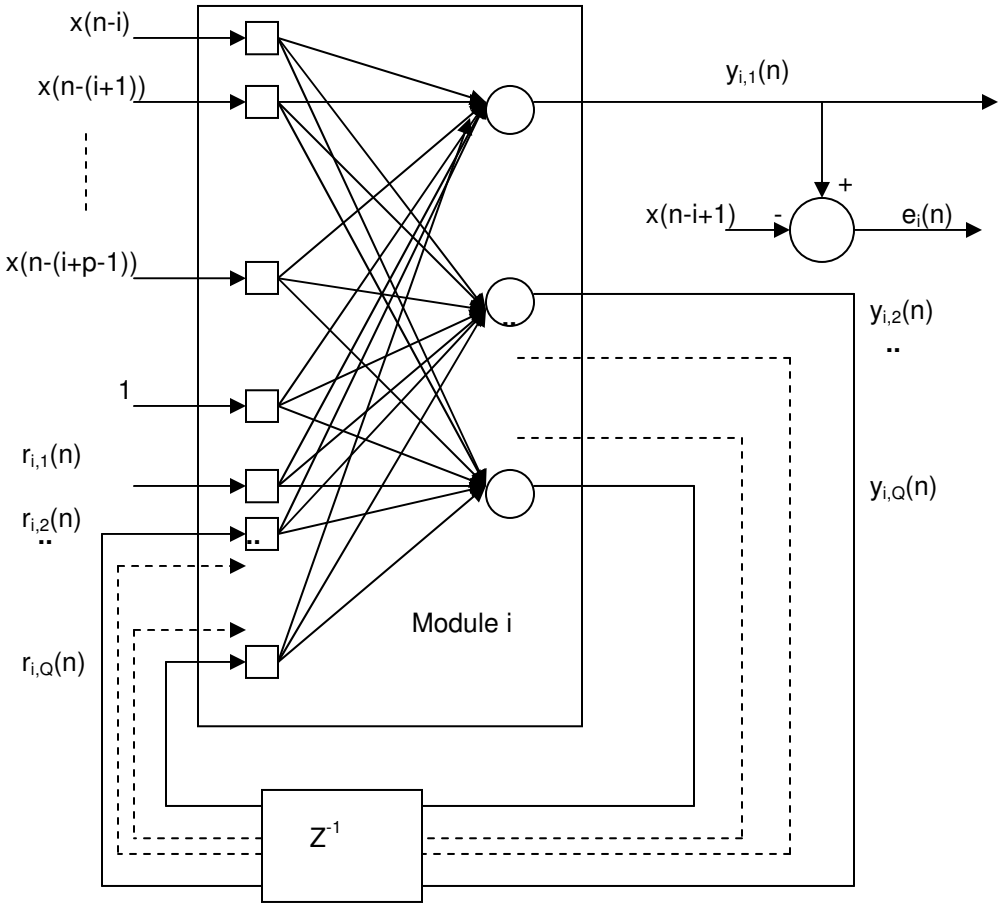

Figure 7.4 Generalized PRNN architecture of i^{th} module

The output of each level $y_{i,k}(n)$ is given by,

$$y_{i,k}(n) = \phi(v_{i,k}(n)) = \frac{1}{1+\exp(-v_{i,k}(n))}, \tag{7.5}$$

where $i = 1, \cdots, T$ and $k = 1, \cdots Q$. The function $v_{i,k}(n)$ is the net internal activation of the k^{th} neuron and $y_{i,k}(n)$ is the output of the k^{th} neuron at the i^{th} module at the n^{th} time point [94].

The synaptic weight matrix $\mathbf{W}$ for each module is a $(p+Q+1)-by-Q$ matrix. Each element of this matrix is represented as $w_{k,i}$ which is the weight of the connection between k^{th} neuron from the i^{th} input node. The weight matrix W is given by,

$$\mathbf{W} = [\mathbf{w}_1, \cdots, \mathbf{w}_k, \cdots \mathbf{w}_Q], \tag{7.6}$$

where w_k is a $(p+Q+1)-by-1$ vector defined by,

$$\mathbf{w}_k = [w_{k,1}, w_{k,2}, \cdots, w_{k,p+Q+1}]^T. \tag{7.7}$$

The input signal $x(n)$ contains the samples $x(1), x(2), \cdots, x(N)$. At any time instant n the external input applied to module i is given by,

$$x_i(n) = [x(n-i), x(n-(i+1)), \cdots, x(n-(i+p-1))]^T, \tag{7.8}$$

where p is the nonlinear prediction order. The other input vector applied to the module i is the feedback from the output of module i and it is given by,

$$r_i(n) = [r_{i,1}(n), r_{i,2}(n), \cdots, r_{i,Q}(n)]^T. \tag{7.9}$$

Each module also has a fixed bias input. Therefore at the n^{th} time point, the output $y_{i,k}(n)$ of neuron k in module i is described by,

$$y_{i,k}(n) = \phi(v_{i,k}(n)), \tag{7.10}$$

where $v_{i,k}(n)$ is given by,

$$v_{i,k}(n) = \sum_{i=1}^{p} w_{k,i} * x(n-(i+p-1) + w_{k,p+1} + \sum_{p+2}^{p+Q+1} w_{k,i} * r_{i,i-(p+1)}(n), \tag{7.11}$$

where the weight $w_{k,p+1}$ represents the bias, the index $i = 1,\cdots,T$ and $k = 1,\cdots Q$.

The feedback signal for module i contains the first neuron's output of the adjacent module $i+1$ and one step delayed output signals from module i. Thus the feedback input $r_i(n)$ is given by,

$$\begin{aligned} r_i(n) &= [y_{i+1,1}(n), r_i^{'}(n)]^T \\ &= [y_{i+1,1}(n), y_{i,2}(n-1), \cdots, y_{i,Q}(n-1)]^T \end{aligned}, \tag{7.12}$$

where $i = 1,2,\cdots T-1$ and $r_i^{'}(n)$ denotes the feedback signals that originate from the module i. The last module, the module T is a fully connected recurrent neural network with the vector $y_T(n)$ fed back after a one time unit delay. Therefore

$$r_T(n) = y_T(n-1). \tag{7.13}$$

The predicted output from the PRNN is the output of first neuron of the first module, module 1 and is given by,

$$y_{pred}(n) = y_{1,1}(n). \tag{7.14}$$

The output from the PRNN is then sent through a linear subsection consisting of a tapped delay line filter as given in Figure 7.3. The weight matrix of this linear subsection is given by,

$$w_i = [w_{i,0}, w_{i,1}, \cdots, w_{i,q-1}]^T, \tag{7.15}$$

where q is the total number of taps. The output of the linear subsection, which is the actual predicted output, is then given by,

$$\hat{x}(n+1) = w_i^T y_{pred}(n). \tag{7.16}$$

The output $\hat{x}(n+1)$ is the prediction of the actual sample $x(n+1)$ of the input signal.

7.3 Implementation of the PRNN Network

The PRNN network for modeling the HRV and EEG signals is implemented with the following parameters. The nonlinear subsection consists of 8 modules *i.e* $T = 8$. Each module has 16 input neurons, 1 bias input, one input from the output of module $i+1$ and

one input feed back input from the module i. The linear subsection contains 12 taps. Therefore using the past 36 samples of the input, the 37th sample is predicted.

7.4 Modeling of HRV Signals

The HRV signals are predicted using the architecture given in Section 7.2 and 7.3. The eight types of HRV signals NSR, VF, AF, ISCH, CHB, LBBB, PVC and SSS segments, the corresponding modeled segments using Elman method and the PRNN method are shown in Figure 7.5 and Figure 7.6. Two main criteria, SNR and NRMSE are used to evaluate the performance of the nonlinear models.

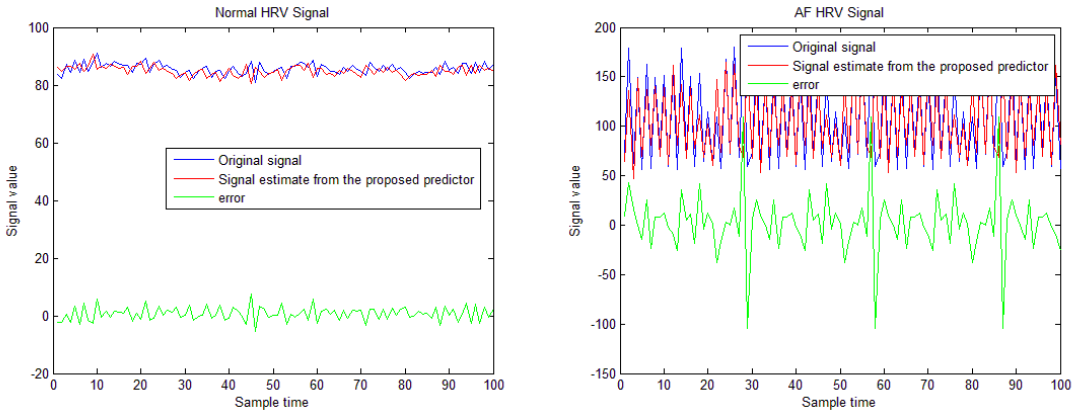

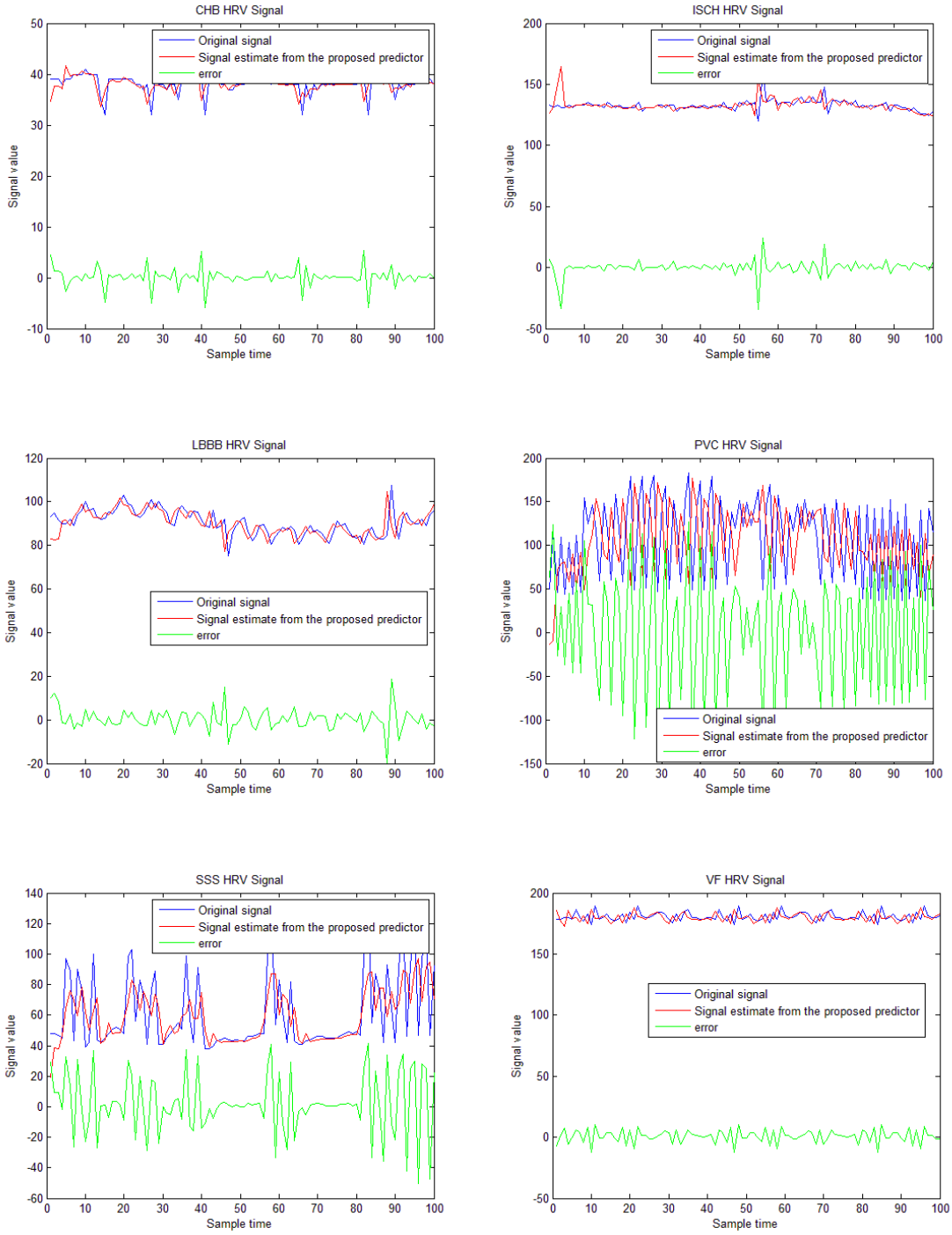

Figure 7.5 Original, reconstructed and error signals for various HRV signals using the Elman network.

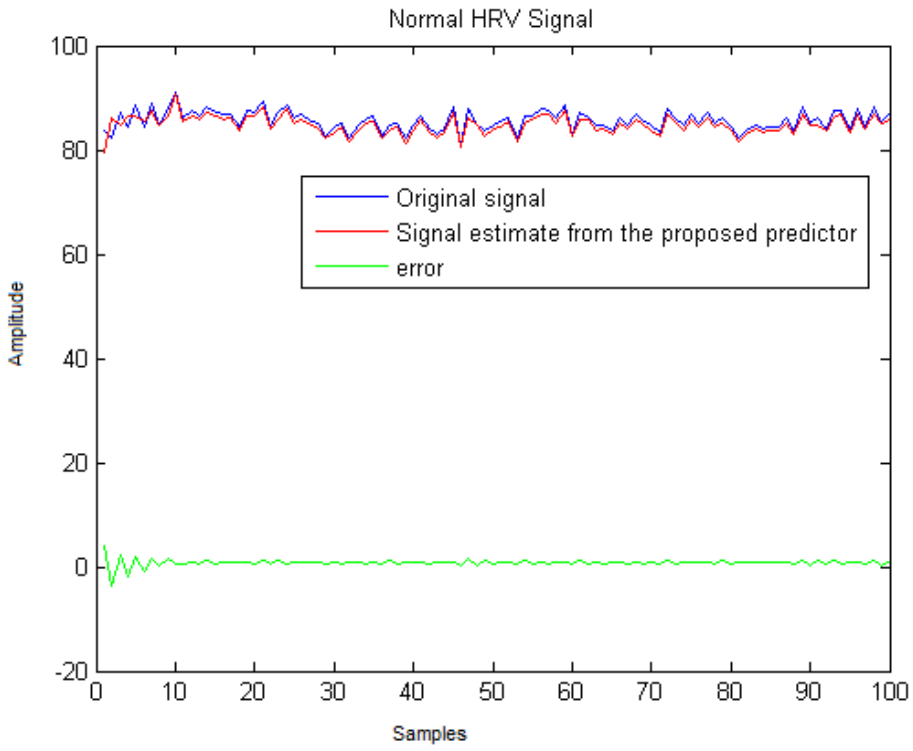
Normal HRV Signal
Original signal
Signal estimate from the proposed predictor
error
Amplitude
Samples
100
80
60
40
20
0
-20
0
10
20
30
40
50
60
70
80
90
100

(a)

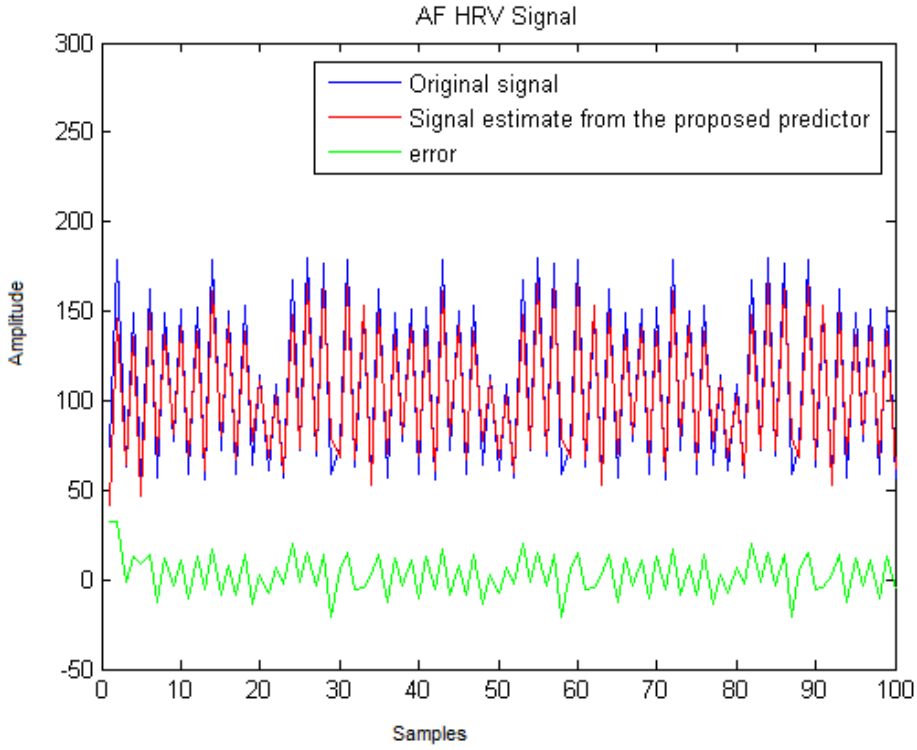
AF HRV Signal
Original signal
Signal estimate from the proposed predictor
error
Amplitude
Samples
300
250
200
150
100
50
0
-50
0
10
20
30
40
50
60
70
80
90
100

(b)

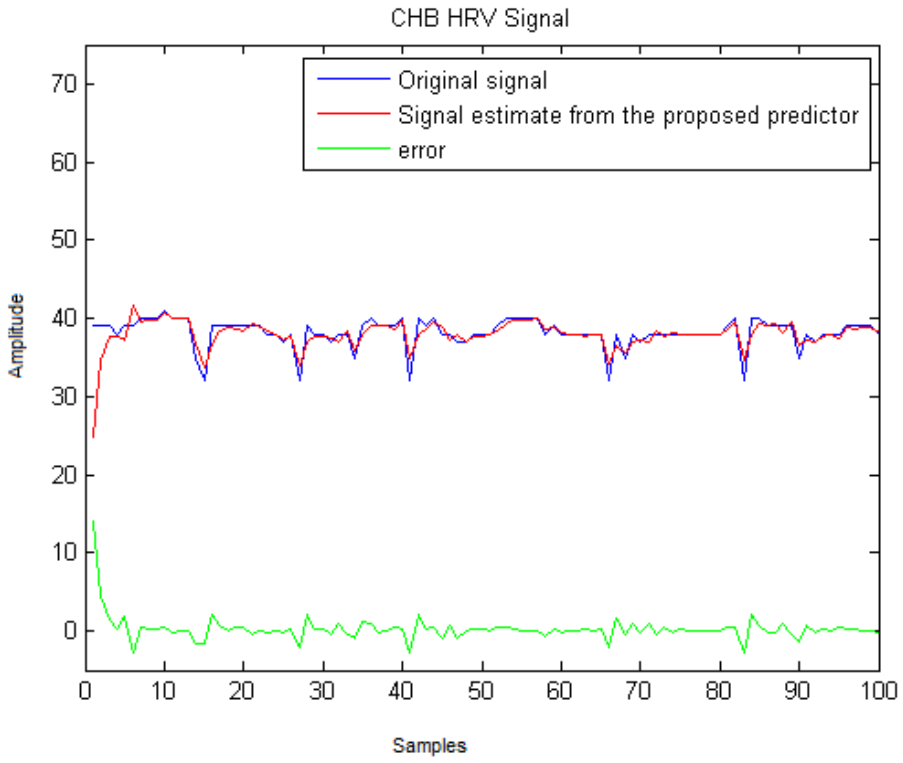
CHB HRV Signal
Original signal
Signal estimate from the proposed predictor
error
Amplitude
Samples
0
10
20
30
40
50
60
70
80
90
100

(c)

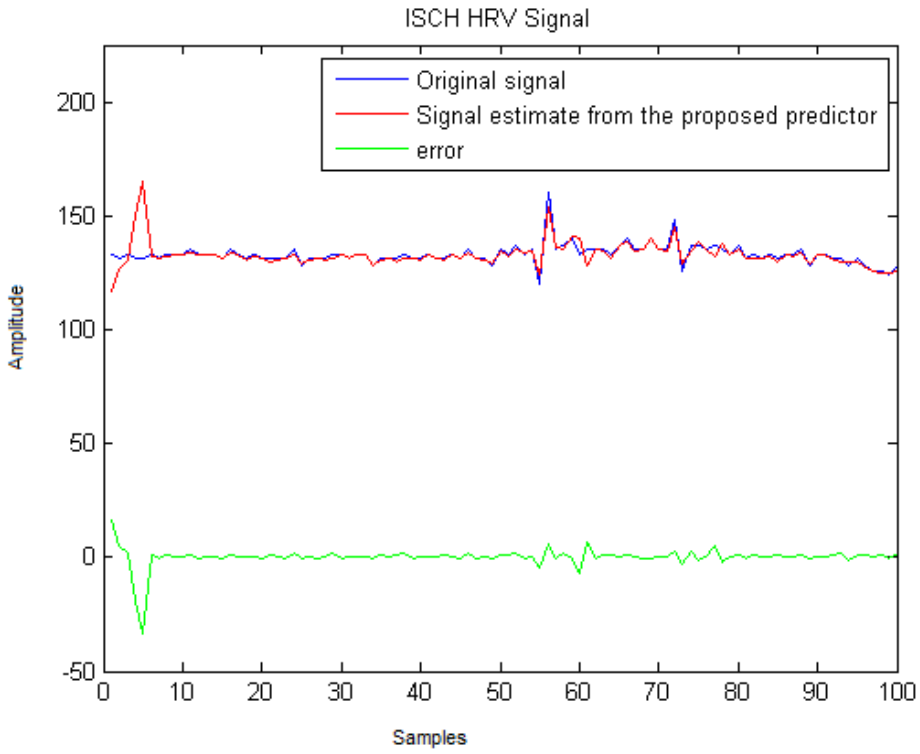
ISCH HRV Signal
Original signal
Signal estimate from the proposed predictor
error
Amplitude
Samples
-50
0
50
100
150
200
0
10
20
30
40
50
60
70
80
90
100

(d)

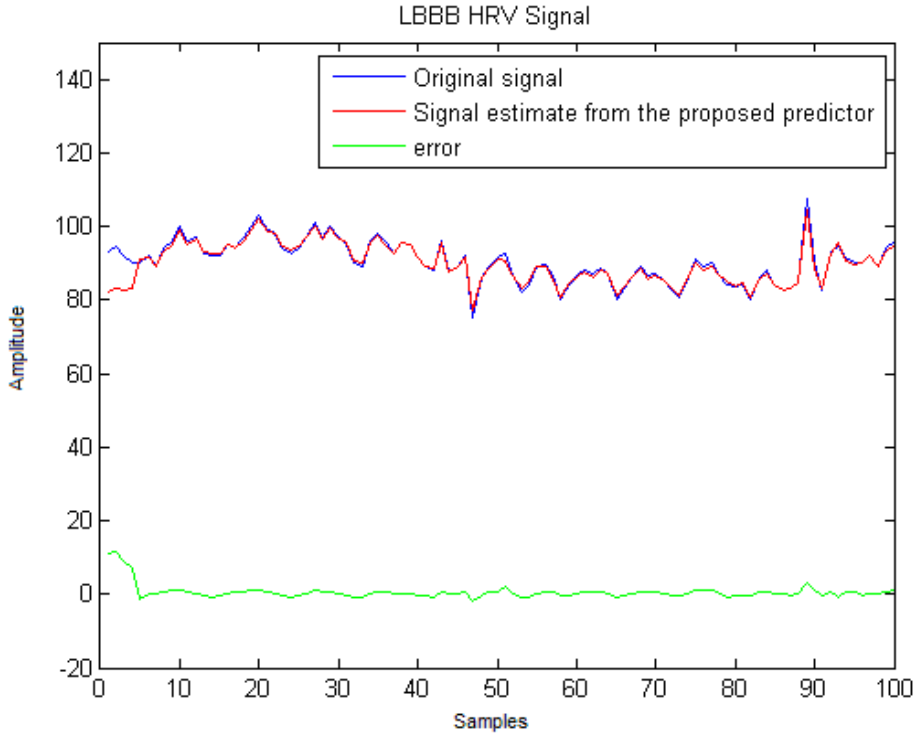
LBBB HRV Signal
Original signal
Signal estimate from the proposed predictor
error
Amplitude
Samples
140
120
100
80
60
40
20
0
-20
0
10
20
30
40
50
60
70
80
90
100

(e)

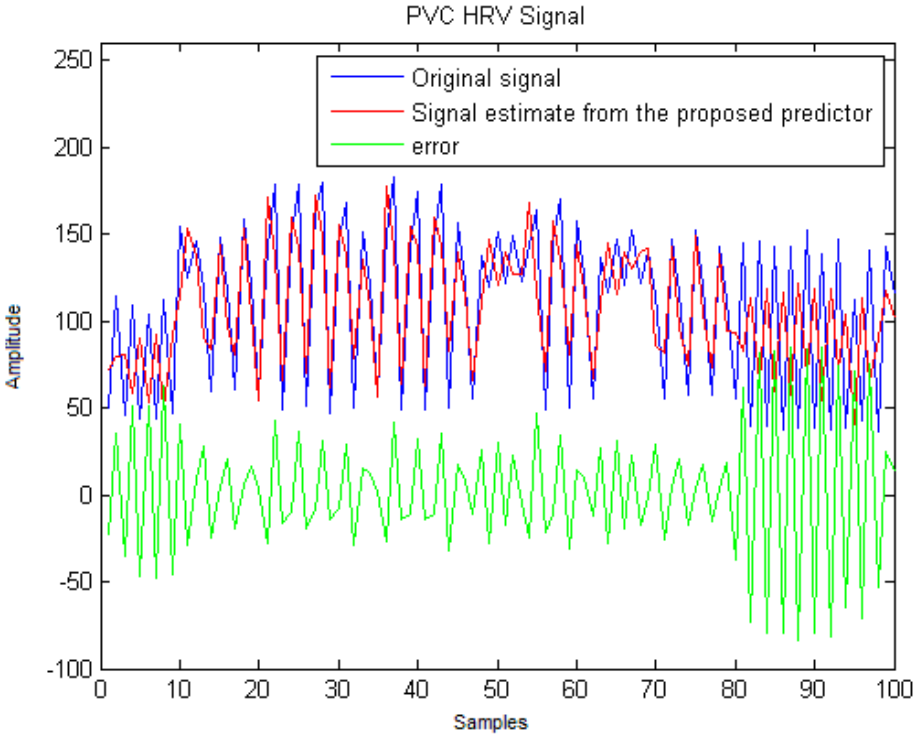
PVC HRV Signal
Original signal
Signal estimate from the proposed predictor
error
Amplitude
Samples
250
200
150
100
50
0
-50
-100
0
10
20
30
40
50
60
70
80
90
100

(f)

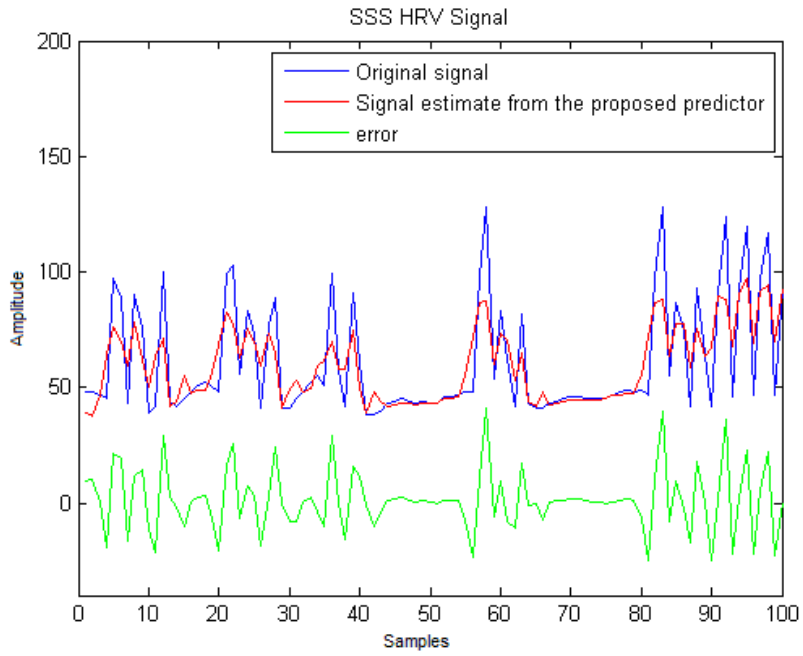

(g)

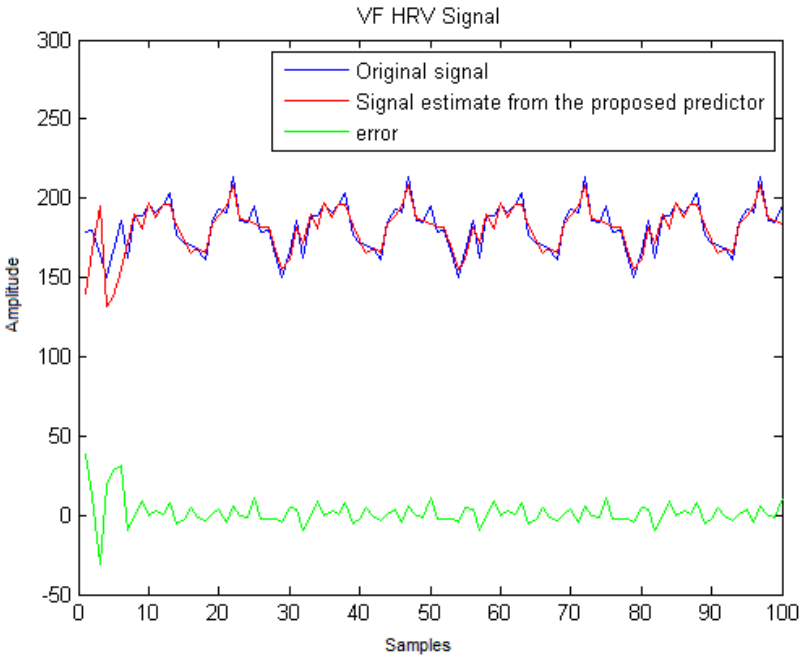

(h)

Figure 7.6 Original, reconstructed and error signals for various HRV signals using the PRNN network.

HRV signal types	Elman	PRNN
NSR	0.35±0.18	0.29±0.11
AF	16.56±2.37	10.42±2.13
VF	2.87±1.11	0.93±0.26
CHB	6.37±1.51	5.26±1.04
ISCH	10.21±2.21	9.24±2.11
PVC	27.65±2.87	22.47±2.85
SSS	18.22±3.72	17.69±2.64
LBBB	2.56±1.62	2.24±1.16

Table 7.1 NRMSE (%) values of the predicted HRV signals from the Elman and PRNN model.

HRV signal types	Elman	PRNN
NSR	21	25
AF	31	32
VF	31	35
CHB	27	28
ISCH	25	27
PVC	27	32
SSS	28	30
LBBB	22	25

Table 7.2 SNR values of the predicted HRV signals from the Elman and PRNN model.

HRV SIGNAL TYPES	LF/HF RATIO				
		ELMAN MODEL		PRNN MODEL	
	ORIGINAL SIGNAL	PREDICTED SIGNAL	% difference	PREDICTED SIGNAL	% difference
NSR	0.8635	0.8424	2.4465	0.8794	1.8382
LBBB	0.2441	0.2612	7.0224	0.2591	6.1620
PVC	1.3453	1.2781	4.9953	1.3369	0.6245
AF	0.5498	0.5592	1.7011	0.5613	2.0830
VF	0.2853	0.2986	4.6554	0.2912	2.0618
CHB	1.1532	1.2368	7.2456	1.2154	5.3899
ISCH	2.9948	3.1196	4.1688	3.0329	1.2737
SSS	0.4185	0.4397	5.0743	0.4467	6.7471

Table 7.3 Comparison of LF/HF ratio of the predicted signals with the original signal.

The Elman and PRNN modeling are applied to eight different types of HRV signals discussed in Chapter 3. The original NSR, VF, AF, ISCH, CHB, LBBB, PVC and SSS segments, the corresponding Elman and PRNN modeled segments and the error signals are shown in Figure 7.5 and Figure 7.6. The SNR values calculated for the predicted signals are given in Table 7.2. It can be seen that the SNR of the predicted signal from PRNN network is greater than 25. The SNR of the predicted signals from the PRNN model is better than for the signals of the Elman model. For critical abnormalities such as VF, PVC, ISCH, AF, CHB and SSS, the SNR is significantly higher in the predicted signals from the PRNN model. The % NRMSE values is computed for the

modeled signals and given in Table 7.1. It can be seen that the error is less for the PRNN model compared to the Elman model.

7.4.1 Validation of the Signal Model

Chaotic measures	**NSR**	**PVC**	**LBBB**	**AF**	**VF**	**CHB**	**SSS**	**ISCH**
D_2	3.6202	2.3032	3.218	2.5812	2.93	2.7674	2.3626	3.3006
λ_1	0.515	0.6692	0.473	0.581	0.4386	0.1892	0.835	0.2308
H	0.6614	0.9234	0.6616	0.8224	0.7648	0.7708	0.881	0.687
KSEN	0.6216	0.5188	0.4452	0.4888	0.442	0.4708	0.3158	0.3556
APEN	1.777	1.5532	1.5096	1.576	1.1146	0.9724	1.5868	0.7756
SEN	1.6816	1.1634	1.2472	1.2336	1.1116	0.8978	1.3198	1.1794
REN	3.487	2.4726	2.7284	2.6324	2.356	2.2422	2.7738	2.468
$D^{Higuchi}$	1.3954	1.2374	1.3418	1.2406	1.2766	1.2934	1.2622	1.3728
D^{Katz}	1.6082	1.3106	1.5522	1.4152	1.5152	1.4238	1.3756	1.5206

Table 7.4 Chaotic measures of the modeled HRV signal - Elman method

The generated HRV signals are validated using NRMSE, SNR and LF/HF ratio measures. The NRMSE given in Table 7.1 indicates the predicted signal to be a close follower of the actual signal with the PRNN model performing better than the Elman model in the HRV signal types considered. The simulated normal HRV signal from the PRNN model closely follows the original signal with the NRMSE less than 0.3. Overall, the PRNN model generates signal with less signal amplitude difference and with a higher SNR. The modeled signal closely follows the original signal in the time domain. In frequency domain, the results of LF/HF ratio measure as given in Table 7.3 indicate the

perseverance of the frequency domain features in the predicted signal. The % difference of the LF/HF ratio of the modeled and actual signal is less then 10%. The modeled signals are also validated using the chaotic measures discussed in Chapter 3.

Chaotic measures	**NSR**	**PVC**	**LBBB**	**AF**	**VF**	**CHB**	**SSS**	**ISCH**
D_2	3.6001	2.2966	3.209	2.5806	2.915	2.7437	2.3563	3.3003
λ_1	0.5075	0.6446	0.4715	0.5705	0.4293	0.1796	0.8275	0.2119
H	0.6362	0.8982	0.6523	0.8092	0.7354	0.7594	0.851	0.6705
KSEN	0.5973	0.5074	0.4371	0.4669	0.4255	0.4639	0.2969	0.3478
APEN	1.7635	1.5316	1.4898	1.573	1.1023	0.9712	1.5784	0.7678
SEN	1.6558	1.1517	1.2436	1.2168	1.0858	0.8789	1.2949	1.1497
REN	3.484	2.4663	2.7242	2.6312	2.338	2.2161	2.7669	2.444
$D^{Higuchi}$	1.3777	1.2137	1.3259	1.2253	1.2733	1.2667	1.2361	1.3464
D^{Katz}	1.5941	1.3103	1.5411	1.4026	1.4876	1.4169	1.3678	1.5203

Table 7.5 Chaotic measures of the modeled HRV signal - PRNN method

The results of the chaotic measures of the synthesized HRV signals modeled using the Elman method and the PRNN method are given in Table 7.4 and Table 7.5, respectively. By comparing the results with the results of the actual signal given in Table 3.3, it can be seen that the chaotic measures of the synthesized using PRNN method closely follows the actual signal results. The variation of the chaotic measures is more than 10% for the synthesized signals using Elman method as compared to the actual signal. The chaotic measures are distinct for each class when the signals are synthesized using PRNN method and a p-value of <0.01 is obtained when subjected to ANOVA test.

The p-value indicates good statistical significance for the results with a confidence interval of 90%. A p-value < 0.07 is obtained for the results of the Elman method. This indicates the PRNN method models the underlying process that generates the signal, more precisely than the Elman method.

7.5 Modeling of EEG Signals

The non linear modeling techniques discussed in Section 7.2 and 7.3 are used to model the three categories of the EEG signals – normal, background and epileptic. The original EEG signals and the corresponding reconstructed signal using PRNN method and error are given in Figure 7.7 and Figure 7.8. The NRMSE and SNR values of the predicted signals are given in Table 7.6 and Table 7.7. It can be seen that the predicted signals using PRNN method has a lower NRMSE and higher SNR values.

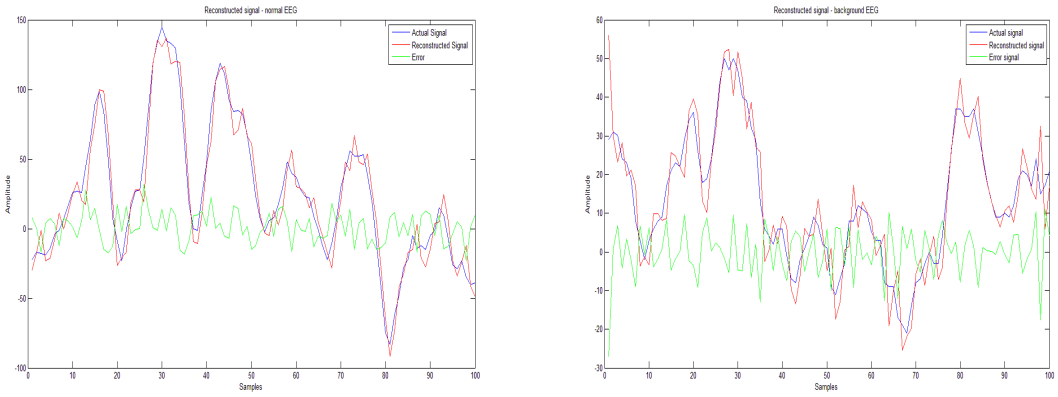

(a) (b)

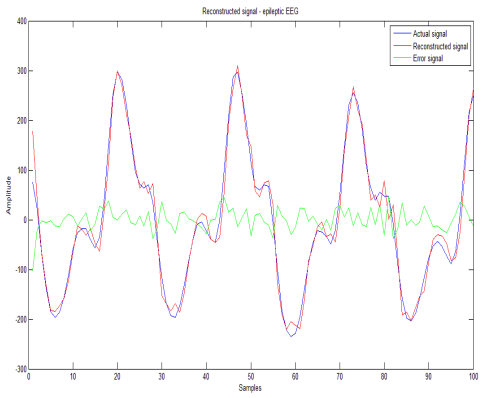

(c)

Figure 7.7 Original, reconstructed and error signals for EEG signals using the Elman network.

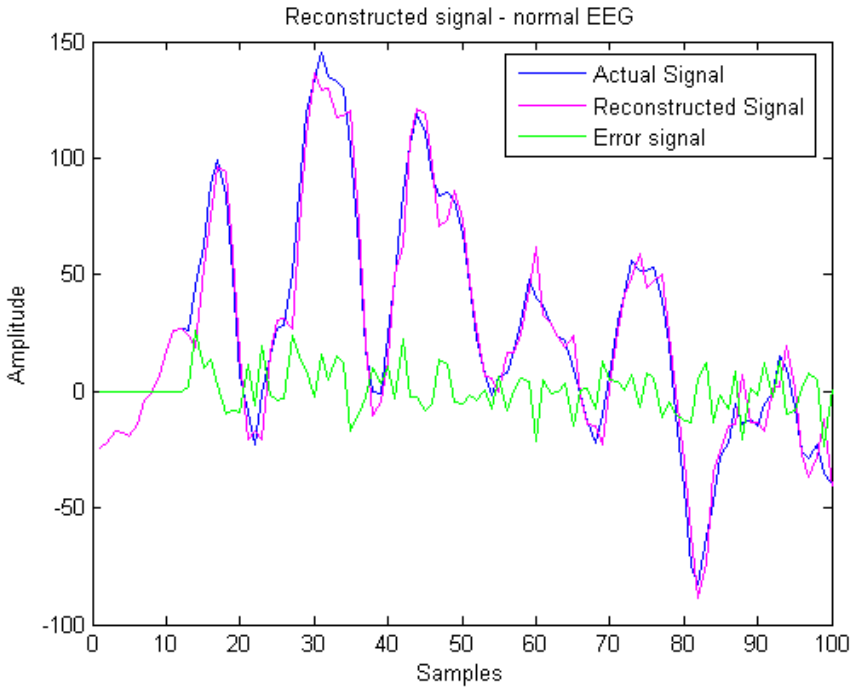

(a)

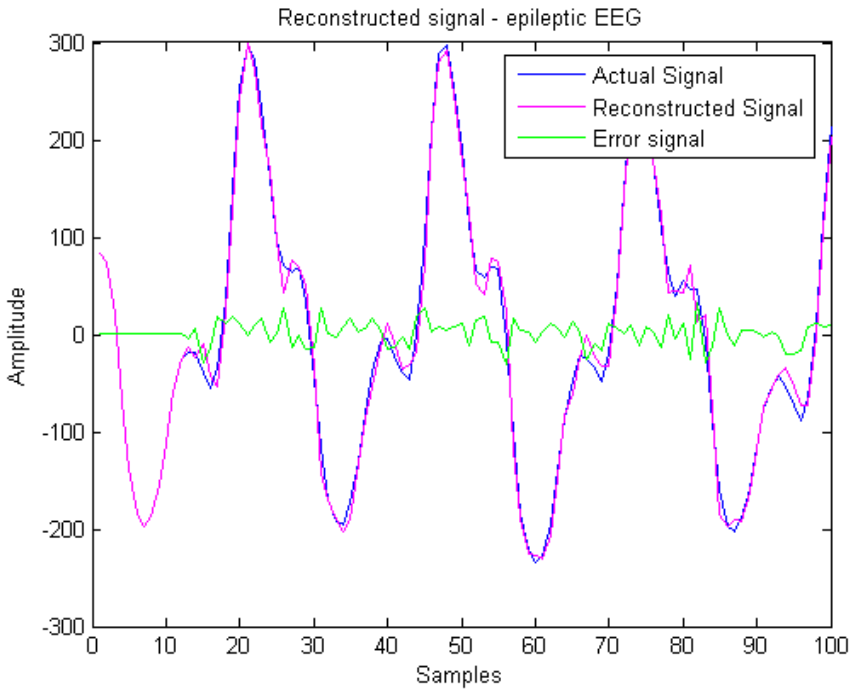

(b)

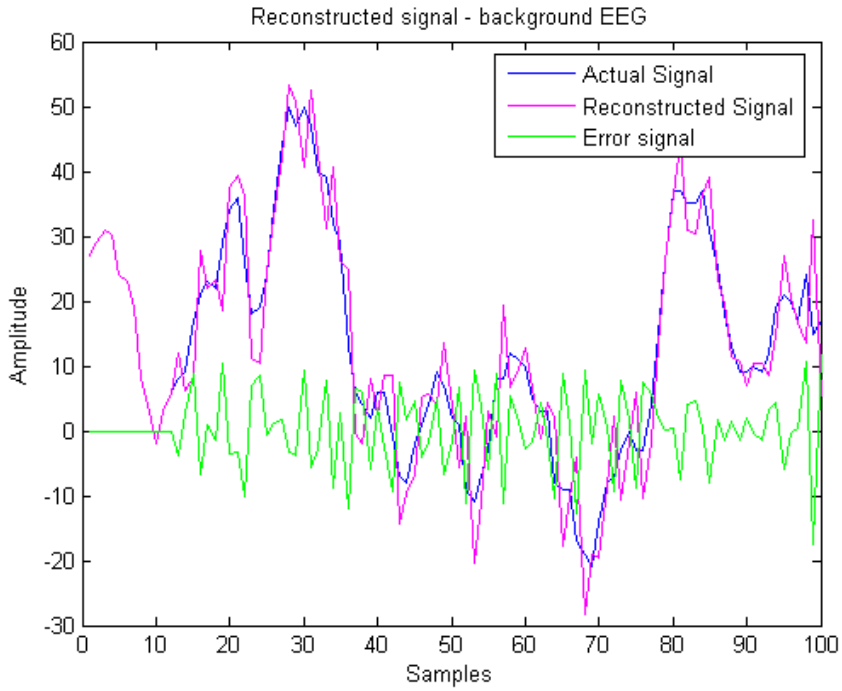

(c)

Figure 7.8 Original, reconstructed and error signals for EEG signals using the PRNN network.

7.5.1 Validation of the Signal Model

The synthesized EEG signals are validated using the nonlinear characteristic measures discussed in Chapter 4. Results of the characteristics measures of the modeled normal, background and epileptic EEG signals using Elman and PRNN method are given in Table 7.8 and Table 7.9, respectively. It can be seen that for all the categories of the EEG signals, nonlinear model using the PRNN method perform better than the Elman method. It can be seen that the characteristic measures are distinct for the three categories.

EEG signal	**Elman**	**PRNN**
Normal	7.683$\pm$1.242	5.321$\pm$1.631
Background	5.876$\pm$1.769	4.322$\pm$1.341
Epileptic	12.491$\pm$1.665	8.965$\pm$1.348

Table 7.6 NRMSE (%) values of the predicted EEG signals from the Elman and PRNN model.

EEG signal	**Elman**	**PRNN**
Normal	18	24
Background	18	22
Epileptic	17	22

Table 7.7 SNR values of the predicted EEG signals from the Elman and PRNN model.

Chaotic	**Normal**	**Epileptic**	**Background**
D_2	4.7731	3.8513	4.2311
λ_1	0.1903	0.1734	0.1891
H	0.3124	0.3397	0.3265
KSEN	0.5876	0.4791	0.5198
APEN	0.6932	0.6278	0.6608
SEN	-0.2333	-0.7432	-0.4992
REN	-0.2121	-0.1993	-0.1914
$D^{Higuchi}$	1.4972	1.2983	1.3528
D^{Katz}	1.8123	1.4511	1.5112

Table 7.8 Chaotic measures of the modeled EEG signals - Elman method

Chaotic	**Normal**	**Epileptic**	**Background**
D_2	4.8490	3.8960	4.2881
λ_1	0.1970	0.1790	0.1902
H	0.3186	0.3480	0.3338
K	0.5955	0.4859	0.5295
APEN	0.7014	0.6381	0.6670
SEN	-0.2274	-0.7391	-0.4905
REN	-0.2024	-0.1972	-0.1872
$D^{Higuchi}$	1.5052	1.3265	1.3790
D^{Katz}	1.8386	1.4825	1.5373

Table 7.9 Chaotic measures of the modeled EEG signals - PRNN method

7.6 Comparison of Linear and Nonlinear Modeling Techniques

The results of the linear and nonlinear modeling are discussed in Chapter 6 and Chapter 7. First, the linear modeling using parametric and nonparametric methods are discussed and the modeled HRV and EEG signals are given. The modeled signals are compared in terms of NRMSE, SNR and the chaotic measures. From the results tabulated in Table 6.1 and Table 7.1, it can be seen that the NRMSE is considerably lower for the nonlinear modeling techniques. Of the four modeling techniques used, the NRMSE is the lowest for all the eight classes of the reconstructed HRV signals using PRNN method. The results of SNR of the reconstructed HRV signals using linear and nonlinear methods are given in Table 6.1 and Table 7.2 respectively. The SNR values are higher for signals modeled using nonlinear methods, more specifically using the PRNN method. The results are in agreement with the results of NRMSE that the noise is lesser in the signals modeled using PRNN technique. The same trend is exhibited for EEG signals as well and is shown in Table 6.5, Table 7.6 and Table 7.7. The reduction in error when using PRNN technique is because the PRNN technique models the linear and nonlinear components of the underlying system dynamics effectively. The linear method such as Welch and Burg method models only the linear components and does not take into account the nonlinear dynamics of the system. The Elman network models the underlying nonlinear dynamics but fails to model the inherent linear dynamics of the system. The PRNN technique

combines both the linear and nonlinear dynamics of the system and hence successfully models the HRV and EEG signals with lower NRMSE and higher SNR values. This result is supported by the results of the characteristics measures given in Table 6.3 – 6.4, Table 6.6 – 6.8, Table 7.4 – 7.5 and Table 7.8 – 7.9. From the results, it is seen that the nonlinear and chaotic measures extracted from the modeled signals using linear techniques are not significant for each case. This may be because the linear models are unable to completely characterize the nonlinearity in the signal. The result of the Elman method is better than the linear methods but not as good as PRNN method. This is due to the fact that the network being purely nonlinear fails to model the inherent linear components of the signal. The HRV and EEG signals modeled using PRNN technique exhibited similar characteristics as the actual signal. This demonstrates the capability of the PRNN modeling technique to model the underlying dynamics of the process. The proposed PRNN predictor outperformed the linear methods and the Elman method in terms of NRMSE, SNR and the characteristic measures.

7.7 Conclusion

Of the two techniques discussed, it can be seen that the PRNN model can generate more reliable and accurate HRV and EEG signals. The reconstructed signals from the PRNN model exhibit higher SNR and less NRMSE. The modeling ability of the PRNN model in synthesizing the HRV and EEG signals is better than that of the linear models also. This is because the HRV and EEG signals are inherently chaotic and nonlinear. The

PRNN model can model the nonlinear aspects of the underlying system better than the linear model. The true power and advantage of neural networks lies in their ability to represent both linear and non-linear relationships and in their ability to learn these relationships directly from the data being modeled.

Chapter 8 Conclusion

8.1 Conclusion

Recent technological developments in the medical field have resulted in sophisticated health care and increased chances of survival. For example, large majority of people who had CA have survived by implantable and portable defibrillators. Neuronal damage occurs within few minutes of CA and brain function starts to degrade rapidly. The neuronal damage usually goes unnoticed in the earlier stages until visible signs of permanent consequent start to appear. During this period, the brain has at least partially damaged and its functions cannot be restored. Sometimes it reaches the extent whereby the heart is functioning and brain is damaged. This leads to the brain dead condition. Hence it is highly crucial to device methods to analyze the heart and brain signals and monitor the cardiac and mental health. In this work, various methods to analyze the heart and brain signals and techniques for detection of cardiac and mental health are proposed.

In this work, HRV and EEG signals are characterized using nonlinear measures. A feature library with eleven features is developed for the eight classes of HRV signals. Extracted features are tested for statistical significance using ANOVA test. The results generated a p-value that is less than 0.1 in all cases. This indicates that the results are statistically significant with a confidence level of 90%. The discriminating ability of the

feature set is tested by classifying the signals using the feature set. Three different classifiers NN classifier, fuzzy classifier and ANFIS classifier are proposed for this purpose. Using the feature set, these classifiers detected the eight classes of cardiac abnormalities with an accuracy of more than 90%. The results demonstrated the usability and suitability of the extracted feature set in the diagnosis of cardiac diseases.

The EEG signals of normal and epileptic subjects are analyzed using the nonlinear time series analysis techniques expecting to extract quantitative measures that can reliably distinguish the EEG of an epileptic subject from that of a normal subject. The results of our analysis demonstrated the potential of complexity measures such as D_2, λ_1, H, D^{katz}, $D^{Higuchi}$, $KSEN$, SEN, $APEN$ and REN in quantifying the EEG signals of normal and epileptic subjects. It is clearly shown that the values are higher for normal subject compared to that of epilepsy. The statistical results also support the discriminating ability of these measures in identifying epileptic and normal EEG signals. These measures can serve as quantitative descriptors of EEG in automatic identification of normal and epileptic EEG signals. The analysis of nonlinear dynamics in EEG signals serve as an aid in understanding the underlying physiological processes in the brain. These features are used for classification of EEG signals as well. The three classifiers used for classification of HRV signals are used for classification of EEG signals as well. The three classifier architectures classify EEG signals with an accuracy of about 90%. The ANFIS classifier outperformed the other two classifiers in identification of EEG signals.

To further understand the characteristics and enhance the analysis of the signals, it is necessary to model the signals. The synthesized signals are valid only if they exhibit similar characteristics as the original signal. In this work, we proposed to model the HRV and EEG signals using linear techniques, nonlinear techniques and finally by a combination of linear and nonlinear techniques to model the HRV and EEG signals. The performances of all the models are compared in detail.

First, we discussed the modeling of the HRV and EEG signals using linear techniques. The parametric modeling using Burg's method and nonparametric modeling using FFT – Welch method is implemented. The performances of the models are evaluated using the performance measures such as the NRMSE and SNR. The synthesized signals are validated using the characteristic measures. Results indicate that the Burg's method perform better than the FFT method. From the results, it is seen that the nonlinear and chaotic measures extracted from the modeled signals are not significant for each case. This is attributed to the fact that the linear models are unable to capture the underlying nonlinearity in the original signal.

To overcome this problem, we proposed to use the nonlinear techniques (using Elman method) to model the HRV and EEG signals. The results obtained using this predictor has a higher variation in terms of the characteristics feature values of the signal. This is because the network is able to capture the nonlinearity and not the linearity in the signals. This led us to propose a new predictor (PRNN) that takes models both the nonlinear and linear dynamics of the underlying process.

From the results, it is seen that the PRNN model generated more reliable and accurate HRV and EEG signals. The synthesized signals from the PRNN model exhibit higher SNR and lower NRMSE values. This is supported by the results of the chaotic analysis of the synthesized HRV and EEG signals. The PRNN model can model the nonlinear aspects of the underlying system better than the linear model. The true power and advantage of neural networks lies in their ability to represent both linear and non-linear relationships and in their ability to learn these relationships directly from the data being modeled. This characteristic is successfully demonstrated by the proposed PRNN predictor.

8.2 Recommendations for Future Work

With the current analysis as the base work, further studies can be conducted in the future to improve the system as recommended below:

- The most imperative recommendation for future work is to analyze the HRV and EEG signals from the same subjects. Currently in our work, this is not implemented due to the constraints in obtaining the validated data.

- The analysis can be extended to other types of EEG signals recorded with conditions such as dementia, change in consciousness, brain death , sleep disorders and catatonia.

- Improvements can be made on the decision-making algorithm. The results of the three networks can be combined by developing a hybrid decision making algorithm and a final decision can be made by using fuzzy logic rule or any other artificial intelligence methods.

- The system can be enhanced to analyze and classify more classes and the degree of abnormality.

References

[1] Broomhead D.S. & G.P. King, "Extracting qualitative dynamics from experimental data", *Physica D,* vol. 20, pp.217-236, 1986.

[2] Simm C.W., M.L. Sawley, F. Skiff & A. Pochelon, "On the Analysis of Experimental Signals for Evidence of Deterministic Chaos", *Helvetica Physica Acta*, vol.60, pp.510-516, 1987.

[3] Denker M. & G. Keller, "Rigorous statistical procedures for data from dynamical systems", *Journal of Statistical Physics*, vol.44, pp.67-93, 1986.

[4] Guckenheimer J. & P. Holmes, *Nonlinear Oscillations, Dynamical Systems and Bifurications of Vector Fields*, Springer-Verlag: Berlin, 1983.

[5] Essex, T. Lookman & M.A.H. Nerenberg, "The Climate Attractor over Short Time Scales", *Nature*, vol.326, pp.64-66, 1987; M.A.H. Nerenberg & C. Essex, paper presented at the Spring Meeting of the American Geophysical Union, Baltimore Maryland, May 29-June 1, 1990.

[6] Roux J.C., R.H. Simoyi & H.L. Swinney, "Observation of a strange attractor", *Phsyica D*, vol.8, pp.257-266, 1983.

[7] Hauser W. A. & D. C. Hesdorffer, *Epilepsy: frequency, causes, and consequences*, New York: Epilepsy Foundation of America, 1990.

[8] Kandel E. R., J. H. Schwartz, & T. M. Jessel, *Principles of Neural Science*, 3rd ed. Prentice-Hall: NJ, 1991.

[9] Engel J. Jr., & T. A. Pedley, *Epilepsy: A comprehensive Textbook*, Lippencott Raven Press: Philadelphia, 1998.

[10] Kantz H. & T. Schreiber, *Nonlinear Time Series Analysis*, Cambridge Univ. Press:U.K, 1997.

[11] Basar E., *Chaos in Brain Function*, Springer-Verlag: Berlin, 1990.

[12] Duke D. & W. Pritchard, *Measuring Chaos in the Human Brain*, World Scientific: Singapore, 1991.

[13] Jansen B.H. & M.E. Brandt, *Nonlinear Dynamical Analysis of the EEG*, World Scientific: Singapore, 1993.

[14] Kaplan D.K. & J.R. Cohen, "Searching for Chaos in fibrillation", *Annals NY Academic Science*, vol.11, pp. 367-374, 1991

[15] Cohen M.E., D.L Hudson & P.C. Deedwania, "Applying continuous chaotic modeling to cardiac signal analysis", *IEEE Engineering In Medicine and Biology Magazine*, vol.15, pp. 97-102, 1996.

[16] Fell J., K. Mann, J. Roschke & M.S. Gopinathan, "Nonlinear analysis of continuous ECG during sleep I. Reconstruction", *Biological Cybernetics*, vol. 82, pp.477-483, 2000.

[17] Khadra L, A.S. Al-Fahoum, & H. Al-Nashash, "Detection of life-threatening cardiac arrhythmias using wavelet transformation", *Medical & Biological Enginering & Computing*, vol. 35, pp. 626-632, 1997.

[18] Al-Fahoum A.S. & I. Howitt, "Combined wavelet transformation and radial basis neural networks for classifying life-threatening cardiac arrhythmias", *Medical & Biological Engineering & Computing*, vol.37, pp.566-573, 1999.

[19] Paul S.A, J.N. Watson, G.R. Clegg, P.A. Steen & C.E. Robertson, " Finding Coordinated Atrial Activity During Ventricular Fibrillation Using Wavelet Decomposition", *IEEE Engineering In Medicine and Biology Magazine*, vol.21(1), pp. 58-61, 2002.

[20] Sun Y, K.L. Chan & S.M. Krishnan, "Arrhythmia detection and recognition in ECG signals using nonlinear techniques", *Annals of Biomedical Engineering*, vol.28, Supplementary 1, S1-37, 2000.

[21] Owis M.I., H. Ahmed, Abou-Zied, A.M. Youssef, & Y.M. Kadah, " Study of features on nonlinear dynamical modeling in ECG arrhythmia detection and classification", *IEEE Transactions on Biomedical Engineering*, vol. 49(7), pp.733-736, 2002.

[22] Dingfei Ge, N. Srinivasan & S.M. Krishnan, "Cardiac arrhythmia classification using autoregressive modeling", *BioMedical Engineering OnLine*, vol.1(1): 5, 2002.

[23] Task Force of the European Society of Cardiology & North American Society of Pacing and Electrophysiology. Heart rate variability - standards of measurement, physiological interpretation, and clinical use, *Circulation*, vol.93, pp.1043-1065, 1996.

[24] Narayana Dutt D. & S.M. Krishnan, "Application of Phase space techniques to the analysis of cardiovascular signals", *Proceedings of IEEE EMBS Conference*, Atlanta, U.S.A., October 13-19, 1999.

[25] Radhakrishna Rao K. A., Vikram Kumar Yergani, D. Narayana Dutt, T.S. Vedavathy, " Characterizing Chaos in heart rate variability time series of panic disorder patients", *Proceedings of ICBME - Biovision 2001*, India, pp.163-167, December 21-24, 2001.

[26] Boccaletti S., C. Grebogi, Y.C. Lai, H. Mancini & D. Mazaet, " The control of chaos: Theory and applications", *Physics Reports*, vol.329, pp.108-109, 2000.

[27] Bessar E., *Biophysical and Physiological Systems Analysis,* Addison-Wesley, London, Methuen, 1960.

[28] Callaway E., P.R. Harris, "Coupling between cortical potentials from different areas", *Science*, vol.183, pp.873-875, 1974.

[29] Babloyantz A., C. Nicolis, J.M. Salazar, "Evidence of chaotic dynamics of brain activity during the sleep cycle", *Physical Letters*, A vol.111, pp.152-157, 1985.

[30] Rapp P.E., T. Bashore, J. Martinerie, A. Albano & I. Zimmerman, "A Dynamics of brain electrical activity", *Brain Topography*, vol.2, pp.99-118, 1989.

[31] Guevara, M.R., Glass L., M. Mackey & A. Shrier, "Chaos in neurobiology", *IEEE Transations on Systems Man & Cybernatics SMC*, vol.13(5), pp.790-798, 1983.

[32] Jaeseung J., C. Jeong-Ho, S.Y. Kim & H. Seol-Heui, "Nonlinear dynamical analysis of the EEG in patients with Alzheimer's disease and vascular dementia", *Journal of Clinical Neurophysiolgy*, vol.18(1), pp.58-67, 2001.

[33] Faure P & Korn H, "Is there chaos in the brain? Concepts of nonlinear dynamics and methods of investigation", *Life Sciences*, vol.324, pp.773–793, 2001.

[34] Stam C.J., T.C.A.M. Van Woerkom & R.W.M. Keunen, "Non-linear analysis of the electroencephalogram in Creutzfeldt-Jakob disease", *Biological Cybernetics*, vol.77, pp.247-256, 1997.

[35] Rezek I.A. & S.J. Roberts, "Stochastic complexity measures for physiological signal analysis", *IEEE Transactions on Biomedical Engineering*, vol.45, pp.1186-1191, 1998.

[36] Lehnertz K, C.E. Elger, "Can epileptic seizures be predicted? Evidence from nonlinear time series analyses of brain electrical activity", *Physics Review Letters*, vol.80, pp.5019-5023, 1998.

[37] Martinerie J, C. Adam, M. Le van Quyen, M. Baulac, B. Renault & F.J. Varela, " Can epileptic crisis be anticipated?", *Nature Medicine*, vol.4, pp.1173-1176, 1998.

[38] Wackermann J., "Beyond mapping: estimating complexity of multichannel EEG recordings", *Acta Neurobiologiae Experimentalis*, vol. 56, pp.197-208, 1996.

[39] Stam C.J., Hessels van der Leij, R.W.M. Keunen & D.L.J. Tavy, "Nonlinear EEG changes in postanoxic encephalopathy", *Theory Bioscience*, vol.118, pp.209-218, 1999.

[40] Schraag S., U. Bothner, R. Gajraj, G.N. Kenny & M. Georgieff, "The performance of electroencephalogram bispectral index and auditory evoked potential index to predict loss of consciousness during propofol infusion", *Anesthesia and Analgesia*, vol.89, pp.1311-1315, 1999.

[41] Jing H. & M. Takigawa, "Topographic analysis of dimension estimates of EEG and filtered rhythms in epileptic patients with complex partial seizures", *Biological Cybernetics*, vol. 83, pp.391-397, 2000.

[42] Lehnertz K. & C.E. Elger, "Spatio-temporal dynamics of the primary epileptogenic area in temporal lobe epilepsy characterized by neuronal complexity loss", *Electroencephalography and Clinical Neurophysiology*, vol.95, pp.108-117, 1995.

[43] Casdagli M.C., D.I. Leonidas, R.S. Savit, R.L. Gilmore, S. N. Roper & J. C. Sackellares, "Non-linearity in invasive EEG recordings from patients with temporal lobe epilepsy", *Electroencephalography and Clinical Neurophysiology*, vol.102, pp.98-105, 1997.

[44] Andrzejak R.G., G. Widman, K. Lehnertz, C. Rieke, P. David & C.E. Elger, "The epileptic process as nonlinear deterministic dynamics in a stochastic environment: an evaluation on mesial temporal lobe epilepsy", *Epilepsy Research*, vol.44, pp.129-140, 2001.

[45] Lehnertz K., J. Arnhold, P. Grassberger & C.E. Elger, *Chaos in Brain*, World Scientific, Singapore, 2000.

[46] Arnhold J., K. Lehnertz, P. Grassberger & C.E. Elger," A robust method for detecting interdependences: application to intracranially recorded EEG", *Physica D.*, vol. 134, pp.419-430, 1999.

[47] Gevins A. & M. Aminoff, "Electroencephalography: Brain electrical activity," in *Encyclopedia of Medical Devices and Instrumentation*, J. Webster, Ed. New York: Wiley, pp. 1084–1107, 1988.

[48] Niedermeyer E. & F. Silva, *Electroencephalography : Basic Principles, Clinical Applications, and Related Fields*. Baltimore, MD: Williams & Wilkins, 1993.

[49] James C. & D. Lowe, "Using dynamical embedding to isolate seizure components in the ictal EEG," in *1st International Conference on Advances in Medical Signal and Information Processing*, Bristol, United Kingdom, pub. no. 476, pp. 158–165, September 4-6, 2000.

[50] Xu-Sheng Z., R. Roy & E. Jensen, "EEG complexity as a measure of depth of anesthesia for patients," *IEEE Transactions on Biomedical Engineering*, vol.48, pp.1424–1433, 2001.

[51] Borel C. & D. F. Hanley, "Neurological intensive care unit monitoring," in *Critical Care Clinics. Symposium on Neurological Intensive Care*, M. C. Rogers & R. J. Traysman, Eds. Philadelphia, PA, pp. 223–239, 1985.

[52] Agarwal R., J. Gotman, D. Flanagan & B. Rosenblatt, "Automatic EEG analysis during long-term monitoring in the ICU," *Electroencephalography and Clinical Neurophysiology*, vol. 107, pp. 44–58, 1998.

[53] Goel V., A. Bambrink, A. Baykal, R. Koehler, D. Hanley & N. Thakor, "Dominant frequency analysis of EEG reveals brain's response during injury and recovery," *IEEE Transactions on Biomedical Engineering*, vol. 43, pp. 1083–1092, 1996.

[54] Geocadin R., R. Ghodadra, T. Kimura, H. Lei, D. Sherman, D. Hanley & N. Thakor, "Anovel quantitative EEG injury measure of global cerebral ischemia," *Clinical Neurophysiology*, vol. 111, pp. 1779–1787, 2000.

[55] Bezerianos A., S. Tong, A. Malhorta & N. Thakor, "Information measures of brain dynamics," in *Nonlinear Signal and Image Processing Conference*, Baltimore, MD, 2001.

[56] Rosso O., S. Blanco, J. Yordanova, V. Kolev, A. Figliola, M. Schurmann & E. Basar, "Wavelet entropy: A new tool for analysis of short duration brain

electrical signals," *Journal of Neuroscience Methods*, vol. 105, pp. 65–75, 2001.

[57] Bai O., M. Nakamura, A. Ikeda & H. Shibasaki, "Nonlinear Markov process amplitude EEG model for nonlinear coupling interaction of spontaneous EEG," *IEEE Transactions on Biomedical Engineering*, vol. 47, pp. 1141–1146, Sept. 2000.

[58] Andrezejak R.G., F. Mormann, G. Widman, T. Kruez, C.E. Elger & K. Lehnertz, "Improved spatial characterization of the epileptic brain by focusing on nonlinearity," *Epilepsy Research,* vol. 69, pp.30-34, 2006.

[59] Kruez T, R.G. Andrezejak, F. Mormann, A. Kraskov, H.Stoegbauer, C.E. Elger, K. Lehnertz & P. Grassberger, "Measure profile surrogates: A method to validate the performance of epileptic seizure prediction algorithms," *Physical Review E,* vol. 69, pp.061915, 2004.

[60] Sherman D., A. Bambrink, R. Ichord, V. Dasika, R. Koehler, R. Traystman, D. Hanley & N. Thakor, "Quantitative EEG during early recovery from Hypoxic-Ischemic injury in immature piglets: Burst occurrence and duration," *Clinical Neurophysiology*, vol. 30(4), pp. 175–183, 1999.

[61] Goldberger A.L., L.A.N. Amaral, L. Glass, J.M. Hausdorff, P.Ch. Ivanov R.G. Mark, J.E. Mietus, G.B. Moody, C.K. Peng & H.E. Stanley, "PhysioBank, PhysioToolkit, and PhysioNet: Components of a New Research Resource for Complex Physiologic Signals", *Circulation,* vol. 101(23), pp. e215-e220, 2000.

[62] Pan J. & W.J. Tompkins, "Real Time QRS Detector algorithm", *IEEE Transactions on Biomedical Engineering*, vol.32(3), pp.230-233, 1985.

[63] Mandelbrot B.B., *The Fractal Geometry of Nature,* W.H. Freeman and Co., New York, 1983.

[64] Higuchi T., "Aproach to an irregular time series on the basis of the fractal theory," *Physica D*, vol. 31, pp.277-283, 1988.

[65] Katz M., "Fractals and the analysis of waveforms," *Computers in Biology and Medicine*, vol. 18(3), pp.145-156, 1988.

[66] Accardo M. A., M. Carrozzi, & F. Bouquet, "Use of the fractal dimension for the analysis of electroencephalographic time series," *Biological Cybernetics*, vol. 77, pp. 339-350, 1997.

[67] Takens F., *Detecting strange attractors in turbulence: Dynamical Systems and Turbulence*, ed. Rand, D. A. & Young, L.-S., New York: Springer-Verlag, pp.366-81, 1981.

[68] Abarbanel Henry D. I., *Analysis of Observed Chaotic Data*, Springer-Verlag New York, 1996.

[69] Sauer T., J.A. Yorke & M. Casdagli, "Embedology", *Journal of Statistical Physics*, vol.65, pp.579-616, 1991.

[70] Grassberger P. & I. Procaccia., "Characterization of strange attractors", *Physical Review Letters*, vol.50(5), pp.346-349, 1983.

[71] Theiler J, S. Eubank, S. Longtin, B. Galdrikian & J. Farmer, "Testing for nonlinearity in time series: the method of surrogate data," *Physica D*, vol.58, pp.77-94, 1992.

[72] Eckmann J. P., S.O. Kamphorst & D. Ruelle, "Recurrence Plots of Dynamical Systems", *Europhysics Letters*, vol.4, pp.973-977, 1987.

[73] Theiler J., "Spurious dimension from correlation algorithms applied to limited time-series data", *Physical Review A*, vol.34(3), pp.2427-2432, 1986.

[74] Wolf, J.B. Swift, L.H. Swinney & J.A. Vastano, "Determining Lyapunov exponent from a time series," *Physica D*, vol. 16, pp.285-317, 1985.

[75] Dangel S., P.F. Meier, H.R. Moser, S. Plibersek & Y. Shen, "Time series analysis of sleep EEG," *Computer assisted Physics*, pp.93-95, 1999.

[76] Woo M.A, W.G. Stevenson, D.K. Moser, R.B. Trelease & R.H. Harper, "Patterns of beat-to-beat heart rate variability in advanced heart failure," *American Heart Journal*, vol.123, pp.704-707, 1992.

[77] Tulppo M.P, T.H. Makikallio, T.E.S. Takala, T. Seppanen & H.V. Huikuri, "Quantitative beat-to-beat analysis of heart rate dynamics during exercise", *American Journal of Physiology*, vol.271, pp.H244-H252, 1996.

[78] Huikuri H.V., T.H. Makikallio , C.K. Peng, A.L. Goldberger, U. Hintze & M. Moller, "Fractal correlation properties of R-R interval dynamics and mortality in patients with depressed left ventricular function after an acute myocardial infarction", *Circulation*, vol.101, pp.47-53, 2000.

[79] Grassberger P. & T. Schrieber, "Nonlinear time sequence analysis.", *International Journal of Bifurcation and Chaos*, vol.1(3), pp.512-547,1991.

[80] Fell J. & J. Roschke, "Discrimination of sleep stages: a comparison between spectral and nonlinear EEG measures", *Electroencephalography and Clinical Neurophysiology*, vol.98(5), pp.401-10, 1996.

[81] Quiroga R. Q. & J. Arnhold, "Kulback-Leibler and renormalized entropies: applications to electroencephalograms of epilepsy patients." *Physical Review E* , Stat Physics of Plasmas Fluids and Related Interdiscipilinary Topics 62(6 Pt B), pp.8380-8386, 2000.

[82] Pincus S.M., "Approximate entropy as a measure of system complexity", *Proceedings National Academy of Science*, USA, vol.88, pp.2297-2301,1991.

[83] Bruhn J. & H. Ropcke, "Approximate entropy as an electroencephalographic measure of anesthetic drug effect during desflurane anesthesia", *Anesthesiology*, vol.92(3), pp.715-726, 2000.

[84] Pincus S.M. & A.L. Goldberger, "Physiological time-series analysis: what does regularity quantify?", *American Journal of Physiology*, vol.266, pp.H1643-H1656, 1994.

[85] Thayer J.F & S. A. Moulden., "Estimation of the correlation dimension of heart rate using surrogate data techniques" , *Biomedical Sciences instrumentation*, vol.33, pp. 491, 1997.

[86] Wessel N., A. Voss, H. Malberg, C. Ziehmann, H.U. Voss, A. Schirdewan, U. Meyerfeldt, J. Kurths, "Nonlinear analysis of complex phenomena in cardiological data", *Herzschr Elektrophys*, vol.11, pp.159-173, 2000.

[87] Korhonen I., L.T. Mainardi, H. Yppärilä, T. Musialowicz, "Comparison of linear and non-linear analysis of heart rate variability in sedated cardiac surgery patients", *Proc. of the 23th Annual Conf. of the IEEE-EMBS*, Istanbul, Turkey, Oct 24-28, 2001.

[88] Freeman W.J., M D. Holmes, B C. Burke, & S. Vanhatalo, "Spatial spectra ofscalp EEG and EMG from awake humans", *Clinical Neurophysiology*, 114 (6), pp.1053-1068, 2003.

[89] Bonn university epilepsy data. (http://www.meb.uni-bonn.de/epileptologie/science/physik/eegdata.html)

[90] Sleigh J. W., E. Olofsen, A. Dahan, J. Goede de, A. Steyn-Ross, " Entropies of the EEG: The effects of general anaesthesia", *Proceedings of the 5th international conference on memory, awareness and consciousness*, U.S.A, 2001.

[91] Jelles B., J.H. van Birgelen, J.P.J. Slaets, R.E.M Hekster, E.J. Jonkman & C.J. Stam, "Decrease of nonlinear structure in the EEG of Alzheimers patients compared to healthy controls", *Clinical Neurophysiology,* vol. 110, pp. 1159-1167, 1999.

[92] Jaeseung J., "EEG dynamics in patients with Alzheimer's disease" *Clinical Neurophysiology*, vol.115(7), pp. 1490-1505, 2004.

[93] Lippman R.P., "Pattern classification using neural networks", *IEEE Communication Magazine*, vol.11, pp. 47-64, 1989.

[94] Haykin S., *Neural networks A comprehensive foundation* (2nd ed.), MacMillan College Publishing Company: New York, 1999.

[95] Wasserman P.D., *Advanced Methods in Neural Computing*, Van Nostrand Reinhold, New York, 1993.

[96] Nozaki, Ishibuchi & Tanaka, "Selecting fuzzy if-then rules with forgetting in fuzzy classification systems", *Journal of Japan Society for Fuzzy Theory and Systems*, vol.6(3), pp.585-602, 1994.

[97] Ishibuchi, Murata & Tanaka "Construction of fuzzy classification systems using genetic algorithms", *Journal of Japan Society for Fuzzy Theory and Systems*, vol.7(5), pp.1022-1040, 1995.

[98] George K. & Bo Yuan, *Fuzzy Sets and Fuzzy Logic: Theory and Applications*, Prentice Hall, India, 1995.

[99] Jang Roger J.S., "ANFIS – Adaptive-network-based neuro-fuzzy inference systems", *IEEE Transactions on Systems, Man, and Cybernetics*, vol.20(03), pp.665-685, 1993.

[100] Marple L., *Digital Spectral Analysis with Applications*, Prentice Hall Inc, London, 1987.

[101] Choi B., *ARMA Model Identification*, springer- Verlag, New York, 1992.

[102] Akaike H., "Fitting autoregressive models for prediction", *Annals of the Institute of Statistical Mathematics*, vol. 21, pp.243-247, 1969.

[103] Anita B., S.S. Fernando, P.R. Ana & A. Leite, "A study on the optimum order of autoregressive models for heart rate variability", *Physiological Measurement*, vol. 23, pp. 324-336, 2003.

[104] Papoulis A., *Probability, Random Variables, and Stochastic Processes*, 3rd ed., McGraw-Hill, New York, 1991.

[105] Eckmann J.P., D. Ruelle, "Ergodic theory of chaos and strange attractors," *Reviews of Modern Physics*, vol. 57(3), pp. 617-656, 1989.

[106] Pineda F.J., "Dynamics and architecture for neural computation", *Journal of Complexity*, vol. 4, pp. 216-245, 1988.

[107] Chapeau-Blondeau F. & G. Chauvet, "Stable, oscillatory, and chaotic regimes in the dynamics of small neural networks with delay", *Neural Networks*, vol.5, pp.735-743, 1992.

[108] Van der Maas H.L.J., P.F.M.J. Verschure & P.C.M. Molenaar, "A note on chaotic behavior in simple neural networks", *Neural Networks*, vol.3, pp.119-122, 1990.

[109] Linkens D. & Y. Nyongesa, "Learning systems in intelligent control: an appraisal of fuzzy, neural and genetic algorithm control applications", *IEEE Proceedings on Control Theory and Applications*, vol.134(4), pp.367-385, 1996.

[110] Parlos A., K. Chong & A. Atiya, "Application of the recurrent multilayer perceptron In modelling complex process dynamics", *IEEE Transactions on Neural Networks*, vol.5, pp.255-266, 1994.

[111] Draye J., D. Pavisic & G. Libert, "Dynamic recurrent neural networks: a dynamical analysis", *IEEE Transactions on Systems Man and Cybernetics*, Part B, vol.26, pp. 692-706, 1996.

[112] Elman J. L., "Distributed representations, simple recurrent networks, and grammatical structure", *Machine Learning*, vol.7, pp.195–225, 1991.

[113] Haykin S. & L. Li, "Nonlinear adaptive prediction of stationary signals", *IEEE Transactions on Signal Processing*, vol.43(2), pp.526-535, 1995.

[114] Elman J. L, "Finding structure in Time", *Cognitive Science*, vol.14, pp.179-211, 1990.

[115] Elman J. L., "Learning and development in neural networks: The importance of starting small", *Cognition*, vol.48, pp.71–99, 1993.